TRANSPORTATION RESEARCH RECORD 607

Bridge Design, Testing, and Evaluation

TRANSPORTATION RESEARCH BOARD

COMMISSION ON SOCIOTECHNICAL SYSTEMS
NATIONAL RESEARCH COUNCIL

NATIONAL ACADEMY OF SCIENCES
WASHINGTON, D.C. 1976

Transportation Research Record 607
Price $3.60
Edited for TRB by Marjorie Moore and Susan Lang

subject area
27 bridge design

Transportation Research Board publications are available by ordering directly from the board. They may also be obtained on a regular basis through organizational or individual supporting membership in the board; members or library subscribers are eligible for substantial discounts. For further information, write to the Transportation Research Board, National Academy of Sciences, 2101 Constitution Avenue, N.W., Washington, D.C. 20418.

Notice

The project that is the subject of this report was approved by the Governing Board of the National Research Council, whose members are drawn from the councils of the National Academy of Sciences, the National Academy of Engineering, and the Institute of Medicine. The members of the committee responsible for the report were chosen for their special competence and with regard for appropriate balance.

This report has been reviewed by a group other than the authors according to procedures approved by a Report Review Committee consisting of members of the National Academy of Sciences, the National Academy of Engineering, and the Institute of Medicine.

The views expressed in this report are those of the authors and do not necessarily reflect the view of the committee, the Transportation Research Board, the National Academy of Sciences, or the sponsors of the project.

Library of Congress Cataloging in Publication Data
National Research Council. Transportation Research Board.
Bridge design, testing, and evaluation.

(Transportation research record; 607)
1. Bridges–Design–Addresses, essays, lectures. 2. Bridges–Testing–Addresses, essays, lectures. 3. Bridges–Evaluation–Addresses, essays, lectures. I. Title. II. Series.
TE7.H5 no. 607 [TG300] 380.5'08s[624.2] 77-9251
ISBN 0-309-02582-6

Sponsorship of the Papers in This Transportation Research Record

GROUP 2–DESIGN AND CONSTRUCTION OF TRANSPORTATION FACILITIES
W. B. Drake, Kentucky Department of Transportation, chairman

Structures Section
Arthur L. Elliott, California Department of Transportation, chairman

Committee on General Structures
W. J. Wilkes, Federal Highway Administration, chairman
Frank D. Sears, Federal Highway Administration, secretary
William L. Armstrong, Dan S. Bechly, N. H. Bettigole, Martin P. Burke, Jr., Daniel E. Czernik, Arthur L. Elliott, Donald C. Frederickson, George G. Goble, William A. Kline, Heinz P. Koretzky, Robert M. Olson, Adrian Pauw, Gordon R. Pennington, Wendell M. Smith

Committee on Steel Bridges
John W. Fisher, Lehigh University, chairman
J. Hartley Daniels, Lehigh University, secretary
Dan S. Bechly, Russell L. Chapman, Jr., Lionel F. Currier, Arthur L. Elliott, Gerard F. Fox, Karl H. Frank, T. V. Galambos, Carl H. Gronquist, Wayne Henneberger, William A. Kline, Andrew Lally, Joseph M. McCabe, Jr., Roy L. Mion, Frank D. Sears, Michael M. Sprinkel, Ivan M. Viest, Charles H. Wilson

Committee on Concrete Bridges
Cornie L. Hulsbos, University of New Mexico, chairman
John M. Hanson, Wiss, Janey, Elstner and Associates, secretary
T. Alberdi, Jr., John F. Cavanaugh, W. Gene Corley, Hotten A. Elleby, Norris L. Hickerson, David S. Huval, Walter J. Jestings, Heinz P. Koretzky, H. G. Kriegel, George F. Leyh, Charles C. Mitchell, Joseph H. Moore, Emile G. Paulet, Dominick L. Somma, David A. Van Horn, Earle E. Wilkinson

Committee on Dynamics and Field Testing of Bridges
Robert F. Varney, Federal Highway Administration, chairman
Charles F. Galambos, Federal Highway Administration, secretary
James W. Baldwin, Jr., Edwin G. Burdette, Paul F. Csagoly, Conrad P. Heins, Jr., Cornie L. Hulsbos, Henry L. Kinnier, Celal N. Kostem, Robert H. Lee, Kenneth H. Lenzen, Norman G. Marks, Fred Moses, M. Noyszewski, Leroy T. Oehler, Frederick H. Ray, Ronald R. Salmons, W. W. Sanders, Jr., William H. Walker, George W. Zuurbier

Lawrence F. Spaine, Transportation Research Board staff

Sponsorship is indicated by a footnote on the first page of each report. The organizational units and the officers and members are as of December 31, 1975.

Contents

Abridgment

Analysis of a Horizontally Curved Bridge Through a Geometric Structural Model

Paul J. Brennan, James A. Mandel, and Charles M. Antoni, Department of Civil Engineering, Syracuse University
Rolf Leininger, Stopen Consulting Engineers

Mathematical analysis is an important adjunct to experimental work and forms a guide to the design and interpretation of tests. The inverse is also significant, and a theory based on mathematical analysis needs to be verified by experimentation or prototype testing. In the study described, a mathematical model was developed and a physical model was designed and used. The physical model was used to verify the mathematical analysis and to provide evidence of the action of horizontally curved highway bridges.

The studies were particularly planned to develop information on the stress and deformation characteristics of a small-scale structure proportioned to the major dimensions of the prototype span—Ramp CBW over Huyck Stream of the Mall Arterial Highway, Interstate 540 in Albany, New York. This single span contains four welded plate girders 1.5 m (60 in) deep, interconnected by seven radial cross frames and a lower horizontal bracing system between each exterior and first interior girder. The radii of the inner and outer girders are 45.7 and 53 m (150 and 174 ft) with lengths of 26.8 and 31.1 m (88 and 102 ft). The deck is a reinforced concrete slab of 19-cm (7.5-in) design thickness placed at 21.6 cm (8.5 in) on corrugated forms.

The small-scale structure was mathematically and experimentally analyzed for three dead load conditions and five live load conditions. The analytical and experimental results of each of these loading conditions were compared for stress, moment, and deformation across four sections of the structure. In addition, end reactions were determined as were forces in members of the diaphragms. Significant comparisons between theory and small structure testing under wet concrete dead loading and five live loadings are given in Tables 1 and 2, and comparisons of transverse distribution of moments at the center section for theory, small structure testing, and prototype testing are given in Table 3.

MATHEMATICAL ANALYSIS OF HORIZONTALLY CURVED BRIDGE AS THREE-DIMENSIONAL STRUCTURE

A three-dimensional method of analysis previously developed in the Department of Civil Engineering at Syracuse University was extended and adapted for analysis of the structural frame of horizontally curved girder bridges, with and without an integral deck. With this analysis each member of the structure is considered to be acting normally and to be located in its true position in the structure. Analysis is performed by a computer program (1).

The input to the program consists basically of the geometrical and physical properties of the bridge and the applied loadings. Program output includes the rotations and displacements of the joints of the bridge and the internal forces and moments in all members of the bridge. The program is general and can accommodate most configurations of curved or straight bridges, both with and without a concrete deck.

DESCRIPTION OF THE SMALL-SCALE STRUCTURE

The mathematical analysis was verified by experimentation on a small-scale structure that was geometrically scaled to the field prototype bridge. The design of the small-scale structure was done in accordance with similitude relations (2) by using dimensions in length, mass, and time, and this design was reproduced at a scale of 1 to 8.33 to extremely close tolerances. All steel members of the prototype were type 304 stainless steel members in the small-scale structure. Concrete was used for the deck. The framing of the small-scale structure is shown in Figure 1.

Three dead load tests were performed on the structure without deck. After the dead load testing was completed, stainless steel shear studs were welded to the top flange of each girder and corrugated sheet metal forms were placed on the girders. After the concrete deck was cured, the sidewalks were placed.

Publication of this paper sponsored by Committee on General Structures.

EXPERIMENTAL PROGRAM

The assembled bridge was supported at one end by four load cells, one under each girder. Loads were applied to the structure through gravity. One hundred fifty-four electrical resistance strain gauges were bonded to the structure at critical locations and terminated in signal conditioning units or switching and balancing units. Vertical and rotational deformation measurements were made by using dial gauges.

The small-scale structure was analyzed for deflections, axial forces, bending moments, and torsional moments by the three-dimensional method of analysis. The same eight independent sets of loadings used for mathematical analysis were applied to the scale structure. These consisted of (a) supplemental loading for steel framing, (b) wet concrete, (c) wet concrete followed by supplemental loadings, and (d) live loads in five different positions. All loadings of the bridge model were done in increments of one-fourth of the total load to be added.

Table 1. Comparison of results of analytical and experimental wet concrete loading at midspan of bridge.

Variable	Girder	Three-Dimensional Theory			Experiment
		Condition A	Condition B	Condition C	
Bending moment, J	RC 40	3575	3727	3906	3423
	RC 39	2538	2451	2509	2649
	RC 38	748	700	666	752
	RC 37	643	632	516	644
	Total	7504	7509	7597	7468
Deflection, mm	RC 40	2.845	3.099	3.404	3.861
	RC 39	2.464	2.566	2.718	2.946
	RC 38	2.032	2.083	2.108	2.261
	RC 37	1.600	1.626	1.524	1.473

Note: 1 J = 0.737 ft-lbf; 1 mm = 0.039 in.

Table 2. Bending moments and bottom flange average stresses at center section.

Live Load Position	Girder	Bottom Flange Average Stress (kPa)		Moment (J)	
		Experiment	Theory	Experiment	Theory
1	RC 40	11 549	12 949	1785	2000
	RC 39	9 170	9 439	1062	1096
	RC 38	4 895	5 254	192	203
	RC 37	2 689	-241	113	-101
	Total			3152	3198
2	RC 40	10 467	10 991	1616	1695
	RC 39	10 411	9 067	1198	1051
	RC 38	7 709	7 364	294	283
	RC 37	4 709	3 558	203	147
	Total			3311	3176
3	RC 40	7 309	8 639	1130	1333
	RC 39	8 295	8 557	961	994
	RC 38	10 411	10 170	407	396
	RC 37	7 295	7 909	305	340
	Total			2803	3063
4	RC 40	5 309	6 640	825	1028
	RC 39	7 260	7 612	836	881
	RC 38	12 894	12 211	497	475
	RC 37	10 756	12 990	452	554
	Total			2610	2938
5	RC 40	3 861	5 178	600	802
	RC 39	6 412	6 929	746	802
	RC 38	14 500	13 349	565	520
	RC 37	12 859	16 865	542	712
	Total			2453	2836

Note: 1 kPa = 0.145 lbf/in^2; J = 0.737 ft-lbf.

SMALL-SCALE STRUCTURE TEST RESULTS

After each structural test on the small-scale structure, theoretical data were compared with experimental data. Strain gauge readings were converted to stress by using a computer program written for this study. Maximum stresses were computed from a zero base that was the average of the initial and final zero readings.

Bending moments for the dead load conditions were computed by using the stress distribution determined experimentally, and the area of the applicable portion of each member was used to compute the tensile and compressive force resultants. The moments were computed by using these resultants and the lever arm between them. Wet concrete loading experimental bending moments were compared with the analytical moments (Table 1). For this loading condition, the following three conditions of torsional restraint of the girders were studied by using the three-dimensional analyses.

Condition	Description
A	Torsional restraint at each diaphragm and halfway between each diaphragm at each girder
B	Torsional restraint at each diaphragm and at the lateral bracing
C	Torsional restraint at each diaphragm

Five live loadings were applied to the structure, and wheel spacing and intensities were scaled to the Federal Highway Administration test vehicle that was used to test the Huyck Stream prototype bridge in Albany. These loads were placed sequentially across the transverse centerline of the bridge. Theoretical values of lower flange average stresses were determined from the computed moments by using the lower flange section modulus. Experimental moment values were computed by using this same lower flange section modulus and the average experimental lower flange stress. These values are given in Table 2.

Table 3. Transverse distribution of bending moments at center section.

Load Type	Girder	Percentage Distribution of Moment		
		Experiment	Theory	Prototype Field Test
Wet concrete	RC 40	45.8	51.4	47.0
	RC 39	35.4	33.0	37.5
	RC 38	10.1	8.8	9.0
	RC 37	8.6	6.8	6.4
Live load, position 1	RC 40	56.6	62.5	51.9
	RC 39	33.7	34.3	35.4
	RC 38	6.1	6.4	6.6
	RC 37	3.6	-3.1	6.1
Live load, position 2	RC 40	48.8	53.4	45.6
	RC 39	36.2	33.1	35.3
	RC 38	8.9	8.9	9.1
	RC 37	6.1	4.6	10.0
Live load, position 3	RC 40	40.3	43.5	38.5
	RC 39	34.3	32.5	33.3
	RC 38	14.5	12.9	13.4
	RC 37	10.9	11.1	14.7
Live load, position 4	RC 40	31.6	35.0	30.7
	RC 39	32.0	30.0	28.8
	RC 38	19.1	16.2	16.8
	RC 37	17.3	18.8	23.7
Live load, position 5	RC 40	24.4	28.3	25.5
	RC 39	30.4	28.3	27.4
	RC 38	23.0	18.3	17.6
	RC 37	22.1	25.1	29.5

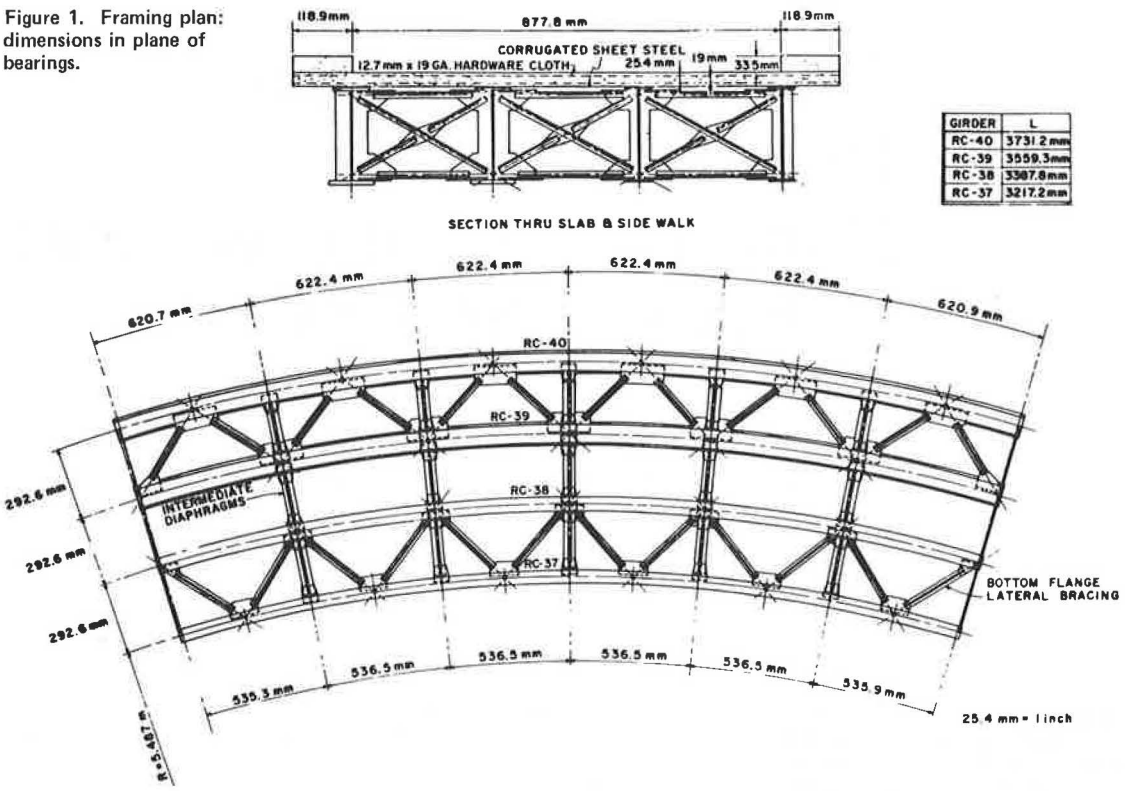

Figure 1. Framing plan: dimensions in plane of bearings.

CONCLUSIONS

Tests of a small-scale structure, geometrically similar to a field prototype, produced useful and valuable data. This tool, properly and carefully used, provides excellent information for evaluating mathematical analyses. The studies on this structure indicate that there is close correlation between theoretical and experimental moment values, and this is particularly evident in data given in Table 3 in which the distribution of the total moment across the center section to each girder is shown by percentage for wet concrete loading and for five live load positions. These distributions are compared with the results of the field tests on the full-size bridge performed by the New York State Department of Transportation and the Federal Highway Administration (3). As noted in this table, the distribution of moments determined from theory, small-scale structure testing, and field testing of the full-sized bridge is in close agreement.

ACKNOWLEDGMENTS

This study was supported by the Engineering Research and Development Bureau, New York State Department of Transportation. Besides the authors, Benjamin A. Wasil and graduate research assistants James D. Cooper, Joseph I. Peck, and John L. Zegarelli were active in the research. Charles Neuman and Bruce Stillman also participated. Robert Roeckelein machined the components and directed assemblage of the bridge.

REFERENCES

1. P. J. Brennan and J. A. Mandel. Users Manual Program for Three Dimensional Analysis of Horizontally Curved Bridges. Federal Highway Administration, U.S. Department of Transportation, Aug. 1975.
2. P. J. Brennan, C. M. Antoni, R. Leininger, and J. A. Mandel. Analysis for Stress and Deformation of a Horizontally Curved Girder Bridge Through a Geometric Structural Model. Department of Civil Engineering, Syracuse Univ., Research Rept.
3. D. B. Beal and R. J. Kissane. Field Testing of Horizontally Curved Steel Bridges: Second Interim Report. Engineering Research and Development Bureau, New York State Department of Transportation, Research Rept. 1.

Abridgment

Thermal Stresses and Deformations in Nonprismatic Indeterminate Composite Bridges

Jack H. Emanuel, University of Missouri—Rolla
J. Leroy Hulsey, North Carolina State University

A review of the literature indicates that thermal stresses warrant increased consideration in design (4, 6). This paper presents a method for determining thermally induced stresses and strains in composite girder bridges and structures with nonprismatic sections subjected to any temperature distribution. It also gives the expected stress range of a typical four-span composite highway bridge with a concrete deck and steel stringer at two arbitrary temperatures.

SLAB AND BEAM STRESSES AND STRAINS

Remove intermediate supports and end restraints, if any, and assume that the composite bridge structure is a simply supported structure in which the slab is separated from the beam. Let the slab be completely restrained in the longitudinal and transverse directions and subjected to temperature effects.

Although it acts as a simple beam before boundary conditions and compatibility are introduced, the slab strains freely in the longitudinal direction. To achieve free movement and satisfy equilibrium, a longitudinal force P'_{ts_k} and a moment M'_{ts_k} are superimposed on the thermally induced force and moment that resulted from the restrained condition.

For the interface strains and curvatures to be compatible, an interface force system of shears and couples, similar to those of Zuk (7) and Aleck (1), must be applied at the ends of prismatic, or constant curvature, segments of the separated slab and beam as shown in Figure 1. The final strains, stresses, curvatures, and deflections may be found after the magnitudes of the interface forces are determined and all deformations have been found to be consistent with the boundary conditions.

The final slab strain at any section is the sum of the strain under unrestrained movement and that resulting from equilibrium and compatibility, which, for a slab in plane strain, is

$$\sigma_{xs_k} = -[\alpha_s E_s T_{s(y)_k}/1 - \mu_s] + (P'_{ts_k}/A_s) + (M'_{ts_k} y_s/I_s) + [(1/A_s) + (cy_s/I_s)]F_k - (y_s/I_s)Q_k \quad (1)$$

where

- s = slab,
- k = segment, if nonprismatic,
- σ_{xs_k} = final slab stress in a determinate member,
- α_s = thermal coefficient of expansion,
- E_s = modulus of elasticity,
- $T_{s(y)_k}$ = change in temperature as a function of vertical distance,
- μ_s = Poisson's ratio,
- P'_{ts_k} and M'_{ts_k} = force and moment superimposed on restrained separated slab to achieve free movement,
- A_s = cross-sectional area of slab,
- I_s = moment of inertia of slab,
- c = half of depth of slab (+ up or down),
- y_s = distance measured from centroidal axis, and
- F_k and Q_k = interface shear force and moment.

In a similar manner, the final beam strain of a determinate member at any section is the sum of the strain under unrestrained movement and that resulting from equilibrium and compatibility, which, for a beam in plane stress, is

$$\sigma_{xb_k} = -\alpha_b E_b T_{b(y)_k} + (P'_{tb_k}/A_{b_k}) + (M'_{tb_k} y_{b_k}/I_{b_k}) + [-(1/A_{b_k}) + (\bar{d}_k y_{b_k}/I_{b_k})]F_k + (y_{b_k}/I_{b_k})Q_k \quad (2)$$

where b = beam and $\bar{d}_k$ = distance from centroidal axis to top of beam (+).

COMPATIBILITY OF COMPOSITE SECTION

For the original composite structure, compatibility requires that the slab strain and curvature be equal to the beam strain and curvature at the interface.

Equating longitudinal interface strains and simplifying yield

Publication of this paper sponsored by Committee on General Structures.

$$\left\{[n(1-\mu_s^2)/A_s] + 1/A_{b_k} + [n(1-\mu_s^2)c^2/I_s] + (\bar{d}_k^2/I_{b_k})\right\} F_k + \left\{\bar{d}_k/I_{b_k} - [n(1-\mu_s^2)c/I_s]\right\} Q_k = [(P'_{tb_k}/A_{b_k}) - (M'_{tb_k}d_k/I_{b_k})] - n(1-\mu_s^2)[(P'_{ts_k}/A_s) + (M'_{ts_k}c/I_s)] \quad (3)$$

where n = modular ratio E_b/E_s.

Equating curvatures of the slab and the beam at the interface and simplifying yield

$$\left\{\bar{d}_k/I_{b_k} - [n(1-\mu_s^2)c/I_s]\right\} F_k + \left\{1/I_{b_k} + [n(1-\mu_s^2)/I_s]\right\} Q_k = [n(1-\mu_s^2)/I_s] M'_{ts_k} - (1/I_{b_k}) M'_{tb_k} \quad (4)$$

Figure 1. Interface shears and moments on separated slab and beam.

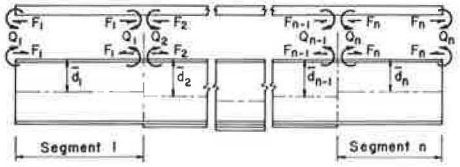

Figure 2. Longitudinal unit stresses resulting from assumed constant temperature gradient in slab and beam.

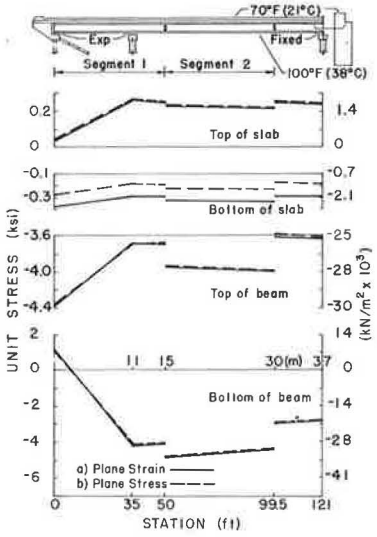

Figure 3. Longitudinal unit stresses resulting from assumed linear temperature gradient in slab and constant gradient in beam.

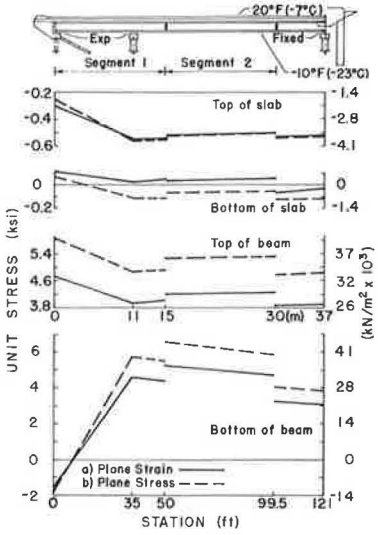

The unknown quantities F_k and Q_k may be obtained by solving equations 3 and 4 simultaneously. The equations are best solved numerically for specific problems.

With F_k and Q_k known, the longitudinal interface stress in a determinate slab and beam may be obtained from equations 1 and 2 respectively. Final slab and beam stresses in an indeterminate member may be found by superimposing equations 1 and 2 with the elastic stresses obtained from the moment and thrust diagram.

EXAMPLE BRIDGE

Variations of stress resulting from thermal loading may be illustrated by applying assumed temperature gradients to a typical four-span, nonprismatic, six-stringer, continuous, four-lane composite highway bridge with expansion rollers except for the center pier. The reference temperature is 21° C (70° F).

Assumed temperature gradients and a comparison of the thermal stresses calculated for the interior girder for (a) plane strain in the slab in the transverse direction and plane stress in the beam and (b) plane stress in both slab and beam by the theoretical method are shown in Figures 2 and 3.

SUMMARY

The procedure presented provides a practical means for considering nonprismatic bridge structures subjected to thermal loading.

The thermal coefficient of expansion for limestone-aggregate concrete has been substantiated by the authors to be approximately $7.2 \times 10^{-6}/°C$ ($4.0 \times 10^{-6}/°F$) and was assumed for the example bridge calculations.

Maximum longitudinal stresses in the slab for the two assumed thermal loadings were 1810 kPa (262 lbf/in^2) for the constant temperature gradients and -3920 kPa (-568 lbf/in^2) for the linear slab and constant beam gradients.

Maximum longitudinal beam stresses were -33 880 and -33 670 kPa (-4910 and -4880 lbf/in^2) by methods a and b for the constant gradients. For the linear slab and constant beam temperature gradients, the maximum longitudinal stresses were 36 360 and 45 130 kPa (5270 and 6540 lbf/in^2) for methods a and b. The actual stresses would probably be between the values of methods a and b, depending on the actual transverse slab restraint. Comparable significant thermal stresses have also been found by other investigators (2, 3, 5).

Although directed toward thermal behavior, the derivations presented are general in nature and may be used to account for other internal effects, e.g., shrinkage strain, provided an equivalent temperature distribution is used.

REFERENCES

1. B. J. Aleck. Thermal Stresses in a Rectangular Plate Clamped Along an Edge. Trans., ASME, Vol. 71, 1949, pp. 118-122.
2. C. Berwanger. Thermal Stresses in Composite Bridges. Proc., ASCE, Specialty Conference on Steel Structures, Engineering Extension Series, No. 15, Univ. of Missouri—Columbia, June 1970, pp. 27-36.
3. C. Berwanger and Y. Symko. Thermal Stresses in Steel-Concrete Composite Bridges. Canadian Journal of Civil Engineering, Vol. 2, No. 1, 1975, pp. 66-84.
4. J. H. Emanuel and others. An Investigation of Design Criteria for Stresses Induced by Semi-Integral End Bents: Phase I—Feasibility Study. Missouri Cooperative Highway Research Program, Univ. of

Missouri—Rolla, Final Rept. 72-9, 1973.
5. Y. N. Liu and W. Zuk. Thermoelastic Effects in Prestressed Flexural Members. Journal of Prestressed Cóncrete Institute, Vol. 8, No. 3, June 1963, pp. 64-85.
6. J. C. Reynolds and J. H. Emanuel. Thermal Stresses and Movements in Bridges. Journal of Structural Division, ASCE, Vol. 100, No. ST1, Proc. Paper 10275, Jan. 1974.
7. W. Zuk. Thermal Behavior of Composite Bridges—Insulated and Uninsulated. HRB, Highway Research Record 76, 1965, pp. 231-253.

Thermal Stress Analysis of Concrete Bridge Superstructures

M. Radolli, M. M. Dillon Ltd., Cambridge, Ontario
R. Green, Department of Civil Engineering, University of Waterloo, Ontario

Only mean temperature changes are generally considered in the design of concrete bridge superstructures. Because of daily changes in both ambient temperature and intensity of solar radiation, temperature differentials also exist in concrete superstructures. These temperature differentials induce stresses throughout the depth of concrete structures, which are generally not included in current design procedures. This paper describes the heat transfer processes that occur between the atmosphere and a concrete superstructure and also the climatic conditions necessary for the development of temperature differentials during both summer and winter. Temperature-time analyses, computed by using a one-dimensional heat flow analysis, indicate that the distribution of temperature throughout the depth of a superstructure is nonlinear and is a function of superstructure depth. Stresses associated with the nonlinear temperature gradients are described. These stresses can be several times those due to live load, especially in continuous systems. The stresses predicted from the idealized distributions are compared to those obtained by using the heat flow analysis. The results indicate that the idealized distributions have limited design value. Simple empirical design expressions are developed for both thermal stresses and curvature. These are based on typical climatic data for summer and winter conditions and can be applied to a variety of cross-sectional superstructure geometries. An example of the stresses induced by thermal loading on a two-span box-girder superstructure is given.

Limited data are available to assist the bridge designer concerned with the stresses induced in a concrete bridge superstructure by heating and cooling effects (1, 2, 3, 4). Current AASHTO specifications include probable temperature ranges to be used in design and generally offer guidance only with respect to expansion and contraction of straight structures. Mean temperature conditions in actual structures can differ appreciably from the ranges suggested (4, 5). No guidance is provided to designers concerned with serviceability problems in deep concrete superstructures where significant temperature differentials are possible. For example, temperature differentials approaching 22°C (40°F) (a frequently specified temperature rise) have been observed between the top and bottom of a deep (1.4-m or 4.5-ft) concrete box girder (6).

Publication of this paper sponsored by Committee on General Structures.

Some bridge design specifications or recommendations do consider differential as well as mean temperature effects (2, 3, 4). German Industrial Standard (DIN) 1072 and British Standard 153 recognize the presence of a temperature gradient through the depth of a bridge superstructure and give design values for gradients in both steel and concrete structures (3). However, little or no guidance is offered regarding the vertical distribution of the temperature differential throughout the depth of a concrete bridge superstructure. Procedures for calculating the forces and stresses induced in the superstructure by such temperature differentials are also lacking.

Why is there concern about temperature gradients in concrete bridge superstructures? Much of the design experience embodied in current specifications is based on the study of structures with both cross-sectional and plan geometries designed and constructed several years ago. The results of these studies may not be typical of superstructures currently designed and constructed. For example, concrete box girder superstructures are a recent innovation, and field observations indicate temperature differentials of more than 22°C (40°F) can exist between the upper and lower flanges of a box girder system (6). This temperature differential gives rise to local stresses that are nearly four times those attributed to full live load. Studies of a two-span prestressed concrete structure have indicated tensile stresses of more than 3450 kPa (500 lbf/in^2) directly above the intermediate support as a result of moderate temperature differentials (7). Such stress values are of importance in the design of prestressed concrete structures where cracking in the absence of live load is undesirable. Further evidence is available where damage has been attributed to thermally induced stresses (8, 9, 10, 11).

HEAT FLOW THROUGH A CONCRETE SUPERSTRUCTURE

The distribution of temperature throughout the depth of a concrete superstructure must be known if the resulting stresses, reactions, and deformations are to be calculated. It has been possible to correlate weather data with the surface temperatures of exposed pavements during heating and cooling cycles (12). However, the in-

fluence of changes in climatic conditions, with both time and location, and the factors controlling the heat gained or lost by a superstructure do not allow the direct application of the results obtained from the study of pavements to concrete superstructures.

An exposed concrete bridge deck is continually losing and gaining heat—from solar radiation, radiation to or from the sky or surrounding objects, and convection to or from the surrounding atmosphere. In the daytime, and especially during the summer, the heat gain is greater than the heat loss, resulting in a temperature increase throughout the depth. During a typical winter night, the converse is true, and the temperature in the superstructure decreases. Heat input typical of a summer day results in positive temperature gradients in the deck in which the top surface is warmer than the bottom. Negative gradients, in which the top surface is cooler than the bottom, result from a net heat loss.

The heat flow processes for typical summer and winter conditions are shown in Figure 1. Because of the poor thermal conductivity of concrete, these processes can result in temperature gradients in a concrete structure and changes in mean temperature.

Large positive temperature gradients occur during a day with high solar radiation, clear skies, a large range of ambient temperature, and a light wind. High mean temperatures, on the other hand, are associated with a high intensity of solar radiation combined with a high, almost constant, ambient air temperature. Negative temperature gradients develop during cooling periods associated with evening conditions. When the mean bridge temperature exceeds the ambient temperature at a particular time, more radiant energy is lost from the exposed top surface of a bridge superstructure than from the sheltered bottom surface.

Weather data suitable for use in a heat flow analysis considering both radiant and convective heat exchange on the upper and lower surfaces of a bridge deck vary with both time and location. Conditions at a given time and position must be considered. Observations for the months of May to August in Toronto indicate that the change in daily ambient air temperature is approximately 10°C (18°F), and the daily intensity of solar radiation on a horizontal surface has a mean value of 23 MJ/m^2 (550 langleys). Consideration of these values leads to the choice of the climatic data shown in Figure 2a as being representative of a day of high-intensity solar radiation and above-average temperature change. Similarly, data representative of a clear, still winter night in January were selected for the heat loss condition (Figure 2b).

Heat flow through a bridge superstructure varies during the diurnal cycle and is a non-steady-state process. Hence, laws governing steady-state heat flow are not applicable to exposed structures, and any analysis of the response of such structures to heat flow must consider the variation of temperature throughout the depth of the structure with time.

A one-dimensional heat flow analysis similar to that used by Emerson (5) was developed, and the resulting partial differential equation was solved by using the finite difference method. The appropriate boundary conditions considered for the heat flow analysis and the material constants assumed for the concrete are given in Table 1.

The assumption of unidirectional heat flow from the exposed surfaces of the concrete superstructure to the interior is not strictly correct. Comparisons with observed and predicted values of temperature (4, 13) indicate good correlation with unidirectional heat flow analyses, notwithstanding small transverse temperature gradients.

The application of the heat flow analysis for the representative climatic conditions (Figure 2) resulted in the temperature distributions shown in Figure 3 for solid slabs of different depths. Temperature distribution is a function of member depth for both winter and summer conditions. For the summer conditions, the surface temperatures are nearly 11°C (20°F) greater than the maximum ambient air temperature, and the temperature distribution is nonlinear for slab depths greater than approximately 30 cm (12 in). The temperature at the mid-depth of 76 and 122-cm (38 and 48-in) sections is not influenced by the exterior heat, and the change in the mean temperature of these sections is small. Winter temperature gradients do not appear to be so severe as those associated with summer conditions. Thus, a slab with a depth of more than approximately 30 cm (12 in) will, when heated or cooled as a consequence of changing radiation and temperature conditions, be subjected to nonlinear temperature distribution.

THERMAL STRESSES

A nonlinear temperature distribution and the strains associated with this gradient lead to some complexities in the computation of stresses. Structural designers do not usually consider the effect of initial strains in the analysis of sections. Figure 4 shows a typical member with an arbitrary cross section and vertical temperature distribution. The temperature varies only in the vertical direction in this analysis. Full restraint is provided to the ends of the member by the moment M and the axial force P.

A member analysis made by assuming that (a) the material is elastic and has temperature-independent properties, (b) plane sections remain plane after bending, and (c) the principle of elastic superposition is valid leads to the following equation for the longitudinal stresses $\sigma_{t,x}$ for a fully restrained member with a nonlinear temperature-induced strain

$$\sigma_{t,x} = - E\alpha\Delta T \tag{1}$$

where

$\sigma_{t,x}$ = longitudinal stress at a fiber located a distance x from the center of gravity,
α = coefficient of thermal expansion,
ΔT = change in temperature, and
E = modulus of elasticity.

The restraining end moment M can be evaluated by

$$M = - \int_{x_1}^{x_2} E\alpha\Delta T\, b_x\, x\, dx \tag{2}$$

and the longitudinal stress associated with this moment $\sigma_{m,x}$ is given by

$$\sigma_{m,x} = x\,(M/I) = -x\left(\int_{x_1}^{x_2} E\alpha\Delta T\, b_x\, x\, dx \Big/ \int_{x_1}^{x_2} b_x\, x^2\, dx\right) \tag{3}$$

where I = moment of inertia.

Similarly the restraining end force P acting on the area A and associated stress $\sigma_{p,x}$ are

$$P = - \int_{x_1}^{x_2} E\alpha\Delta T\, b_x\, dx \tag{4}$$

$$\sigma_{p,x} = P/A = -\left(\int_{x_1}^{x_2} E\alpha\Delta T\, b_x\, dx \Big/ \int_{x_1}^{x_2} b_x\, dx\right) \tag{5}$$

Figure 1. Heat gain and loss processes for (a) summer and (b) winter conditions.

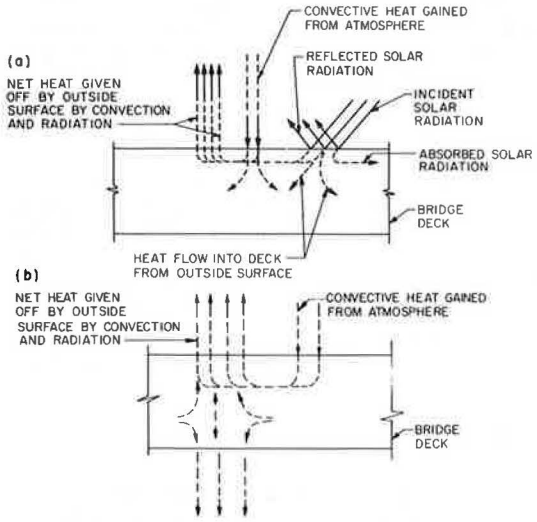

Figure 2. Typical climatic data for (a) high-intensity and (b) low-intensity radiation.

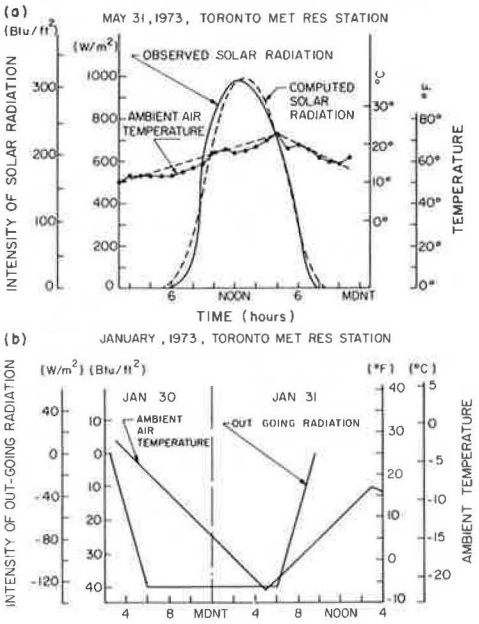

Table 1. Thermal and elastic properties used in one-dimensional heat flow analysis.

Property	Value
Diffusivity, mm^2/s	0.6
Conductivity, W/m·K	13.8
Absorptivity	
Plain concrete	0.5
Bituminous surfacing	0.9
Emissivity	0.9
Specific heat, J	242
Coefficient of expansion	0.000 010 8/°C
Top surface heat transfer coefficient, $W/m^2·K$	
Summer	23
Winter	19
Bottom surface heat transfer coefficient, $W/m^2·K$	
Summer	9
Winter	9
Elastic modulus, GPa	34.5

Note: 1 m^2/s = 10.7 ft^2/s; 1 W/m·K = 0.58 Btu·ft/h·ft^2·°F; 1 J = 0.000 95 Btu; °C = °F/1.8; 1 W/m^2·K = 0.17 Btu/h·ft^2·°F; 1 MPa = 145 lbf/in^2.

Figure 3. Typical temperature distributions during (a) summer and (b) winter.

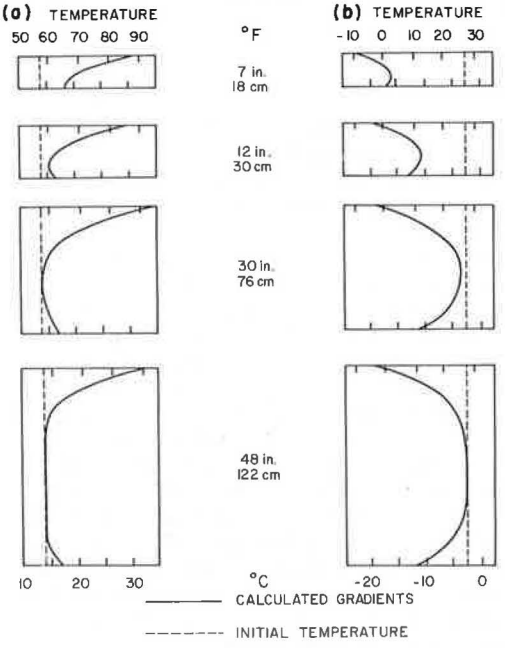

Figure 4. Restrained beam with nonlinear temperature distribution.

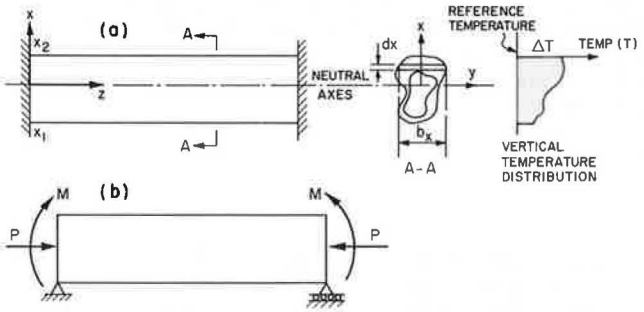

Figure 5. Sectional strains and associated stresses.

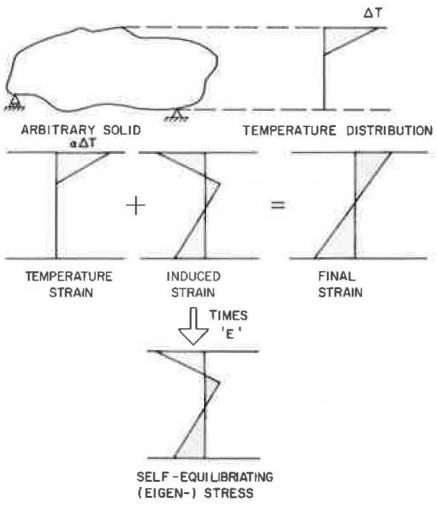

The longitudinal thermal stress σ present in a fiber located a distance x above the center of gravity of a long thin member with no end restraint (13, 14, 15) has the form

$$\sigma_{c,x} = -E\alpha\Delta T - x\,(M/I) - P/A \quad (6)$$

Subtraction of the stresses induced by the restraining forces P and M (equations 3 and 5) leads to equation 6. This latter equation describes the stress state corresponding to a nonlinear temperature gradient in an unrestrained member.

The concept of a stress state in an unrestrained member that is not subjected to external forces may be new for the bridge designer. Reference to Figure 5 may clarify this concept. The nonlinear temperature distribution attempts to induce a nonlinear strain distribution proportional in magnitude to the temperature distribution. Additional strains develop in the section as a consequence of the Euler-Bernoulli hypothesis concerning plane sections. These strains have associated self-equilibrating stresses similar in form to the residual stresses found in fabricated steel members. The self-equilibrating stresses depend directly on the daily heating and cooling cycle and material properties; they do not depend on the support conditions of a structure and, until a satisfactory English-language term is established, will be referred to as eigen stresses.

If the curvature of a member induced by a temperature gradient is restrained by the interior supports of a continuous beam, additional stresses develop. These additional stresses will be referred to as continuity stresses, and the form of the moments and reactions associated with these stresses is shown in Figure 6. The value of maximum thermal continuity stress for the two-span beam is

$$\sigma_{c,z} = {}^3/_2\phi Ec \quad (7)$$

where

$\sigma_{c,z}$ = continuity stress at the support,
ϕ = thermal curvature, and
c = distance to the extreme fiber from the centroidal axis,

and, in general,

$$\sigma_{c,z} = C_1C_2\phi dE \quad (8)$$

where

C_1 = constant developed from the span geometries (1.5 for a two-span system, 1.0 for the interior span of a multispan system),
C_2 = constant developed from the sectional geometry (0.5 for a rectangular section), and
d = member depth.

The total stresses developed in a two-span member for typical summer and winter conditions (Figure 7) consist of both eigen stresses and continuity stresses. As mentioned previously, the eigen stresses are self-equilibrating stresses formed as a consequence of the nonlinear temperature distribution throughout the section depth, and continuity stresses develop because the deflection at point B (Figure 7) is zero. Inspection of the total stress patterns (Figure 7a) indicates that large tensile stresses develop in the web of the member as a consequence of the summer conditions.

Thus, a prestressed concrete member designed for zero tension at support B under dead load plus prestress should be provided with reinforcing steel in the web to cater for these thermally induced tensile stresses. Leonhardt has also noted this requirement based on a simpler analysis (7). Well-distributed steel is required in the flange to cater for the tensile stresses due to the winter condition (Figure 7b).

It is apparent from Figure 6 that summer heating effects change the values of reaction. Some experimental data are available describing reaction change for a three-span bridge, but regrettably values of the intensity of incoming solar radiation were not available (16). Typical values were assumed, and the reaction changes calculated from derived curvature values appear to predict the observed values closely for a day with high solar radiation (18). The observed reaction change results in a moment change of nearly 60 percent of the dead load moment for the double girder three-span structure with spans of 13, 17, and 13 m (44, 55, and 44 ft).

DESIGN CONSIDERATIONS

In the literature, several temperature distributions have been suggested for design (7, 14, 17). The adequacy of these distributions with respect to the prediction of eigen stress and continuity stress values in concrete superstructures does not seem to have been examined previously. Figure 8 shows several suggested temperature distributions. The eigen stresses and curvature values induced by these distributions were computed for summer conditions. It is apparent that the form and magnitude of both the eigen stresses and curvatures are strongly dependent on both assumed temperature difference and temperature gradient. Linear gradients do not induce eigen stresses. Temperature measurements obtained from prototype structures with depths of approximately 1 m (3 ft) correspond most closely to those predicted by a sixth-degree parabola (5). The stresses corresponding to this distribution are very similar in magnitude and distribution to those recommended by Maher, who considers a linear gradient throughout the depth of the top slab of a box girder superstructure (17). The temperature difference (23°C or 40°F) used in the example should be considered as an upper limit (6).

Three representative temperature distributions and the one-dimensional heat flow analysis were used to compute eigen stresses and nondimensional curvatures (ϕd) for various depths of a solid slab. The distributions used and the results obtained are given in Figures 9 and 10. Not all concrete superstructures are solid, and corrections to the analysis for cellular structures are available (18).

Two values of temperature differential (10 and 20°C or 18 and 36°F) were considered for the linear gradient (the Leonhardt gradient). For the Priestley and Maher gradients, a temperature differential of 19°C (35°F) was used. The linear Maher gradient was assumed to extend to 20 cm (8 in) below the surface of the solid superstructure. The sixth-order parabolic distribution suggested by Priestley (14) was used.

Figure 9 shows that the Maher distribution and one-dimensional analysis compare favorably for the prediction of eigen stress values for a wide range of depths. The Priestley distribution appears to have a limited range of applicability, and eigen stresses cannot be predicted by using a linear temperature distribution. The nondimensional curvature versus depth predictions (Figure 10) show that the Maher distribution will overestimate curvature compared to the one-dimensional analysis for shallow members; the Priestley distribution applies only to member depths of between 0.75 and 1.0 m (30 to 40 in), and the Leonhardt distribution is indepen-

Figure 6. Restrained curvature of a member with (a) no temperature gradient, (b) induced curvature, (c) applied loading, and (d) final moments and reactions.

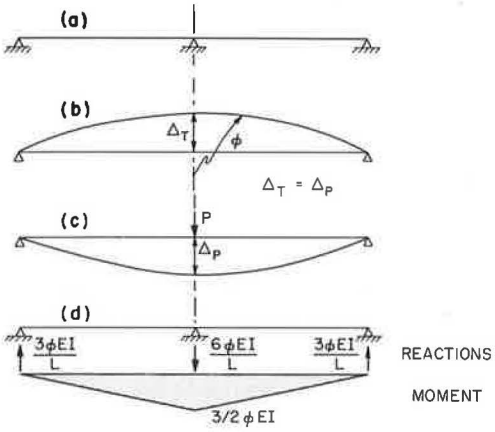

Figure 7. Two-span beam under (a) summer and (b) winter conditions.

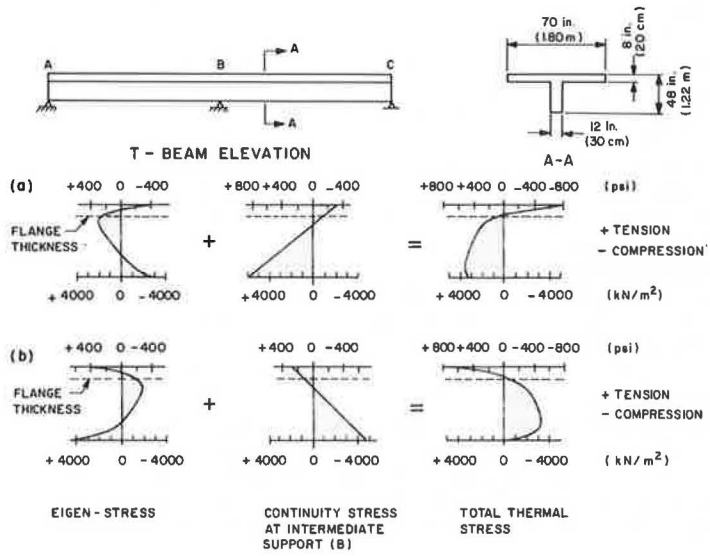

Figure 8. (a) Temperature distributions and resulting (b) eigen stresses and (c) curvature values.

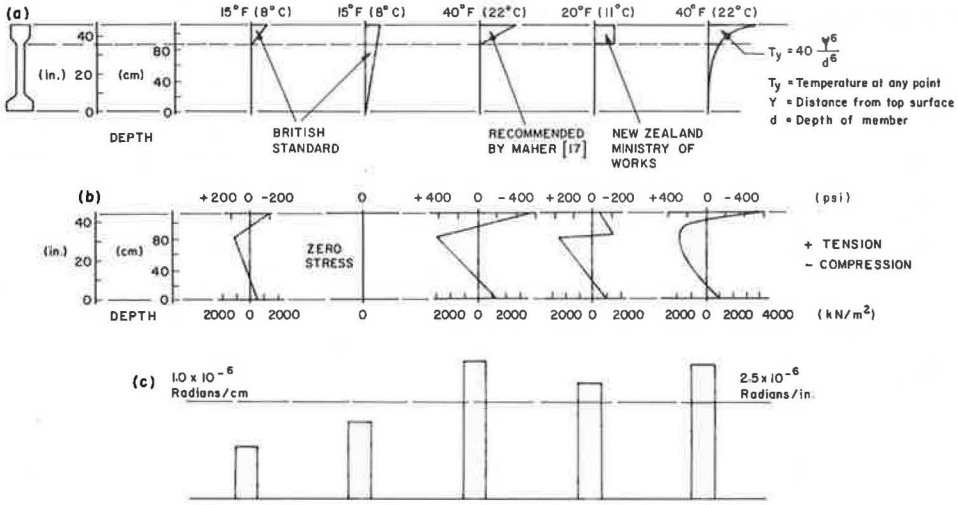

Figure 9. Eigen stress comparisons for various distributions and depths.

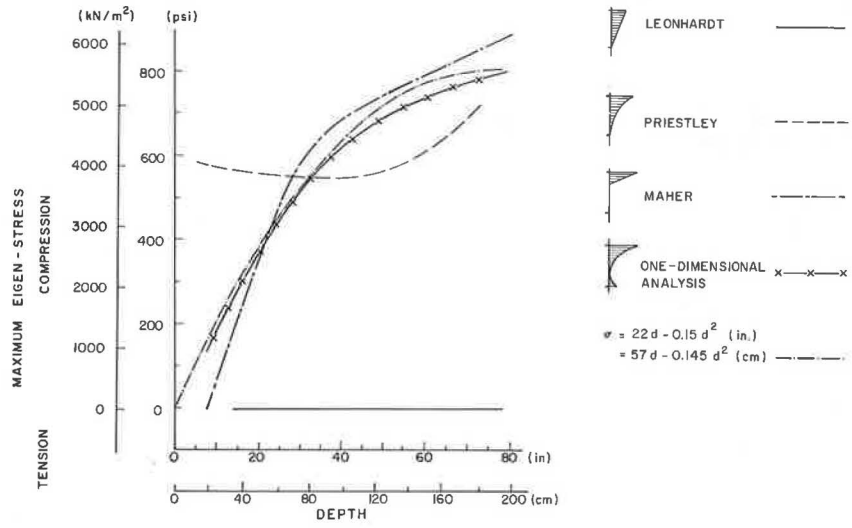

dent of member depth, contrary to the Maher and one-dimensional analysis predictions.

For design purposes, the calculation of the eigen and continuity stresses associated with a given temperature distribution would be tedious. Simple empirical design expressions were developed from Radolli's analyses (18) for use as first approximations in design. The results for summer heating conditions are given in Figures 9 and 10 and allow calculation of both eigen stresses and nondimensional curvature for various depths of slab with relative ease. For depths less than 50 cm (20 in), the nondimensional curvature is assumed to be constant. These expressions are based on climatic conditions for Toronto and are therefore valid for locations of similar climate.

Figures 9 and 10 can be used to predict values associated with winter conditions. It was found that eigen stress values for winter heat flow conditions are nearly identical to the values for summer conditions but of opposite sign; also curvature values are of the opposite sign and are only 60 percent of the summer values. Thus, one set of simple calculations can be used to obtain the stress values associated with thermal loading for both summer and winter conditions.

The results presented apply to a variety of cross-sectional geometries including cellular and T-beam sections (18, 19). Variations in material properties and heat transfer coefficients will influence stress values. However, the changes in the stress values for a wide range of properties and coefficients were found to be within 25 percent of the values presented here (18).

Figure 10. ϕd for various distributions and depths.

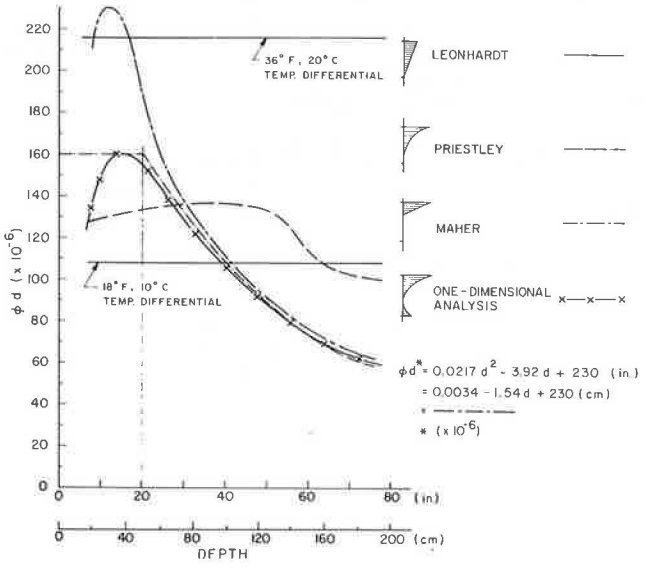

Figure 11. Observed and computed temperature gradients during (a) summer and (b) winter.

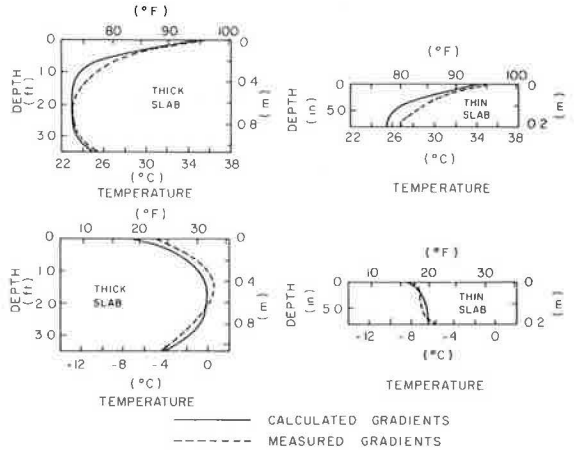

DISCUSSION OF RESULTS

The analyses and results presented for stress are based in part on a one-dimensional heat transfer analysis for a solid slab. A comparison of measured and computed temperature values (Figure 11) confirms the general validity of the analysis.

The effect of thermal loadings associated with summer conditions on the design stress envelopes for typical concrete bridge superstructures has been discussed (19). Figure 12 provides an example of the stresses developed in a two-span posttensioned box girder as a consequence of winter cooling conditions. Surface tensile stresses develop throughout the length of the structure as a consequence of the nonlinear temperature distribution. These tensile stresses influence both the span and support regions of the structure. The serviceability of such a box girder structure could well be affected if additional bonded reinforcing steel is not added for crack control in zones of high tensile stress.

Thermal loadings will not affect the overall strength

Figure 12. Stresses in a box girder bridge: (a) bending moment due to thermal load, (b) total thermal stress, (c) live load and impact stress, and (d) total working stress.

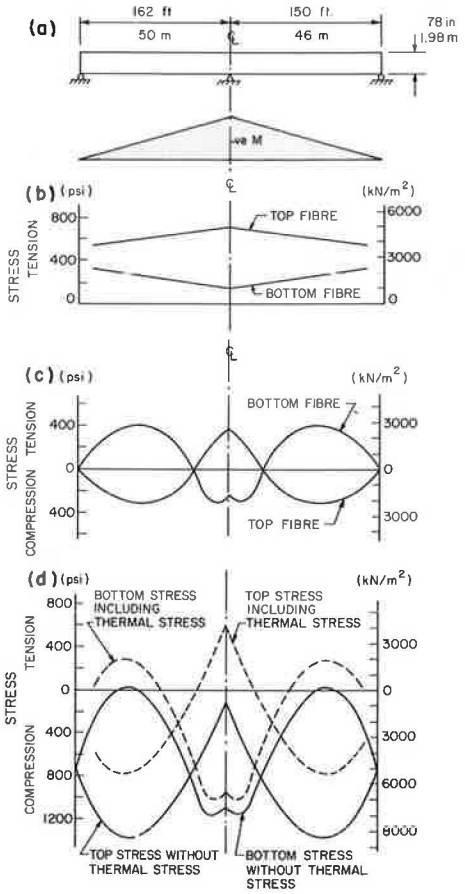

of a continuous superstructure inasmuch as failure of the superstructure will result in a release of the restraints causing thermal stresses. However, heating and cooling of the structure during a normal diurnal cycle combined with lifetime creep and shrinkage must be considered in the serviceability analysis of concrete superstructures.

CONCLUSIONS

Significant flexural stresses are developed in concrete bridge superstructures as a consequence of the heating or cooling of concrete—a material of relatively poor thermal conductivity. Nonlinear temperature gradients develop during a daily heating or cooling cycle. These gradients lead to both eigen and continuity stresses. Simple design formulas are developed that allow the prediction of these stresses and do not require a knowledge of the temperature gradient.

Thermal loading of a superstructure is a serviceability problem and should be so considered. Proportioning of reinforcement in a concrete bridge superstructure should reflect the stress-inducing thermal effects.

ACKNOWLEDGMENTS

The work was carried out with the support of the Transportation Development Agency of Canada, the National Research Council of Canada, and the Department of Civil Engineering, University of Waterloo. This support is gratefully acknowledged.

REFERENCES

1. Standard Specifications for Highway Bridges, Eleventh Ed. AASHO, Washington, D.C., 1973.
2. Design of Highway Bridges. Canadian Standards Association, Rexdale, Ontario, CSA Standard S6-1974, 1974.
3. D. J. Lee. The Theory and Practice of Bearings and Expansion Joints for Bridges. Cement and Concrete Association, London, 1971.
4. M. Emerson. Bridge Temperation and Movements in the British Isles. U.K. Road Research Laboratory, Crowthorne, Berkshire, England, RRL Rept. LR228, 1968.
5. M. Emerson. The Calculation of the Distribution of Temperature in Bridges. U.K. Transport and Road Research Laboratory, Crowthorne, Berkshire, England, TRRL Rept. LR561, 1973.
6. H. Bosshart. Thermal Stress in Prestressed Concrete Bridges. Symposium on Design of Concrete Structures for Creep, Shrinkage and Temperature Changes, Madrid, Final Rept., Vol. 6, 1970, pp. 73-80.
7. F. Leonhardt and W. Lippoth. Folgerungen aus Schäden an Spannbetonbrücken. Beton-und Stahlbetonbau, Vol. 65, No. 10, Oct. 1970, pp. 231-244.
8. J. N. Deserio. Thermal and Shrinkage Stresses—They Damage Structures! ACI, Detroit, Publ. SP27, 1971, pp. 43-49.
9. T. Monier. Cases of Damage to Prestressed Concrete. Heron, Vol. 18, No. 2, 1972.
10. K. H. Weber. Causes of Crack Formation Near Intermediate Supports of Continuous Prestressed Concrete Beams and Their Limitations to Allowable Crack Width. Univ. of Stuttgart, dissertation, 1967.
11. R. D. Larrabee, D. P. Billington, and J. F. Abel. Thermal Loading of Thin-Shell Concrete Cooling Towers. Journal of Structural Division, Proc., ASCE, Vol. 100, No. ST12, Dec. 1974, pp. 2367-2382.
12. E. S. Barber. Calculation of Maximum Pavement Temperature From Weather Reports. HRB, Bulletin 168, 1957, pp. 1-8.
13. W. I. J. Price and R. G. Tyler. Effects of Creep, Shrinkage and Temperature on Highway Bridges in the United Kingdom. Symposium on Design of Concrete Structures for Creep, Shrinkage and Temperature Changes, Madrid, Final Rept., Vol. 6, 1970, pp. 81-93.
14. M. J. N. Priestley. Effects of Transverse Temperature Gradients on Bridges. New Zealand Ministry of Works, Central Laboratories, Rept. 394, Oct. 1971.
15. R. Hoyle. Plane Strain and Plane Stress. In Thermal Stress, Pitman and Sons, London, 1964, pp. 43-51.
16. N. Krishnamurthy. Temperature Effects on Continuous Reinforced Concrete Bridges. Alabama Highway Research, HPR Rept. 58, July 1971.
17. D. R. H. Maher. The Effects of Differential Temperature on Continuous Prestressed Concrete Bridges. Institution of Engineers, Australia, Civil Engineering Trans., Vol. CE12, No. 1, Paper 273, April 1970, pp. 29-32.
18. M. Radolli. Thermal Stresses in Concrete Bridge Superstructures. Univ. of Waterloo, Ontario, MASc thesis, March 1975.
19. M. Radolli and R. Green. Thermal Stress in Concrete Bridge Superstructures Under Summer Conditions. TRB, Transportation Research Record 547, 1975, pp. 23-36.

Lateral Buckling of Pony Truss Bridges

P. Csagoly and B. Bakht, Research and Development Division, Ontario Ministry of Transportation and Communications

At one time, low or pony truss bridges were popular for their economy and ease of construction. With the tremendous increase in commercial vehicle weights, especially after World War II, the load-carrying capacity of these bridges became suspect, and many were taken out of service or replaced by modern structures. An ultimate load test carried out by the Structural Research Section of the Ontario Ministry of Transportation and Communications on a pony truss bridge in 1969 indicated that these bridges possess an inherent strength that far exceeds the value predicted by elementary structural theories. The complex problem of lateral buckling of truss compression chords, which in the past has led to oversimplifying assumptions resulting in underestimation of the bridge strength, has been solved by a computer program based on a modified version of Bleich's method. The program, whose validity has been checked against experimental results, will provide bridge engineers with a better assessment of the load-carrying capacity of pony truss bridges than has been possible in the past. Since there are several hundred pony truss bridges in Ontario alone, it is economically important to determine the extent to which these bridges can usefully serve their purpose.

Low truss bridges that have horizontal wind bracings at the deck level only are usually referred to as pony truss bridges (Figure 1). Now that more efficient modes of construction are available and given the emphasis on aesthetics, steel pony truss bridges might not be constructed in the future. However, there are several hundred pony truss bridges in Ontario and possibly many thousands throughout North America. Most of these bridges are still serving as important traffic carriers on secondary highways and county roads. The increase in the volume of traffic and the weight of commercial vehicles makes it necessary to review the serviceability of the existing pony truss bridges by evaluating their load-carrying capacity. In the present economic environment, the structural strength of a bridge must be fully investigated before a decision is made on whether it should be replaced.

The weakest component of the pony truss bridge is usually the top chord of one of its trusses; for lateral stability these compression members depend on their own stiffnesses and the elastic restraints offered by the web members of the trusses.

This paper presents a method for investigating the lateral stability of pony truss bridges on a more rational basis than has been attempted in the past. The method is an iterative one that takes into account the secondary stresses caused by change in the geometry of the structure due to loading.

METHOD OF ANALYSIS

The problem of lateral instability of the compression chord of a pony truss is essentially that of a beam-column elastically restrained at discrete points. This problem has caught the attention of engineers since the turn of the last century (1, 2, 3, 4). It was Bleich (5, 7) who first solved the problem of stability of a beam-column that has varying sectional properties, is subjected to varying axial loads, and has discrete elastic supports with random spacings. The method is briefly outlined below.

For a pony truss (Figure 2a) with n number of panels, (n - 1) compatibility equations relating moments and beam stiffnesses and (n - 1) equilibrium equations relating moments, deflections, and elastic restraints offered by the transverse portals can be written for (n - 1) intermediate panel points. The very ends of the chord are assumed to be hinged. Thus, together with the assumed end conditions of the end moments being equal to zero, a total of 2n equations can be written from which the (n - 1) unknown moments and (n + 1) unknown deflections can be found for any stable condition of the top chord. For the top to be in an unstable condition, one of the unknown moments and deflections should have an infinite value. Such a condition would result in (n - 1) solutions of which the solution associated with the minimum load would give the critical buckling load for the truss.

Bleich's method ignores the fixity of the ends of the compression chord against rotation and does not account for the discontinuity in the direction of the compression chord, which is a common feature in North American pony truss bridges; the theory had to be modified to con-

Publication of this paper sponsored by Committee on Steel Bridges.

Figure 1. A typical pony truss bridge.

Figure 2. (a) European pony truss used in Bleich's thesis and (b) American pony truss with the numbering system used.

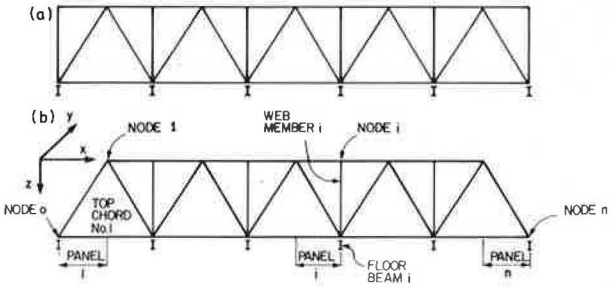

Figure 3. Deflected shape of transverse portal frame.

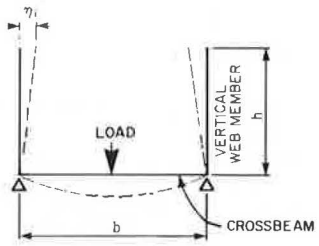

Figure 4. Deformation of a panel length of compression chord on the horizontal plane.

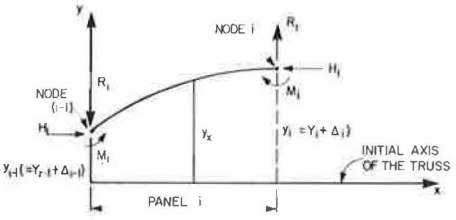

Figure 5. Moments at left shoulder node.

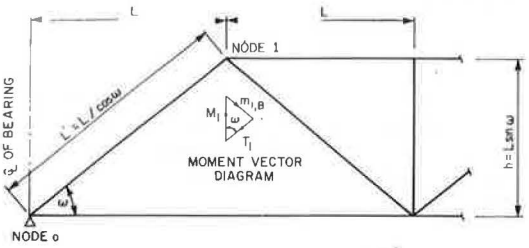

sider these aspects. Bleich's theory was also modified to include live load deflections of the panel points at the interface of the compression chord and the vertical members of the transverse portals. This modification enabled the solution to be obtained for any loading condition, and reduced the solution from that of stability to theory of second-order stresses. Smallest value of the applied load that caused the stress, anywhere along the chord, to exceed the yield stress of the material was regarded as the critical load for the chord.

Derivation of the modified set of equations, which were to be solved by using a computer, was based on the following assumptions.

1. The two trusses are of constant height, and their distance apart is also constant;
2. The lateral restraints offered by the diagonal web members are negligible;
3. The torsional rigidities of the compression chords, which are formed from open sections, are small and can be ignored;
4. The modulus of elasticity and yield stress of steel are constant;
5. Panel lengths are identical; and
6. Vertical members of the transverse portals have uniform flexural stiffness.

Although a solution based on the modified method of analysis can easily be formulated without any of those restrictions, the restrictions were included to avoid unnecessary generality. For brevity, many steps of derivation leading to the resulting equations are omitted. Detailed formulations can be found elsewhere (6).

Notation

The notation used in the equations is defined below.

A_i = function relating to panel i, as defined by equation 7;
a_i = cross-sectional area of the top chord of panel i;
B_i = function relating to panel i, as defined by equation 7;
$2b$ = distance between the centerlines of the two trusses of the bridge;
D_i = lateral rigidity of the transverse portal frame at node i, defined as the force to cause a unit displacement of the top chord node;
$d_{i,m}$ = distance between nodes i and m, measured along x;
E = modulus of elasticity;
$F_{i,1}$, $F_{i,2}$, $F_{i,3}$ = transcendental functions defined by equation 9;
G = shear modulus;
H_i = axial force in chord member of panel i, in the direction of longitudinal axis of the truss;
h = height of the truss;
I_{bi} = moment of inertia of the floor beam at node i;
I_{hi} = moment of inertia of the portal column at node i (or equivalent inertia if the column has non-uniform moment of inertia);
I_i = moment of inertia of the compression chord of panel i, about Y-axis;
J_i = torsional inertia of the compression chord of panel i
K_i = torsional rigidity of the compression chord of panel i
$= GJ_i$
L = length of truss panel;
L' = length of the inclined end member;

M_i = lateral moment acting at node i on the compression chord;
M_x = lateral moment acting on the compression chord at a distance X from the left node of the panel under consideration;
$M_{i,A}$ = lateral moment acting at the left end of the compression chord of panel i;
$M_{i,B}$ = lateral moment acting at the right end of the compression chord of panel i;
n = number of panels in truss;
P = concentrated load acting on cross beam;
R_i = lateral force in top chord member at node i;
S_i = section modulus of the compression chord of node i;
T_1 = torsion in left inclined compression chord;
V_L = left-hand reaction of the truss in lateral direction;
V_R = right-hand reaction of the truss in lateral direction;
V_x = shear force, in Y-direction, at a distance X from the left node of the compression chord of panel i
X = distance of a point from the left node of the panel under consideration;
Y_i = lateral deflection of node i with respect to the specified initial position of the node;
y_i = total lateral deflection of node i with respect to the original axis of the truss;
$\alpha_i, \beta_i, \gamma_i$ = functions relating to panel i and defined by equation 5; and
Δ_i = initial lateral deflection of node i (that prior to the application of load), with respect to the original axis of the truss.

Lateral moment is the moment associated with displacements in the Y-direction, where two horizontal members meet at node i.

Characteristics of Portal Frames

The transverse portal frame, which provides the elastic restraint to the compression chord, is formed from two outstanding vertical members rigidly connected to floor beams, as shown in Figure 3. The rigidity of the portal frame is calculated on the assumption that the ends of the beam are restrained against relative vertical movement. Under loading, the top ends of the vertical, which restrain the movement of the compression chord, deflect inward. If at node i, Y_i is the deflection of the compression chord and η_i is the displacement of the node due to flexure of the floor beam, the resulting lateral force R_i is given by

$$R_i = D_i(Y_i - \eta_i) \tag{1}$$

where D_i is the rigidity of the idealized portal frame shown in Figure 3. It is given by the following relationship:

$$D_i = EI_{bi}/h^2\,[b + (hI_{bi}/3I_{hi})] \tag{2}$$

The value of the inward movement of the top of the portals can be obtained from elementary statics. For example, the value of the inward movement η_i for a portal loaded with a simple concentrated load P, as shown in Figure 3, is given by

$$\eta_i = (Phb^2/4EI_{bi}) \tag{3}$$

Compatibility Equation

A total of (n - 3) compatibility equations are obtained for nodes 2 through (n - 1) as follows:

The flexural behavior of the chord in horizontal plane, as shown in Figure 4, is given by

$$H_iY_x + M_{i-1} + M_i - H_iY_{i-1} + R_iX = EI''_{yx} \tag{4}$$

By introducing

$$\alpha_i^2 = (H_i/EI_i) \quad \gamma_i^2 = (M_{i-1}/EI_i) \quad \beta_i = (R_i/EI_i) \tag{5}$$

the solution of equation 4 is given by

$$Y_x = A_i\sin\alpha_iX + B_i\cos\alpha_i \times X + Y_{i-1} - (\gamma_i^2/\alpha_i^2) - (\beta_iX/\alpha_i^2) \tag{6}$$

where the expressions for A_i and B_i are found from the boundary conditions:

$$A_i = (M_i - M_{i-1} \times \cos\alpha_iL)/(H_i \times \sin\alpha_iL) \quad B_i = (M_{i-1}/H_i) \tag{7}$$

The slope at a point is given by the first differential of the right side of equation 6 with respect to x.

By equating the slopes at the common node of two adjacent panels, the following typical compatibility equation is obtained.

$$\begin{aligned} &Y_{i-1} - 2Y_i + Y_{i+1} - (F_{i,2}/H_iF_{i,3})\,M_{i-1} - (F_{i-1}/H_iF_{i,3}) \\ &\quad + \left\{[G_{(i+1),1}/H_{i+1}F_{(i+1),3}]\right\} M_i - [G_{(i+1),2}/H_{i+1}G_{(i+1),3}]^{M_{i+1}} \\ &\quad = -\Delta_{i-1} + 2\Delta_i - \Delta_i + 1 \end{aligned} \tag{8}$$

where

$$\begin{aligned} F_{i,1} &= G_{i,1} = \sin\alpha_iL - \alpha_iL\cos\alpha_iL \\ F_{i,2} &= G_{i,2} = \alpha_iL - \sin\alpha_iL \\ F_{i,3} &= G_{i,3} = \sin\alpha_iL \end{aligned} \tag{9}$$

Equation 8 is not valid for nodes 1 and (n - 1), the shoulder nodes. On the assumption that both the torsion and moment act on the inclined member but that there is no resultant torsion in the horizontal members (Figure 5), the following compatibility equation is obtained for node 1, the left shoulder node.

$$\begin{aligned} &Y_1\,(1 + \cos^2\omega) - Y_2 - [(\cos^2\omega F_{1,2}/H_1F_{1,3})\,m_{1,A}] \\ &\quad + [(h^2\cos\omega/GJ) + (F_{1,1}\cos\omega/H_1F_{1,3}) - (G_{2,1}/H_2G_{2,3})]\,M_1 \\ &\quad - (G_{2,2}/H_2G_{2,3})\,M_2 = 0 \end{aligned} \tag{10}$$

Equation 10 can be easily adapted for node (n - 1).

Boundary Conditions

By equating the expression for slope at the left end of chord 1, obtained by differentiation of the right side of equation 6, to zero, the equation for the boundary condition is

$$Y_1 + \Delta_1 + (F_{1,1}/H_1F_{1,3})\,m_{1,A} + (F_{1,2}\cos\omega/H_1F_{1,3})\,M_1 = 0 \tag{11}$$

Similarly, an equation for the boundary condition at node n can be obtained.

Equilibrium of Lateral Forces

If we assume that there are no external forces acting on the compression chord, the only lateral forces are those resulting from the interaction of the compression chord and the vertical members of the portal.

Shear force is given by

$$V_x = -EI''''_Y \tag{12}$$

Differentiating equation 4 three times with respect to x and substituting it in equation 12 yield

$$V_L = [\alpha_1 L/\sin(\alpha_1 L)]\ [M_1 \cos\omega - m_{1,A}\cos(\alpha_1 L)/L] \quad (13)$$

The equation for V_R can be similarly formed.

The reaction at node i, due to the interaction of the portal and the compression chord, is given by equation 1. From equations 1 and 3, the following equation for the equilibrium of forces can be obtained.

$$-V_L + \sum_{i=1}^{n} D_i (Y_i - \eta_i) + V_R = 0 \quad (14)$$

Nonlinear Equilibrium Equations

Lateral forces at the interface of the compression chord and the portals change with the lateral deflection of the chord; so do the lateral moments caused by the axial forces. The equilibrium equations, which are necessarily nonlinear in nature, can be formed by equating the moments due to forces on one side of a node to the nodal moment. M_0 in terms of $M_{1,A}$ and $m_{1,A}$ is given by

$$M_0 = m_{1,A}\cos\omega + M_1 \sin^2\omega \quad (15)$$

Taking the moment of forces to the left of node i and equating it to M_i yield

$$-M_i - M_0 - V_0 d_{i,1} + \sum_{n=1}^{i-1} (H_{m+1} - H_m)(Y_i - Y_m) + H_1 Y_i$$

$$+ \sum_{m=1}^{i-1} D_m (Y_m - \eta_m) d_{i,m} = 0 \quad (16)$$

Substituting the expression for V_L and M_0 from equations 13 and 15 respectively and replacing y_i by $(Y_i + \Delta_i)$ from (n - 2) equilibrium equations, in terms of the unknown nodal displacements and moments, for nodes 2 through (n - 1).

SOLUTION

The equations thus formed are solved for the unknown displacements and moments at a given load level. From the nodal moments, the maximum moments and stresses between the nodes are calculated. If none of the members is stressed to the yield limit, the load is increased in steps, and the whole process of forming and solving the equations and calculating the maximum stress within the compression chord is repeated until the stress somewhere in the chord reaches the yield limit. This load is regarded as the maximum load that the truss can carry.

Description of Computer Program

Implementation of the method of analysis was only possible by using a computer. A computer program was developed for this purpose in standard ANSI FORTRAN (and partly in Assembly for the IBM 360 version); it is named LATBUK. The program is available on request from the Engineering Research and Development Branch of the Ontario Ministry of Transportation and Communications.

A step-by-step increment of the specified initial load to reach the lateral buckling load would have consumed a lot of computer time in most of the cases, especially when the initial load was a low guess. A search technique in which the solutions converge within 12 iterations almost irrespective of the initial load was used in the program. The technique consists basically of giving a large increment to the specified initial load and then iterating by either decreasing or increasing the load by an amount equal to half the previous step. The iterations are continued until the critical load within the accuracy of specified load increment is reached. The process is shown in Figure 6.

Validity of the Method of Analysis

For checking the validity of the program and the method of analysis, a Perspex model of a pony truss bridge with six panels and two transverse portals was constructed and tested for various loading conditions. The model was constructed from a 10-mm-thick (0.4-in) Perspex sheet. The dimensions and details of the model are shown in Figure 7. The model was used only to validate the prediction of the lateral deflections by the program.

The program assumes that the top chord is laterally supported only at the interface of the portal column and the top chord. This assumption, although valid in actual bridges, does not hold in the model, especially at the middle node where the diagonals join the chord. The truss was carved from a single sheet of Perspex. Because of the continuity of the members, the middle node was offered some lateral restraint by the inclined members, which at their lower ends were partly restrained against rotation through the portal and truss connection.

To account for the restraint at the middle node, a fictitious portal was placed at the center of the truss in the analysis by the program. The columns of the portal were given the stiffness offered by the two inclined members. One-quarter of the stiffness of the actual transverse beams was arbitrarily apportioned to the beam of the fictitious portal.

Some of the comparisons of the lateral deflections of the top chord as given by the model test and the program are shown in Figure 8. Given the fact that the model was not an exact idealization of a typical pony truss bridge for which the program is written, the program results compare well with experimental results.

The model test ensured that the program can correctly calculate the lateral deflections of the top chord for various loadings. The acid tests for the validity of the program were, however, provided by the test on an existing pony truss bridge and an accidental failure of another. The load test was carried out in 1969 on a bridge close to Exeter, located on the boundary of Perth and Middlesex in Ontario.

The Exeter Bridge consisted of two pony trusses spanning 15.2 m (50 ft). The trusses had eight panels each and were 4.6 m (15 ft) apart. A view of the bridge with the test loads is shown in Figure 9.

The program predicted a failure load of 721 kN (162 000 lbf) for the bridge. In the test the bridge failed through the buckling of one of the top chords under a load of 623 kN (140 000 lbf). The concrete blocks (44.5 kN or 10 000 lbf each) were placed off-center 152 mm (6 in) toward the instrumented truss. The equivalent central load is on the order of 667 kN (150 000 lbf). Furthermore, to ensure the safety of testing personnel, the blocks were always dropped from a height of 25 mm (1 in) to create an impact that would trigger the failure at the critical load. The actual capacity of the bridge was slightly more than 667 kN (150 000 lbf) for a central load position. Inasmuch as the calculated properties of the bridge could not have been exact, the correlation between the predicted failure load and the actual failure load seemed almost fortuitous. Later, anaother opportunity to test the validity of the program was provided by an accidental failure of the Holland Road Bridge at Thorold. This pony truss bridge failed on October 26, 1972, when a three-

Figure 6. Search technique for fast convergence.

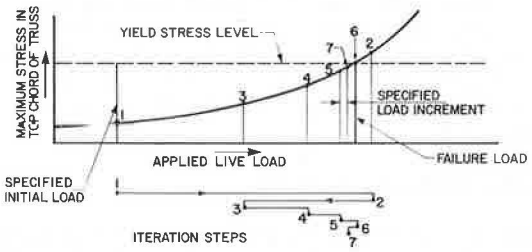

Figure 7. Details of the pony truss bridge model.

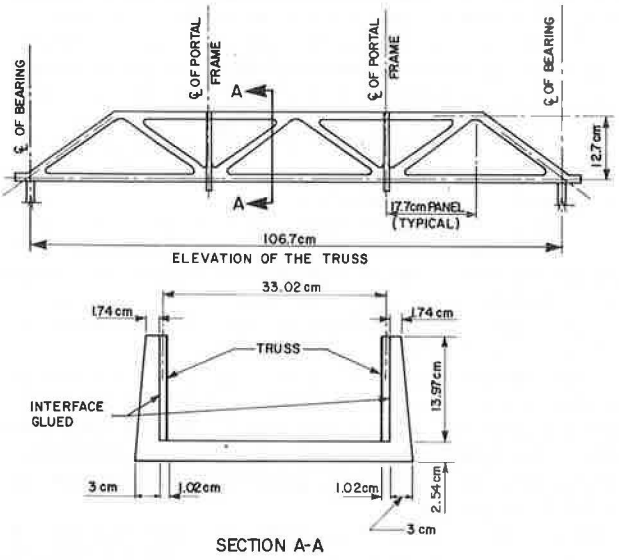

Figure 8. Lateral deflections of the top chord for truss shown in Figure 7.

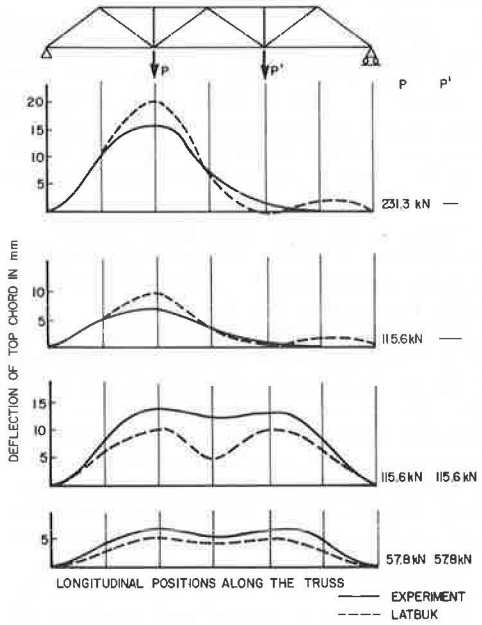

axle tandem truck passed over it. The truck was reported to weigh 20.7 Mg (457 000 lb). The bridge was analyzed by the program for various longitudinal positions of the vehicle. The smallest failure load of the vehicle given by the program was 200 kN (45 000 lbf). There seemed little doubt that the program can predict realistic values of the failure loads for the top chords of pony trusses.

Figure 9. A pony truss bridge with test loads.

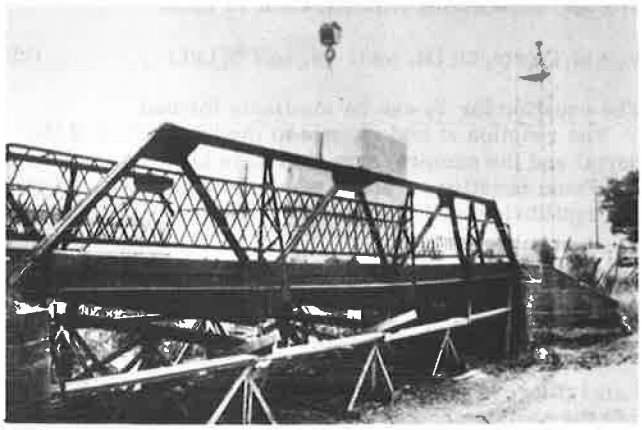

CONCLUSIONS

The behavior of the compression chord of a pony truss cannot be predicted intuitively or by simple hand calculation. Based on the proposed method of analysis, which accounts for the interaction of the compression chord and the transverse portals and for the change of direction of the chord at the shoulder points, a computer program has been written. Comparison of the program results to those of model and full-scale tests has proved the validity of the method. The program can now be used to check the load-carrying capacity of the many existing pony truss bridges before their replacement is contemplated.

REFERENCES

1. E. Engesser. Die Sicherung offener Brucken gegen Ausknichen. Zentralblatt der Bauverwaltung, 1884, p. 415.
2. F. S. Jainski. La flexion des pieces comprimees. Annales des Ponts et Chausees, 2nd Part, 1894, p. 233.
3. H. Muller-Breslau. Die graphische Statik der Baukonstruktionen. Vol. II-2, A. Kroner, Leipzig, 1809.
4. H. Zimmermann. Die Knickfestigkeit der Druck gurte offener Brucken. W. Ernst und Sohn, Berlin, 1910.
5. F. Bleich. Die Knickfestigkeit elasticher stabverbindungen. Der Eisenbau, Vol. 10, 1919.
6. P. F. Csagoly, B. Bakht, and A. Ma. Lateral Buckling of Pony Truss Bridges. Ontario Ministry of Transportation and Communications, Research Rept. 199, 1975.
7. F. Bleich. Buckling Strength of Metal Structures. McGraw-Hill, New York, 1952.

Design Traffic Loads on the Lions' Gate Bridge

Francis P. D. Navin, James V. Zidek, and Caroline Fisk, University of British Columbia, Vancouver
Peter G. Buckland, Buckland and Taylor Ltd.

During the first major renovation of the Lions' Gate Bridge joining Vancouver, British Columbia, to its northern suburbs, there was evidence of deterioration due to the corrosive sea atmosphere. Because traffic loads have increased, both in volume and in mass, since the bridge was built, a set of analytical equations and a computer simulation were developed to estimate the vehicle traffic load on the bridge. The analytical formulation handles the critical vehicle load as a function of the bridge and approach lengths, the number of lanes, the percentage of cars, buses, and trucks in each lane, the number and severity of stoppages, the weight distribution of trucks, and the return period for the critical load. The simulation includes additional factors such as the trickling of vehicles past a stoppage, the time of day and day of the week of the stoppage, the location on the bridge or approach of the stoppage, the stopped lane or lanes, and the duration of the stoppage. The application of these two approaches using traffic data observed on the Lions' Gate Bridge gave practically the same vehicle load per unit length. The resulting design loads were considerably less than those suggested by Ivy and coworkers or Asplund and quite similar to those used in the original analysis.

The Lions' Gate Bridge is an 830-m, three-lane suspension bridge connecting Vancouver, British Columbia, to its northern residential and commercial suburbs and carries approximately 60 000 vehicles per day. The bridge spans a navigational channel 365 m wide and is 1524 m long. The center span is 472.4 m and the two side spans are each 187 m long. A 915-m concrete roadway having three 2.9-m-wide traffic lanes forms the causeway from the Vancouver city center to the bridge. The northern ramp of the suspension bridge is a series of standard truss sections supported on steel columns. Built in 1937-38 by a private land developer, the bridge has been subjected to a corrosive saltwater atmosphere for 37 years and increasingly heavier vehicle loads, particularly of buses and trucks. This study was conducted to confirm the validity of the original traffic loading and to set the legal load limit for heavy vehicles using the crossing.

The validity of the original traffic loading was rather important because the loads were considerably less than any suggested in the available literature, such as the American Association of State Highway Officials (1) or the Canadian Standards Association (2) loads. Further review (3, 4) indicated that no general formula or analytical procedures existed to help designers set the traffic loads on long span bridges. The commercial interests using the bridge for trucking were particularly concerned about the legal load limit because the only other bridge crossing is approximately 8 km to the east.

Vehicle traffic was simulated in the study for two reasons:

1. Early attempts at an analytical solution were not encouraging, and it was fairly certain that an acceptable answer could be obtained by simulation; and
2. The results of the simulation could be used to check an analytical solution if one could be found.

The development of the computer simulation, the simulator, the analytical solution, and a comparison of the results of the two methods are described below.

TRAFFIC LOADING PARAMETERS

The aim of the study was to estimate the maximum traffic load on any general loaded length of bridge with a given return period. The selection of simulation variables was based on the criteria of importance and availability of data. For the simulation, information was needed on

1. The vehicle—weight and length;
2. The bridge—location of stoppage, number of lanes blocked, and direction of center lane;
3. Stoppage—type of event, time to clear event, and time of stoppage by hour and day; and
4. Traffic flow—vehicle mix, maximum vehicle flow by hour and day, spacing of vehicles when stopped and when moving, and speed of moving lanes.

Some of this information was collected by the British Columbia highway department and some by the bridge patrol. Some was supplied through traffic counts (6), and some was estimated.

The distribution of vehicle weights on the bridge was

Publication of this paper sponsored by Committee on Steel Bridges.

a critical component in the study. The weight of cars and buses was set at 1360 and 13 600 kg respectively. Truck weights were found to follow a gamma distribution having a mean of 0.7 registered gross vehicle weight (GVW). The traffic weight was a function of the length of vehicles and their spacing. The length of buses and trucks with a GVW of more than 5400 kg was set at 12 m (5), and all others were set at 5 m. The speed-spacing relationship was determined by experiments on the bridge. Control vehicles were driven at constant predetermined speeds across the bridge, and from time-lapse photographs the following empirical relationship between vehicle density and speed was found:

$$D = 1.6/[\bar{\ell} + 1.5 + \bar{\ell}\,(V/16.1)] \quad (1)$$

where

D = density in vehicles per kilometer,
$\bar{\ell}$ = average vehicle length in meters, and
V = vehicle stream speed in kilometers per hour.

This relationship conforms reasonably well to envelope curves of the same variables presented by Wheeler and Troy (8) and others (9). The only unknown in the relationship is the vehicle speed, which is assumed here to be constant over various sections of the bridge and causeway. The speed of vehicles moving in the same direction as the stopped vehicle was reduced to 70 percent of the observed speed, and the speed of vehicles in opposing lanes was reduced by 20 percent. Once the blocked lane was cleared stopped vehicles flowed at 1500 vehicles/h (10).

Stoppages were classified into event categories such as single-lane stoppages (including flat tires and running out of fuel) and more serious events including head-on, sideswipe, and rear-end collisions. The type of event was assumed to determine both the number of lanes blocked and the time to clear the stoppage. The majority of events were assumed to be single lane; only head-on and sideswipe collisions blocked two lanes simultaneously.

The direction (and lane, if applicable) stopped was randomly generated from a cumulative probability distribution describing the amount of vehicle flow in each lane. The time to clear the traffic backup at a stoppage was expressed as

$$t = t_1 + t_2 = t_1(x/x - y) \quad (2)$$

where

t = time to clear all backed-up traffic in minutes,
t_1 = time needed to remove the stopped vehicle in minutes,
t_2 = additional time needed to remove vehicles added to queue after stopped vehicle is removed, in minutes,
x = vehicle flow from a stopped situation in vehicles per minute, and
y = vehicle flow at the time of stoppage in vehicles per minute.

The value of y may be reduced to reflect the traffic that trickles past a single-lane blockage for the two lanes flowing in the same direction. The trickle was estimated at 1200 vehicles/h (11) and the flow after a stop at 1500 vehicles/h. Equation 2 then simplifies to

$$t = t_1(50/y - 20) \quad (3)$$

t_1 was obtained by using a random number generator, with separate upper and lower bounds for mechanical failures and accidents.

Both the time of the day and day of the week of the stoppage influenced the number of heavy vehicles that would be on the bridge. Visual examination of the data films and manual traffic counts indicated that the greatest volume of truck and bus traffic on the bridge was from 7 a.m. to 7 p.m. The data were summarized by hours to give the average upper bound of the vehicle mix by lane. The allocation (percent) of vehicle types in each lane was as follows:

Vehicle Type	Curb Lane	Center Lane
Cars	50	50
Buses	80	20
Trucks	60	40

The time of day also determined the direction of flow in the center lane. Finally the location of the stoppage indicated to what extent the bridge would be loaded and, combined with the length of time the stoppage was in effect and vehicle flows, whether the vehicles actually backed up on the bridge.

Figure 1. Two-lane stoppage.

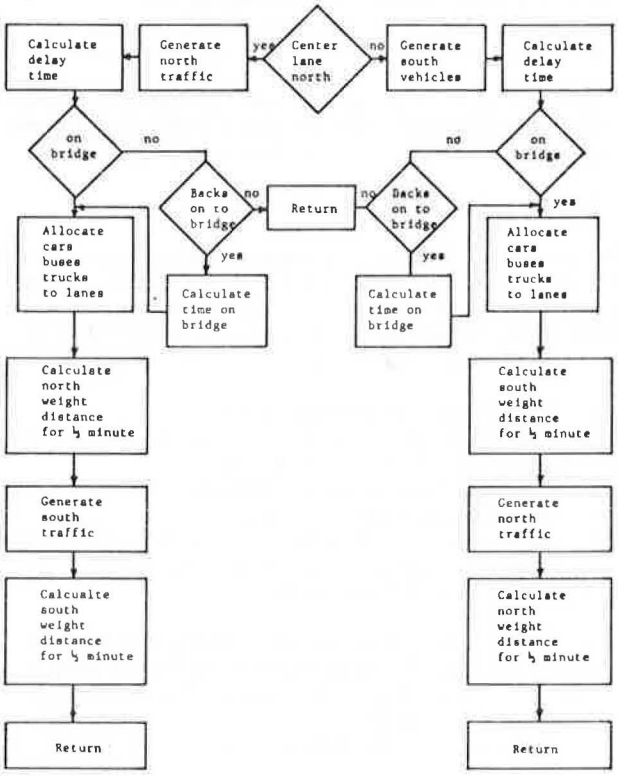

THE SIMULATION

The simulator operated in three distinct steps.

1. All significant events within an analysis period (events that created a backup of traffic on the bridge) were stored.
2. All such events within the analysis period (90 days) were analyzed to determine the maximum loads for several lengths of bridge and all possible combinations of the three lanes.
3. A search produced the maximum of these period maxima, and statistics describing the distribution of the maxima were obtained.

A more detailed accounting of the simulator follows.

There are 12 possible combinations of stopped traffic that may cause a backup on the bridge. The event could be due to mechanical failure, a one-lane accident, a two-lane accident, or a head-on collision, each of which occurs with a known frequency.

Two-lane accidents are simple (Figure 1). The direction of traffic flow in the center lane is determined first. For example, in the northbound center lane, northbound traffic is generated in half-minute intervals. The delay time due to the stoppage is calculated, and the location of the blockage is checked. If the stoppage occurs off the bridge, then a further check is made to determine whether the traffic backs up onto the bridge. If not, the event is rejected, and the simulation returns to the main program. If an accident occurs on the bridge or creates a serious backup of traffic on the bridge, the vehicles going north are distributed among the two northbound lanes and the resulting weight distributions are obtained. Southbound traffic is generated in a similar manner, and the weight distribution is obtained. A return to the main program is then effected.

After the analysis period has been covered by a sufficient number of events, the maximum loading for that period is determined. This is obtained by simply aligning the maximum weight in a 45-m moving section with that of one or two stationary 45-m sections. The program then calculates the maximum weights for single, any two, and all three lanes for loaded lengths in multiples of 45 m up to a maximum of 1100 m. Each maximum value and the associated traffic conditions are stored for forty 90-day analysis periods. These maxima are then used to provide statistics for the Gumbel distribution of maximum values, which estimates the maximum load $w^*_{Y,L}$ to be expected in Y years as

$$w^*_{Y,L} = \bar{w}_{max,L} + g\sigma_{max,L} \quad (4)$$

where

$\bar{w}_{max,L}$ = average of all the maxima observed within each analysis period of Y years,
$\sigma_{max,L}$ = standard deviation of the maximum values,
g = a factor depending on the return period Y expressed as

$$g = (1/\sigma_n)(\ell n\, Y - \bar{y}_n) \quad (5)$$

$\bar{y}_n$ = 0.5436 for the number of years of simulation, and
σ_n = 1.1413, obtained from table of the Gumbel distribution.

Thus,

$$g = 0.88\ell n\, Y - 0.48 \quad (6)$$

This value of g is then used to obtain the maximum weight $w^*_{Y,L}$ expected in a return period of Y years on a loaded length L.

BOUNDARY CONDITIONS

The shape of the curve relating vehicle weight per meter on the vertical axis to loaded length on the horizontal axis was assumed to be a very flat s. At short load lengths, the weight is fixed by the maximum load of single (or a very few) vehicles, and at very long lengths the average vehicle mix determines the weight.

An upper bound to the traffic load is produced by the heaviest vehicle observed on the bridge. Studies in the province (12) and elsewhere (12, 13) found that 1.3 (GVW) is a good upper limit for the weight of overloaded trucks (without special permits). The probability of two or three vehicles of similar weight being on the bridge has been reported by Stephenson (14).

The loads on very long spans are easy to calculate. As the loaded lengths approach infinity, the average load per meter tends to the average mix of vehicles. The limiting value is the number of vehicles in a lane multiplied by their average weight and divided by the length of road occupied. Thus,

$$w^*_{L\to\infty} = (N_C\bar{w}_C + N_B\bar{w}_B + N_T\bar{w}_T)/[N_C(\bar{\ell}_C + 1.5)(1 + R) + N_B(\bar{\ell}_B + 1.5)(1 + R) + N_T(\bar{\ell}_T + 1.5)(1 + R)] \quad (7)$$

where

$w^*_{L\to\infty}$ = average critical weight for a very long length in kilograms per meter,
N = proportion of vehicles,
$\bar{w}$ = average weight of vehicle in kilograms,
$\bar{\ell}$ = average length of vehicle in meters,
C, B, T = subscripts for cars, buses, and trucks,
R = V (0.0621) where V = speed of vehicle in kilometers per hour,
N_C = 0.94 fraction of cars,
N_B = 0.04 fraction of buses,
N_T = 0.02 fraction of trucks,
$\bar{\ell}_C$ = 5 m,
$\bar{\ell}_B = \bar{\ell}_T$ = 12 m,
$\bar{w}_C$ = 1590 kg,
$\bar{w}_B$ = 13 600 kg, and
$\bar{w}_T$ = 12 200 kg.

The maximum critical load over a long length will occur when the traffic is stopped, in which case the average weight per meter for stopped vehicles is given by

$$w^*_{L\to\infty} = 0.94(1590) + 0.04(13\,600) + 0.02(12\,200)/0.94(5 + 1.5) + 0.06(12 + 1.5) = 330 \text{ kg/m on a single lane} \quad (8)$$

Similarly the weights for two and three lanes may be calculated to get the extreme boundary value. The hypothesized shape of the vehicle traffic loading as a function of bridge length is shown in Figure 2. The shorter loaded length on the curve is set by the legal load limit and the very long lengths by the average vehicle mix. The curve in between, the most important, is determined by the complex simulation and, eventually, an analytical solution.

ANALYTICAL SOLUTION

The derivation of the analytical solution is rather long and complex; the following is a condensation. The problem was to find the maximum weight on an infinite number of sections of given length on the bridge. The technique

Figure 2. Hypothetical traffic loading on long span bridges (single-lane example).

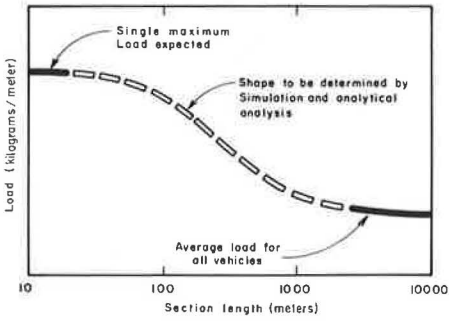

considered an arbitrary bridge length of δ meters and how many (Δ) of these make up the required length. For example, if we wish to know the loading on 300 m, then $\Delta = 300/\delta$. The critical load w* is given by

$$w^* = (1.488/h)\ell n_e \left\{\left[D - \sqrt{D^2 - 4(1 - C)}\right](\sqrt{AB})\right\} \quad (9)$$

where

$A = (k/3n)F + [2(n - k + 1)/3n]G,$
$B = (n - k + 1/3n)F + (2k/3n)G,$
$C = (1 - 1/JZ)^{2/S}$
$D = \sqrt{A/B} + (\sqrt{A/B})^{-1},$
$F = (E\exp hW_o)(E\exp hM_c)(E\exp hM_o),$
$G = (E\exp hW_o)(E\exp hW_c)(E\exp hM_o),$
k = a value such that $K \leq k \leq L,$
$J = L - K,$
$L = K +$ (length of bridge/δ), and

$$1/Z = 1 - \left(1 - Y^{-1}\{1 + [(\Delta - 1)(J - 1)/J]\}^{-1}\right)^{1/J}$$

Before going further the terms and notation must be explained. The bridge and the causeway are composed of n subsections, each of length δ, and numbered K = 1, 2, . . . , n. K is the length of the downstream approach affecting the bridge divided by δ. The unit for measuring Δ is 15 m, which was selected because it is approximately the space occupied by a bus, truck, or two cars. The length of the bridge and causeway is approximately 1500 m. For example, if each causeway is 300 m long and Δ = 5 (units of 15 m), each subsection K is 75 m (5 × 15) long. The total number of subsections n is 20. Each subsection is composed of the relevant portions of all three lanes. The variable Y is the return period (in years) and defines the probability that an event will occur as 1/Y. The number of subsections on the bridge is given by J where K is the number of subsections on the causeway to the bridge and L is the number to the far end of the bridge.

The further calculation of F and G requires additional definitions. Stopped lanes are noted by W and moving ones by M with subscripts o and c denoting outside and center lanes respectively. The proportion of units (δ) on the average containing vehicles is noted by p, the superscript gives the lane and the subscripts C, B, T denote cars, buses, and trucks. T, when not a subscript, also gives the truck weight in kilograms divided by 453.6. The number of trucks and buses at a given instance is noted by N_{T+B}, and q is the average number of trucks plus buses divided by N_{T+B}. The value r is the proportion of heavy vehicles that are either trucks or buses in each lane. S is the number of annual events.

Finally the value of h, the constant used to produce a continuous equation from a discrete probability distribution, may be selected to ensure that the boundary conditions are met. The value originally selected as most appropriate was 0.08, but later analysis has shown h to be a function of the loaded length.

With these definitions and the value of h it is possible to calculate F and G. For the outside lane when stopped:

$$E\exp(hW_o) = (p_C^o e^{8.38h} + p_B^o e^{33h} + p_T^o Ee^{hT})^{\Delta} \quad (10)$$

$$E\exp(hW_o) = (1.955\, p_C^o + 14.013\, p_B^o + Kp_T^o)^{\Delta}$$

and

$$K = Ee^{hT} = (12.5/M - 12)[\exp(T_{max}) - 2.61]$$

if

T_{max} = maximum truck weight = 18 000 kg,
K = 9.787, and
h = 0.08.

The calculations for the inside, middle, stopped lane are

$$E\exp(hW_c) = (p_C^c e^{8.38h} + 14.013\, p_B^c + Kp_T^c)^{\Delta}$$
$$= (1.955 p_C^c + 14.013\, p_B^c + Kp_T^c)^{\Delta} \quad (11)$$

For the moving lanes, calculation for the outside lanes is

$$E\exp(hM_o) = \left\{e^{3.5h}\left[1 + q^o\left(r_T^o\left\{E\exp[h(T - 3.5)] - 1\right\} + r_B^o(e^{29.5h} - 1)\right)\right]^{N_{T+B}^o}\right\}^{\Delta}$$
$$= \left(1.323\left\{1 + q^o[9.591 r_B^o + (0.756K - 1)r_T^o]\right\}^{N_{T+B}^o}\right)^{\Delta} \quad (12)$$

and for the middle lane is

Table 1. Vehicle traffic loads based on existing operating policy.

Section Length (m)	Single Lane		Two Adjacent Lanes		Three Outside Lanes		Three Lanes	
	$\bar{w}_{max,L}$	$\sigma_{max,L}$	$\bar{w}_{max,L}$	$\sigma_{max,L}$	$\bar{w}_{max,L}$	$\sigma_{max,L}$	$\bar{w}_{max,L}$	$\sigma_{max,L}$
45	972	146	1092	146	1149	132	1274	132
90	754	89	728	85	921	85	1059	74
180	610	60	737	54	774	60	911	58
360	500	43	628	37	640	40	775	31
720	432	30	574	37	558	27	711	36
1080	403	25	552	40	524	24	687	42

Notes: Values are in kilograms per meter.
1 kg = 35.3 oz; 1 m = 3.3 ft.

Figure 3. Single-lane traffic loading.

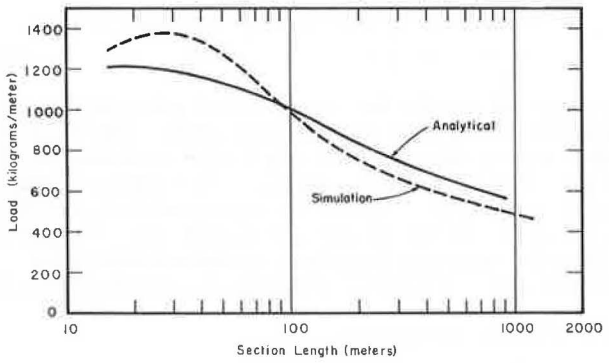

Figure 4. Design traffic load comparison for Lions' Gate Bridge (three-lane example).

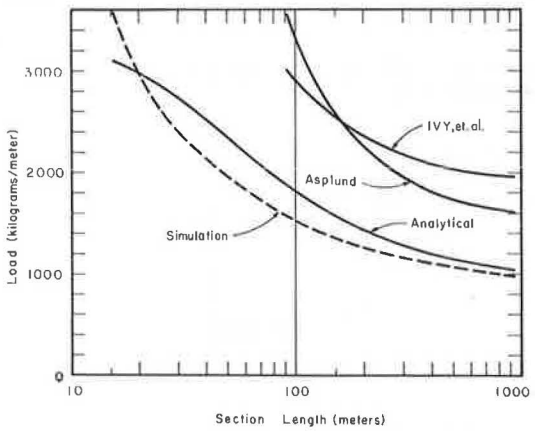

$$E\exp(hM_c) = \left\{ e^{3.5h} \left[1 + q^c \left(r_T^c \left\{ E\exp[h(T - 3.5)] - 1 \right\} + r_B^c (e^{29.5h} - 1) \right) \right]^{N_{T+B}^c} \right\}^{\Delta}$$

$$= \left(1.323 \left\{ 1 + q^c [9.591 r_B^c + (0.756K - 1) r_T^c] \right\}^{N_{T+B}^c} \right)^{\Delta} \quad (13)$$

A complete account of the derivation of the analytical formulation will be published shortly.

RESULTS

As stated earlier two methodologies were used to solve the problem of vehicle loads on the Lions' Gate Bridge. The analytical approach involved the development of probability equations representing traffic flow on the three lanes. The traffic conditions used were from an extreme peak hour. The alternative method simulated traffic flow across the bridge under a variety of conditions. It was possible to hunt for the stoppages that produced the maximum load both within individual lanes and across the total bridge. The resulting arithmetic mean and standard deviation of the maximum live loads on the bridge over a period of 10 years based on current operating policies are given in Table 1. The maximum vehicle traffic load can be calculated from equation 4.

The values of g for return periods of 30, 100, and 1000 years are 2.51, 3.57, and 5.58 respectively. Figures 3 and 4 show the vehicular loading results for existing traffic conditions and a return period of 100 years. The lower curves in Figures 3 and 4 are plotted from the data in Table 1 for three- and one-lane vehicle loads with g = 3.57. The analytical approach gave the upper curves in the figures. Visual inspection of the curves developed by the two methodologies shows very good agreement, which tends to add validity to the results. Beyond 75 m, both curves have essentially the same shape. Figure 3 shows an even closer agreement for a single lane. The maximum difference between the two curves at distances beyond 90 m is 18 percent.

The analytical curve should be higher than the simulation since it took slightly more conservative data and is in any case intended to be an upper bound. The reason that the curves for three lanes show a greater disparity than those for one lane is mainly that the third lane is treated differently in the two methods. Both assume that at least one lane has the traffic flowing at all times. The analytical approach tends to overestimate the load in this lane. The total effect on the bridge is small, however, because the critical side of the bridge is the one with the incident in the outer lane. Therefore, the compatibility of the two methods to measure the effective load on the bridge is more nearly represented by Figure 3 than by the simulated-analytical results in Figure 4.

A comparison of outer estimates and the live loads for existing traffic is shown in Figure 4. At lengths less than 150 m the difference between the Lions' Gate Bridge loads and those of Ivy and others (4) and Asplund is a factor of 1.7. At lengths of 900 m the difference is a factor of 2 for Ivy's curves and 1.6 for Asplund's curves. It would appear that Asplund's curve approaches the Lions' Gate curves at extremely long lengths.

The traffic loadings proposed by Ivy and others (4) and Asplund (15) are approximately similar for bridge lengths between 150 and 300 m. Ivy and coworkers studied the traffic on the lower deck of the San Francisco Bay Bridge reserved for trucks and U.S. army regulations for the movement of convoys. Ivy used the maximum expected loads, and the methodology does not allow the varying of vehicle mix or truck sizes. Asplund assumed that cars were mixed with very heavy trucks and that the vehicle load was 59 000 kg. This altered the very conservative estimates made by Ivy. He then applied simple probability theory to this mixed traffic. Asplund's selection of such a heavy single vehicle is rather arbitrary and does not represent all conditions. Asplund's curve in Figure 4 represents the probability of occurrence as more remote than 1 in 100 000.

The curves developed for the Lions' Gate Bridge reflect a low maximum vehicle load set by legislation over short segments of the bridge. At long lengths, the high percentage of buses using the bridge at rush hours is also apparent. The combination of these two features, unique to the Lions' Gate Bridge, accounts for the relative flatness of the traffic load on loaded lengths.

The resulting traffic load estimates combined with an extensive structural analysis verified the original decision to limit legal truck loads to 12 700 kg. The analysis also indicated that buses, operating under conditions similar to those at present, would not pose any structural problems.

CONCLUSIONS

The Lions' Gate Bridge is a unique three-lane suspension bridge built in 1938. The original traffic loadings for which the bridge was designed reflected vehicle weights and vehicle combinations typical in the late thirties. Since that time, vehicle weights, in particular truck weights, have increased considerably. The structure has also been subjected to many years of corrosive sea atmosphere. The British Columbia highway department required a reevaluation of the structural capabilities of the bridge; trucking companies also took interest in the bridge since any reduction in the legal load limit would greatly increase the distances that trucks had to travel. These two concerns helped to initiate the research presented in this paper.

The methodology developed reflected the need to independently estimate the effect of changing the legal load limit and varying the number of heavy vehicles that might use the bridge. Two methods were developed to estimate the vehicle traffic loads on the bridge: a computer simulation and an analytical formulation.

These methods have been shown to give comparable results. In the most extreme case the absolute difference between the curves is only 18 percent at a length of 60 m on all three lanes. The presence of one large, fully loaded bus or truck would account for this difference. Again for the three-lane case, at long lengths the difference is 75 kg/m. The single-lane agreement is even closer. At a loaded length of 120 m, the difference is only 30 kg/m or 3600 kg total. Although these results do not in themselves confirm the adopted design curve, they do lend credibility to the decision. In the absence of an extensive field survey in which the weight of each vehicle and distance on the highway at the time of an accident were known, the design curve is an optimal choice. The use of existing estimates such as those proposed by Ivy and coworkers, Asplund, or AASHTO would not easily allow the impact of reducing the legal load limit to be studied. Also, the vehicle combination used in those estimates was considerably different from that existing on the Lions' Gate Bridge.

The particular methodology, if generalized, would be particularly useful because it would allow the bridge designer to determine the bridge dimensions to fit a particular vehicle demand specification. If the bridge is along a recreational route, then a small percentage of heavy trucks would be expected. On the other hand, in areas of high industrial concentrations, trucks become more important and thus increased truck usage may be analyzed.

The method allows the traffic engineer and bridge designer to design the approaches and exits from the bridge

in a way that minimizes the potential of vehicles stopping on the bridge. This may be found beneficial in minimizing the vehicular traffic loads on the bridge.

The methodology allows the bridge designer to investigate vehicle traffic loads with a degree of sophistication approaching that used in the structural engineering analysis.

ACKNOWLEDGMENTS

The authors wish to thank the British Columbia Department of Highways for allowing publication of this work, which was contracted for their studies of the Lions' Gate Bridge. Richard Newman, Richard Lockhark, and David Burkholder obtained many of the data used in the study.

Financial support over and above that specifically contracted by the British Columbia highway department was provided by the British Columbia government through Careers '75, the Department of Civil Engineering, and the Centre for Transportation Studies, University of British Columbia.

REFERENCES

1. Standard Specifications for Highway Bridges. AASHO, 1973.
2. Standard S6: Design of Highway Bridges. Canadian Standards Association, 1966.
3. W. Henderson. British Highway Loading. Institution of Civil Engineers, Road Paper 44, March 1954.
4. R. J. Ivy, T. Y. Lin, S. Mitchell, N. C. Raab, V. J. Richey, and C. F. Scheffey. Live Loading for Long-Span Highway Bridges. Trans., ASCE, Paper 2708, 1953.
5. K. W. Crowley. Classification of Vehicles by Length. Port of New York Authority, Research Division Rept. TBR 2-63, 1963.
6. Measures to Improve Bus Transit and Traffic Flow Across the First Narrows Bridge. N. D. Lea and Associates, May 1967.
7. R. Herman, T. Lam, and R. Rothney. An Experiment on Car Size Effects in Traffic.
8. R. I. Wheeler and E. M. Troy. Volume Density Relationships and Their Use in the Study and Prevention of Kinematic Waves in Traffic. Ontario Department of Highways, Canada, Rept. RB 112, June 1966.
9. D. Gerlough and M. Huber. An Introduction to Traffic Flow Theory. Federal Highway Administration, U.S. Department of Transportation, June 1972.
10. Traffic Engineering Handbook. Institute of Traffic Engineers, Washington, D.C., 1965.
11. Highway Capacity Manual—1965. HRB, Special Rept. 87, 1965.
12. F. W. Jung and A. A. Witecki. Determining the Maximum Permissible Weight of Vehicles on Bridges. Ontario Ministry of Transportation and Communications, RR 175, Dec. 1971.
13. P. F. Csagoly and R. A. Dorton. Proposed Ontario Bridge Design Load. Ontario Ministry of Transportation and Communications, RR 186, Nov. 1973.
14. H. K. Stephenson. Highway Bridge Live Loads Based on Laws of Chance. Proc., ASCE, Vol. 83, July 1957.
15. S. O. Asplund. Probabilities of Traffic Loads on Bridges. Proc., ASCE, No. 585, Vol. 81, Jan. 1955.

Fatigue Design of Welded Bridge Details for Service Stresses

Kentaro Yamada and Pedro Albrecht, University of Maryland

An average stress range histogram for truck loads on short-span highway bridges is derived from 106 strain range records reported in the literature. The histogram is used in conjunction with the concept of an equivalent stress range and the allowable constant amplitude stress range values specified by AASHTO to design bridge details for service stresses. Practical application of the method is illustrated with two design examples.

Highway bridge members are designed statically for the maximum stress due to dead and live loads. The dynamic effect of the live load is considered by adding an impact factor. It is well known, however, that a large number of repeated stress cycles may cause fatigue damage to the structural components at stress levels lower than the allowable maximum stress. A safe fatigue design of the structural components is achieved by limiting the value of the stress range caused by the design live load, including impact.

AASHTO specifications (1, 7), article 1.7.3, fatigue design, give the number of repeated stress cycles for which the bridge must be designed and the allowable stress range depending on the type and location of the detail (Figure 1). The allowable stress range values specified by AASHTO correspond to the 95 percent confidence limit for 95 percent survival of beam specimens tested at constant amplitude stress cycling (5, 6). The number of design load cycles is given by the average daily truck traffic (ADTT) for the traveled artery or the number of expected lane loads.

Fatigue design for truck-induced stress ranges is conservative in two respects. First, loadometer studies and strain history records indicate that few trucks have a gross vehicle weight comparable to that of the design truck. A variety of large but light cargos, partially filled trucks, and empty runs produce a frequency distribution curve for truck weights of concave shape with a peak at about 25 percent of the maximum recorded stress range. This is typical of all bridges surveyed. To assume for purposes of fatigue design that all trucks are fully loaded is safe but very conservative.

A more realistic fatigue design should be based on truck-induced stress histories of variable amplitude, which reflect the actual variation in truck weights. This paper derives an average stress histogram for truck loads on short span highway bridges from published data and shows how it can be used in conjunction with the AASHTO constant amplitude stress range values to design bridge details for service stresses.

Fatigue design is conservative in a second way. Several investigators have matched recorded truck weights with induced strains and have consistently observed lower stresses than those predicted by analysis. This is due mainly to the fact that the various analyses and design rules are conservative. It is not a direct result of fatigue design. However, inasmuch as analysis and design rules may be changed to reduce such discrepancies, it is advisable not to relax the fatigue design specifications.

Special permits may be granted for overloads under the AASHTO operating rating (1, 2). Although a discussion of periodic overload effects on fatigue strength is beyond the scope of this paper, it is helpful to point out that preliminary research findings indicate an enhancement of fatigue life at overload frequencies to which bridges are currently being subjected (25).

STRESS HISTORY OF HIGHWAY BRIDGES

As a first step toward a more realistic fatigue design of highway bridge components, the frequency distribution of stress ranges induced under service conditions, commonly referred to as stress range histogram, must be known. During the last decade, stress range histograms for truck traffic on 29 bridges on Interstate and U.S. highways in semirural and metropolitan areas were recorded (14 through 23). Detailed descriptive information on the bridges and characteristic features of the 106 individual stress range histograms reported in these references is presented elsewhere (13). A collection of all 106 stress range histograms is given by Yamada and Albrecht (24).

Publication of this paper sponsored by Committee on Steel Bridges.

Notation

The following symbols are used in this paper:

- ADTT = average daily truck traffic,
- B_1, B_2 = regression coefficients for S-N curve,
- f(x) = probability density function for stress range histogram,
- F_y = yield point of material,
- f_r = stress range,
- $f_{r,RMS}$ = root mean square stress range,
- $f_{r,RMC}$ = root mean cube stress range,
- $f_{r,equiv}$ = equivalent stress range,
- $f_{r,max}$ = maximum stress range in stress histogram,
- $f_{r,RO}$ = fatigue limit or runout level of stress range,
- N = fatigue life,
- N_i = fatigue life under applied stress range f_{ri},
- n_i = applied cycles of stress range f_{ri},
- N_{prop} = number of design stress cycles above the fatigue limit,
- N_{total} = total number of cycles,
- N_{year} = design fatigue life in years,
- P = percentage of frequency occurrence from $x = x_{min}$ to $x = 1.0$, and
- x_{min} = ratio of fatigue limit to maximum stress range.

Bridge Type

A breakdown by type of bridge shows that records were obtained from 16 single-span bridges, 8 three-span continuous bridges, 2 end-anchored bridges, 2 suspended span bridges, and 1 semisuspended span bridge.

Most of the bridges have short spans in which the length between supports varies from 11.6 to 24.4 m (38 to 80 ft). Only five bridges have a span longer than 24.4 m (80 ft): two I-96 bridges over the Grand River in Michigan have spans of 29 and 39.3 m (95 and 128 ft) (14), the Yellow Mill Pond twin bridges on I-95 in Bridgeport, Connecticut, have a span of 34.6 m (113.5 ft) (22), and the Lehigh Canal bridge on US-22 near Bethlehem, Pennsylvania, has a span of 44 m (144 ft) (23).

Rolled sections were used as girders in 20 bridges, of which 19 bridges have welded cover plates. Two bridges with longer spans have welded plate girders (14), and one has riveted plate girders (23). The remaining six bridges are of concrete construction, either reinforced (20) or prestressed (14, 17). In all but 4 of the 23 steel girder bridges (16, 18, 20), the slabs are attached to the girders with shear connectors. The thickness of the concrete deck varies between 15 and 20 cm (6 and 8 in).

Stress Range Histograms

All recorded strain ranges were converted into stress ranges by multiplying by Young's modulus. The number of stress range events in preselected intervals was counted, and the results were presented in the form of a frequency occurrence distribution.

Most strain range measurements, 77 out of 106, were taken with strain gauges attached to the bottom flange either at midspan or near the end of the cover plates. Records from strain gauges attached to slabs (16), reinforcing bars in the slab (16), and tie plates (23) were not included because they are affected by wheel loads rather than truck loads.

For steel girder bridges the stress range intervals, preselected by the investigators for purposes of data presentation, varied from a minimum of 1.4 MPa (200 lbf/in^2) (16) to a maximum of 8.3 MPa (1200 lbf/in^2) (23). Most of the histograms (69 out of 87), had stress range intervals between 2.8 and 4.1 MPa (400 and 600 lbf/in^2). For concrete girders, a value of approximately 0.28 MPa (40 lbf/in^2) was used (14, 17). Two typical histograms with 1.4 and 4.1 MPa (200 and 600 lbf/in^2) stress range intervals are shown in Figure 2. They were recorded at the extreme fiber of the bottom flange at the midspan of simple beams.

The maximum stress range value recorded varied from 1.2 MPa for a prestressed concrete girder (17) to 72.4 MPa (180 to 10 500 lbf/in^2) measured at the bottom flange of the three-span continuous riveted plate girder (23), as shown in Figure 4. Of the 87 steel girder histograms, 35 had a maximum stress range larger than 34.5 MPa (5000 lbf/in^2).

A total of 66 stress range histograms were presented with a cutoff point below which no stress ranges were recorded (17, 20, 21, 22, 23), while the remaining 40 were presented with the lowest interval starting at 0 stress range. Two typical histograms are shown in Figure 3: one with a cutoff point of 4.1 MPa (600 lbf/in^2) obtained from a strain gauge attached to the bottom flange at midspan of a simple beam (22) and one without a cutoff point recorded at the one-quarter point of a simple span welded plate girder (14). Although both histograms have the same stress range interval, the one with the cutoff point shows a descending frequency distribution, while the one without the cutoff point shows an ascending-descending frequency distribution shape. The same characteristics can be seen in the stress range histograms shown in Figures 2 and 4. Most cutoff points in the stress range histograms were chosen between 3.1 and 6.9 MPa (450 and 1000 lbf/in^2). Only 7 out of 106 stress range histograms had cutoff points greater than 25 percent of the highest stress range.

In spite of the variations in $f_{r,max}$ and cutoff points discussed above, the concavity of the frequency distribution curve from the peak frequency at about 25 percent of $f_{r,max}$ to a low value at $f_{r,max}$ is typical of all histograms. To preserve this characteristic feature and to permit a meaningful comparison, the stress range histograms were nondimensionalized with respect to the maximum stress range $f_{r,max}$, and the lowest quartile was deleted.

A uniform cutoff point at 25 percent was selected for the following reasons:

1. Stress ranges below 25 percent of the highest stress range usually fall below the fatigue limit and, hence, do not contribute to fatigue crack propagation.
2. Stresses induced by partial car lane loads were not recorded although their magnitude would be comparable to that for light trucks.
3. Using a cutoff point at 25 percent prevents insignificant low stress ranges from affecting the cumulative frequency distribution at the higher and significant stress ranges.

All 106 nondimensionalized cumulative frequency distributions were then plotted, as shown in Figure 5, together with the computed average. The average of all 106 histograms is shown in Figure 6 in the form of a histogram. It can be expressed by the following probability density function:

$$f(x) = \begin{cases} -12.0(X - 1.0)^3 + 0.07 & 0.25 \leq x \leq 1.0 \\ 0 & \text{otherwise} \end{cases} \quad (1)$$

where $x = f_r/f_{r,max}$ is the nondimensional stress range. Equation 1 is also plotted in Figure 6. When equation 1 is used for variable amplitude design, the nondimensionalized stress ranges are multiplied by the maximum stress range obtained from the stress analysis. The

Figure 1. Allowable constant amplitude stress range values for stress categories D and E.

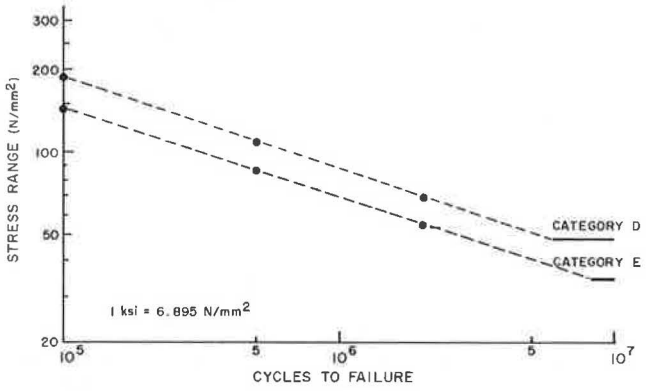

Figure 2. Typical stress range histograms with two extreme stress range intervals.

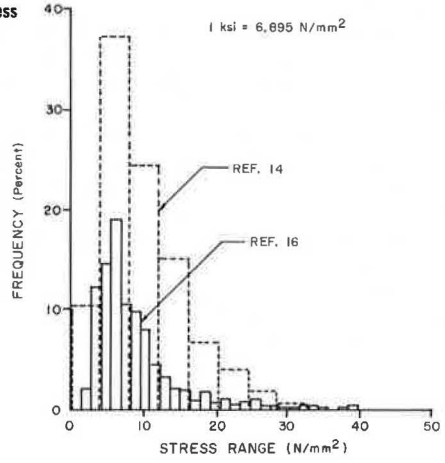

Figure 3. Typical stress range histograms with and without cutoff point.

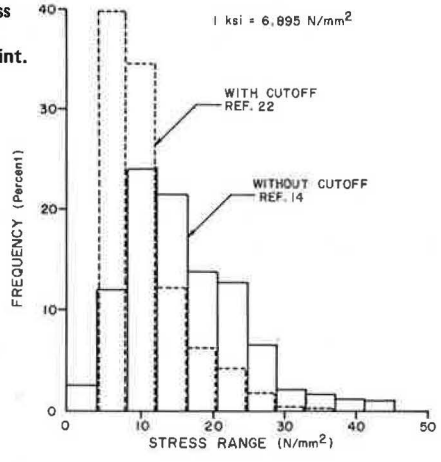

Table 1. RMS and RMC stress range for the average non-dimensionalized stress range histogram.

Cutoff Point	Percentage Above Cutoff Point	RMS Stress Range (MPa)	RMC Stress Range (MPa)
0.25	100.0	0.435	0.459
0.30	76.8	0.472	0.493
0.40	43.0	0.551	0.566
0.50	22.2	0.633	0.644
0.60	10.5	0.719	0.726
0.70	4.5	0.806	0.810
0.80	1.8	0.887	0.889
0.90	0.73	0.949	0.950
1.00	0.0	1.0	1.0

Note: 1 MPa = 145 lbf/in².

Figure 4. Typical stress range histograms with highest and lowest recorded stress range values, $f_{r,\,max}$.

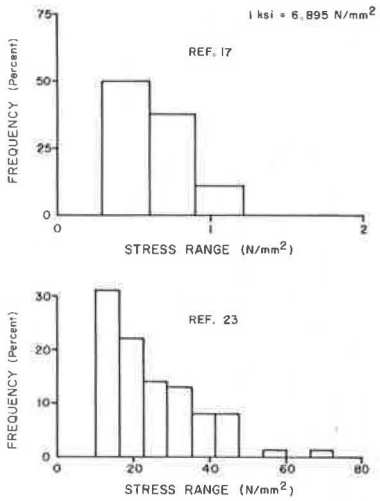

Figure 5. Nondimensional cumulative frequency plot of 106 stress range histograms with cutoff point of 0.25 $f_{r,\,max}$.

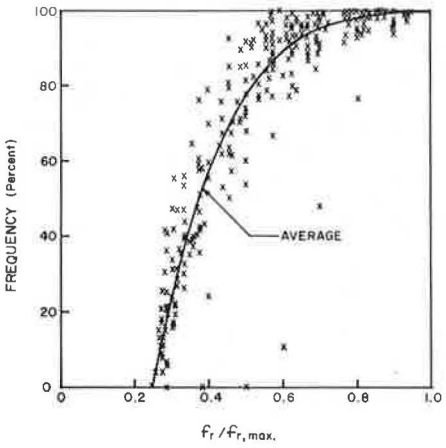

Figure 6. Average nondimensional stress range histogram and probability density function.

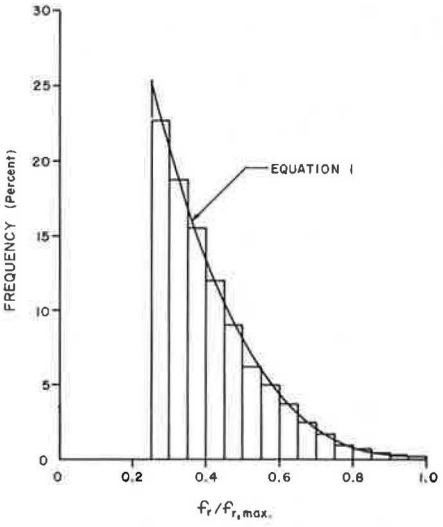

average histogram then accounts for the actual live load variation.

Among the curves investigated for the purpose of best fitting the average cumulative frequency distribution, shown as a step function in Figure 6, were Rayleigh functions. They have been used by others (10), presumably because they follow in general the ascending-descending shape of individual histograms such as those shown in Figure 2. The results of the least squares fit analysis revealed a significant lack of correlation for the Rayleigh curve. Its applicability appears to be questionable also for conceptual reasons. A Rayleigh curve would predict gradually vanishing frequencies at very low loads, where in reality the addition of groups of cars capable of producing comparable stress fluctuations would cause an upward turn in the frequency distribution. Further, retaining the very low stress ranges reduces the equivalent stress range, as discussed below, and leads to nonconservative estimates of variable amplitude fatigue life.

FATIGUE LIFE PREDICTION

The fatigue life of structural components consists of a crack initiation phase and a crack propagation phase. Severe stress concentrations at weldments and the existence of microcracks and slag inclusions at weld borders tend to reduce the crack initiation phase to a small number of cycles compared with the total fatigue life. Therefore, the initiation phase is usually neglected, and the analysis of the useful life is based on crack propagation alone. The assumption is conservative for purposes of design and indeed necessary because undesired weld cracking can preempt entirely the initiation phase.

Stress Range Versus Fatigue

The constant amplitude fatigue life of weldments is determined experimentally. The data are usually presented as a log-log plot of stress range versus fatigue life (S-N) with the mean life given by

$$\text{Log } N = B_1 + B_2 \log f_r \qquad (2)$$

B_1 and B_2 are regression coefficients obtained from a least squares fit. The AASHTO specifications (1) classify all structural details in five stress categories, A through E, according to their fatigue resistance. For each stress category, the constant amplitude stress range is specified as a function of the design life on the basis of the 95 percent confidence limit for 95 percent survival obtained from the statistical analysis of the pertinent test data. For example, allowable stress ranges for stress categories C and D(1) are shown by the solid points and lines in Figure 1.

At low values of stress range, a fatigue limit or a runout level exists for each detail below which fatigue cracking will not occur even after application of a large number of load cycles, usually on the order of 10 million. The safe fatigue limit for details in stress categories C and D is shown by solid lines in Figure 1.

Equivalent Constant Amplitude Stress Range

Recently, the concept of an equivalent constant amplitude stress range has been advanced (10). It is defined as the constant amplitude stress range that will give the same fatigue life as the variable amplitude stress history. Barsom (3) successfully used the root mean square stress range, $f_{r,RMS}$, to correlate fatigue crack propagation rates under constant and variable amplitude cycling.

The RMS stress range is defined as the square root of the mean sum of squares of all stress ranges:

$$f_{r,RMS} = \left(\sum_{i=1}^{s} n_i f_{ri}^2 \Big/ N \right)^{1/2} \qquad (3)$$

where

N = total number of cycles,
s = number of stress range levels, and
n_i = number of stress range cycles at each level.

Equation 3 can be derived from the condition that the strain energy induced by a total of N variable amplitude stress cycles must be the same as the strain energy caused by the application of N stress cycles of constant amplitude, $f_{r,RMS}$.

Combining Miner's theory with the S-N curves fitted to fatigue test data suggests, however, that an exponent of 3 rather than 2 should be used in equation 3. This is shown below.

The Palmgren-Miner theory (8) is an empirical, cumulative damage criterion for evaluation of variable amplitude fatigue life. Its widespread use can be attributed to both the simplicity of the method and the ease of application. The Palmgren-Miner theory states that the damage caused by a number of stress cycles, n_i, can be expressed as a fraction of n_i to the number of cycles, N_i, required to fail the component at the same stress range level. Failure occurs when the summation of the fractions for each level adds up to unity.

$$\sum_{i=1}^{s} (n_i/N_i) = 1.0 \qquad (4)$$

By substituting the anti-log of equation 2 into equation 4, the Palmgren-Miner criterion is given by

$$\sum_{i=1}^{s} (n_i/10^{B_1} f_{ri}^{B_2}) = 1.0 \qquad (5)$$

If the equivalent constant amplitude stress range, $f_{r,equiv}$, causes failure, the life, N, can be expressed by the anti-log of equation 2 as

$$N = 10^{B_1} f_{r,equiv}^{B_2} \qquad (N f_{r,equiv}^{-B_2}/10^{B_1}) = 1.0 \qquad (6)$$

Equating the identities expressed by equations 5 and 6 and solving for the equivalent stress range yield

$$f_{r,equiv} = \left(\sum_{i=1}^{s} n_i f_{ri}^{-B_2} \Big/ N \right)^{-(1/B_2)} \qquad (7)$$

Equation 7 is of the same form as equation 3 except the exponent is different. If $-B_2 = 3$, as found for most structural details (5, 6), is substituted, the equivalent stress range is given by a so-called root mean cube stress.

$$f_{r,RMC} = \left[\sum_{i=1}^{s} (n_i f_{ri}^3/N) \right]^{1/3} \qquad (8)$$

As previously explained, a runout level of stress range, $f_{r,RO}$ (also called fatigue or endurance limit) is assumed when a large number of cycles, usually on the

order of 10 million, do not produce any fatigue cracking. Therefore the stress range levels below the fatigue limit should be deleted from the calculation of RMS or RMC stresses. Root mean square and root mean cube stresses for the average stress range histogram, equation 1, were computed for several values of fatigue limit, expressed as a fraction of the maximum stress range. The results are given in Table 1. For example, if the fatigue limit of a given detail is 50 percent of the maximum design stress range, only 22.2 percent of all trucks cause stress ranges above the fatigue limit, and its RMS and RMC stress ranges are given by 0.633 and 0.644 of $f_{r,max}$. The difference between the RMS and RMC stress ranges is approximately 5 percent when $f_{r,RO} = 0.25\ f_{r,max}$ and decreases further as the relative fatigue limit increases.

These small differences explain partially why good correlation between constant and variable amplitudes test data can be obtained by plotting the fatigue lives against the root mean square stress range. The RMC stress range is based, however, on a sounder theoretical and experimental foundation.

The Fracture Mechanics Approach

In contrast to Miner's empirical theory, the fracture mechanics approach is based on the physical phenomena of fatigue crack propagation. It has been used with success to correlate observed fatigue lives with the computed number of cycles required to propagate a fatigue crack from an average initial size to failure, for both constant and variable amplitude fatigue. It also explains why the slope of all S-N curves is the same and about numerically equal to the slope of curves in log-log plots of crack growth rate versus range of stress intensity factor. The value of the slope is about 3 for structural details and steels.

It can be shown that both Miner's theory (equation 4) and the root mean cube stress range concept (equation 8) are special cases of the fracture mechanics approach. They give identical variable amplitude fatigue life prediction (13) provided that (a) the crack initiation phase is negligible, (b) no interaction exists between the stress range levels, (c) only stress ranges above the fatigue limit are retained, and (d) the slopes of the S-N curves and the crack growth rate curves are about 3. Substantial experimental evidence can be presented in support of each one of the four conditions.

APPLICATION

A more realistic fatigue design of welded bridge details for service stresses can be performed with the aid of (a) an average stress range histogram for highway bridges, (b) the concept of an equivalent stress range, and (c) the allowable constant amplitude stress range values specified by AASHTO. The following design procedure is recommended.

1. Find the maximum stress range, $f_{r,max}$, at the detail due to live load and impact.
2. Compute $x_{min} = f_{r,RO}/f_{r,max}$, where the runout stress range, $f_{r,RO}$, is defined in the AASHTO specifications (more than 2 million cycles).
3. Find the equivalent RMC stress range, $f_{r,RMC}$.
4. Compute the percentage of frequency occurrence, P, of the stress cycles above the fatigue limit by integrating the probability density function, f(x), from $x = x_{min}$ to $x = 1.0$. This is the percentage of stress range cycles that contribute to crack propagation. Alternatively read the RMC stress range directly from Table 1.
5. From the S-N plot for the appropriate stress category, read the propagation life, N_{prop}, corresponding to the equivalent stress range, $f_{r,RMC}$ (Figure 1).
6. Divide the propagation life, N_{prop}, by the percentage of frequency occurrence to obtain the total truck traffic, $N_{total} = N_{prop}/P$.
7. Compute the expected fatigue life in calendar years from $N_{year} = N_{total}/(360 \times ADTT)$.

REFERENCES

1. Standard Specifications for Highway Bridges. AASHTO, 1974.
2. Manual for Maintenance and Inspection of Bridges. AASHTO, 1976.
3. J. M. Barsom. Fatigue-Crack Growth Under Variable-Amplitude Loading in ASTM A514-B Steel. ASTM, Special Technical Publ. STP 536, 1973, pp. 147-167.
4. T. R. Gurney. Fatigue of Welded Structures. Cambridge Press, 1968.
5. J. W. Fisher, K. H. Frank, M. A. Hirt, and B. M. McNamee. Effect of Weldments on the Fatigue Strength of Steel Beams. NCHRP, Rept. 102, 1970.
6. J. W. Fisher, P. A. Albrecht, B. T. Yen, D. J. Klingerman, and B. M. McNamee. Fatigue Strength of Steel Beams With Welded Stiffeners and Attachment. NCHRP, Rept. 147, 1974.
7. J. W. Fisher. Guide to 1974 AASHTO Fatigue Specifications. American Institute of Steel Construction, 1974, pp. 29-31.
8. M. A. Miner. Cumulative Damage in Fatigue. Journal of Applied Mechanics, Trans., ASME, Vol. 67, Sept. 1945, pp. A-159—A-164.
9. W. H. Munse. Fatigue of Welded Steel Structures. Welding Research Council, 1964.
10. C. G. Schilling, K. H. Klippstein, and R. J. Reilly. Simulated Traffic Fatigue Loading of Steel Bridges. Preprint, Specialty Conference on Metal Bridges, ASCE, Nov. 1974, pp. 379-410.
11. J. E. Stallmeyer and W. H. Walker. Cumulative Damage Theories and Application. Journal of Structural Division, Proc., ASCE, Vol. 94, No. ST12, Dec. 1968, pp. 2739-2750.
12. J. P. Tang and J. T. P. Yao. Random Fatigue-Literature Review. Univ. of New Mexico, Albuquerque, Technical Rept. CE-22(70) NSF-065, July 1970.
13. K. Yamada. Fatigue Behavior of Structural Components Subjected to Variable Amplitude Loading. Univ. of Maryland, College Park, PhD dissertation, 1975.
14. G. R. Cudney. The Effects of Loadings on Bridge Life. Michigan Department of State Highways, Research Rept. R-638, Sept. 1967.
15. T. R. Douglas and J. B. Karrh. Fatigue Life of Bridges Under Repeated Highway Loading. Alabama Highway Research, HPR Rept. 54, April 1971.
16. C. P. Heins and A. D. Sartwell. Tabulation of 24 Hours Dynamic Strain Data on Four Simple Span Girder-Slab Bridge Structures. Civil Engineering Department, Univ. of Maryland, College Park, Progress Rept. 29, June 1969.
17. W. T. McKeel, C. E. Maddox, H. L. Kinnier, and C. F. Galambos. A Loading History Study of Two Highway Bridges in Virginia. Virginia Highway Research Council, Charlottesville, Final Rept. VHRC 70-R48, June 1971.
18. D. C. Sartwell and C. P. Heins. Tabulation of Dynamic Strain Data on a Girder Slab Bridge Structure During Seven Continuous Days. Civil Engineering Department, Univ. of Maryland, College Park, Progress Rept. 31, Sept. 1969.

19. A. D. Sartwell and C. P. Heins. Tabulation of Dynamic Strain Data on a Three Span Continuous Bridge Structure. Civil Engineering Department, Univ. of Maryland, College Park, Progress Rept. 33, Nov. 1969.
20. D. W. Goodpasture. Stress History of Highway Bridges. Department of Civil Engineering, Univ. of Tennessee, Dec. 1972.
21. P. O. Christiano and L. E. Goodman. Bridge Stress Range History. HRB, Highway Research Record 382, 1972.
22. D. G. Bowers. Loading History of Span 10 on Yellow Mill Pond Viaduct. HRB, Highway Research Record 428, 1973, pp. 64-71.
23. J. W. Fisher, B. T. Yen, and N. V. Marchica. Fatigue Damage in the Lehigh Canal Bridge. Fritz Engineering Laboratory, Lehigh Univ., Bethlehem, Penn., Rept. 386.1, Nov. 1974.
24. K. Yamada and P. A. Albrecht. A Collection of Live Load Stress Histograms of U.S. Highway Bridges. Univ. of Maryland, College Park, Civil Engineering Rept., 1975, pp. 39-144.
25. P. Albrecht, A. Abtahi, and G. R. Irwin. Fatigue Strength of Overloaded Bridge Components. Univ. of Maryland, College Park, Civil Engineering Rept., 1975.

Stresses in Orthotropic Deck of Rio-Niteroi Bridge Under Traffic

J. Hartley Daniels, B. T. Yen, and John W. Fisher, Fritz Engineering Laboratory, Lehigh University

The six-lane President Costa e Silva Bridge between Rio de Janeiro and Niteroi over Guanabara Bay in Brazil spans the main shipping channel with two parallel three-span continuous steel box girders 848 m (2782 ft) long. The box girders are joined by an orthotropic steel deck with asphalt surfacing. A thorough field study was conducted of the steel box girders under erection and service load conditions. As part of this investigation, the service life behavior of the orthotropic steel deck was examined. Field studies were carried out on a portion of the orthotropic deck to determine the stress history under a random traffic sample so that the fatigue susceptibility of the welded details could be assessed. The investigation revealed that the orthotropic deck will provide satisfactory service throughout its life. Indications are that certain splices of the trapezoidal deck stiffeners may have the potential for fatigue crack growth. Periodic inspection of these splices will provide ample safeguards and ensure that their capacity is not impaired.

In light of the recent failures during construction of four bridges similar to the Rio-Niteroi bridge (1), a thorough field study of the steel box girders and the orthotopic deck of the bridge was made under erection and service loading conditions (2). Because experiments in England on orthotropic steel bridge deck panels (3) demonstrated that fatigue cracks can be generated in the stiffener-to-floor beam connection welds, the field study included stress measurements on part of the orthotropic deck under a random traffic sample. This study was carried out from May 30 to June 5, 1974.

The orthotropic deck was instrumented over the end support of an end span where the plate thickness is reduced (2). Figure 1 shows the general location of the deck gauges. Local stresses were determined under vehicular traffic, particularly in the stiffening elements and near the welded connection between the deck and the stiffening elements. Traffic flow on the bridge was also recorded, some of it photographically.

Investigations in the United States since 1960 demonstrate the applicability of stress measurements obtained in the field when the serviceability of highway bridge structures is assessed (4, 5, 6, 7). These investigations were also very helpful in the development of the current specifications for failure design that are based on existing data and detailed classifications (8, 9, 10, 11).

INSTRUMENTATION AND TRAFFIC DATA

Thirty-three 0.64-cm-long (¼-in) electrical resistance foil strain gauges were mounted in five groups as shown in Figure 2. A quarter-bridge, three-wire hookup was used, which automatically provided lead-in wire and temperature compensation to all gauges. All gauges were located to provide

1. Representative strain data on the orthotropic deck cross section,
2. Strains near the splice plates on the sides and bottom of the trapezoidal stiffeners,
3. Strains at the junction of the deck plate and web A of the north box (Figure 1), and
4. Strains at the junction of the deck plate and floor beam 17.

Figure 3 shows the analog traces in stress units determined from the strain at gauges 5, 21, and 33. These are typical of the traces from all gauges. The elastic modulus was taken as 207 000 MPa (30×10^6 lbf/in^2). Only truck traffic and other large vehicles generated strains sufficiently large to be detected.

A total of 642 truck records were obtained. These were distributed over 19 daylight hours of the 7-day field study. Each truck record was correlated with each strain record. Of the 642 trucks, 120 of them were photographed as they passed over floor beam 17. A typical photograph is shown in Figure 4. The deck markings in the figure identify the transverse location of each truck in relation to the gauges near floor beam 17. The transverse graduated strip is directly over floor beam 17. The narrow strip parallel to the traffic is directly over web A. The wide strip is a lane marker. The five small crosses are located approximately above the midpoint of the five groups of gauges.

The stress range distribution at gauges 5, 21, and 33 is shown in Figure 5. Stress range is the difference be-

Publication of this paper sponsored by Committee on Steel Bridges.

tween a maximum stress as determined from the analog strain trace and the next minimum stress (Figure 3). Gauges experiencing high maximum stresses also experienced high stress ranges.

A continuous count of all bridge traffic on an hourly basis, 24 h/day and 7 days/week, was made available by the bridge authority from toll booth information acquired at the Niteroi approach from March 4, 1974, to May 31, 1975.

The distribution of westbound trucks by number of axles is shown in Figure 6. A comparison of the data shows similar axle distributions during both sample periods. The eastbound distribution (Rio to Niteroi) during the 14-month period is similar. Hence, it is reasonable to assume that the composition of truck traffic in the field sample is typical for the entire structure at least up to May 31, 1975.

No loadometer survey is available in Brazil. Therefore, the frequency of occurrence of axle weight or gross weight could not be determined directly. These were indirectly computed by comparing the strain response at selected gauges, due to passage of a sample of trucks of known lateral (lane) position, with the strain response from controlled load tests using a test truck of known axle weights and known lateral position. The test truck had two axles.

The two-axle truck made 13 crawl run passes and 7 speed run passes over the deck gauge locations near floor beam 17. The speed runs were made at approximately 55 to 60 km/h (35 to 38 mph).

Figure 7 shows the variation in maximum stress ranges at gauges 21 and 33 during the crawl and speed runs. Each curve is essentially an experimental influence line for stress range. Similar curves were obtained for the other gauges. The double hump in each curve is a result of the influence of wheels (front axle) or wheel groups (duals on rear axle). For most gauges, particularly the transverse gauges on the deck plate and stiffeners, the strains produced by the front and rear axles do not interact. A relatively small interaction did occur at gauge 33 as expected.

The axle and gross vehicle weights of selected trucks were computed by using the influence line for gauge 33. The results are shown in Figure 8. Inasmuch as closely spaced (tandem) axles cause a single strain response, the distribution of axle group weights instead of individual axle weights is presented. Figure 8 shows a skewed distribution of axle group weights, which indicates that large numbers of relatively small axle group weights can be expected. Because the orthotropic deck is mainly responsive to axle group weights and wheel or wheel group loads, each truck may generate two or more cycles. However, given the lateral position of traffic and the frequency and loading of trucks, probably only one stress cycle is significant in the fatigue analysis.

Figure 1. Location of deck gauges adjacent to floor beam 17.

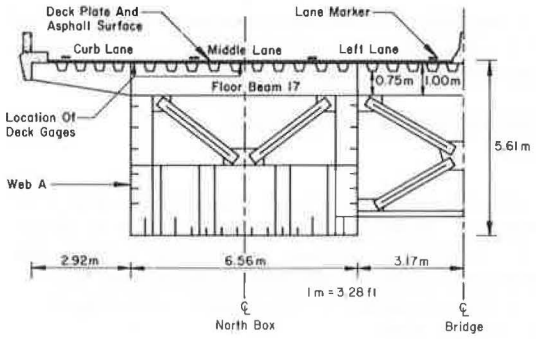

Figure 2. Location and type of strain gauges on underside of orthotropic deck as viewed from below.

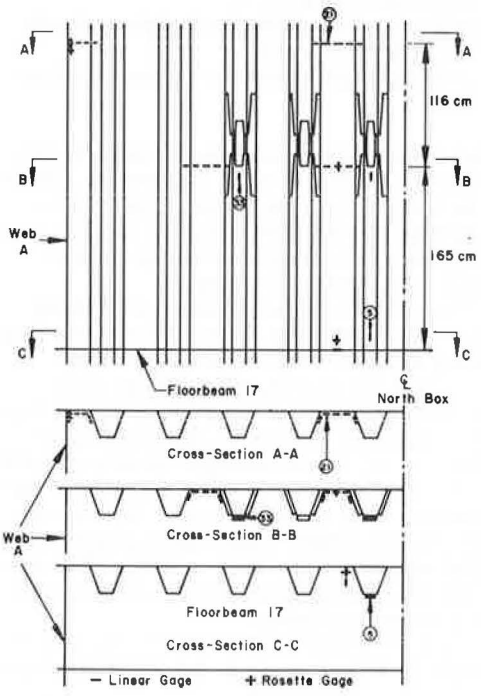

Figure 3. Typical analog traces for gauges 5, 21, and 33 produced by a 12-channel ultraviolet oscillograph trace recorder.

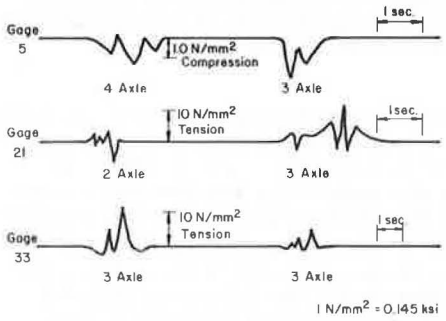

Figure 4. Typical trucks (traveling west from Niteroi to Rio de Janeiro) passing over floor beam 17 of north box.

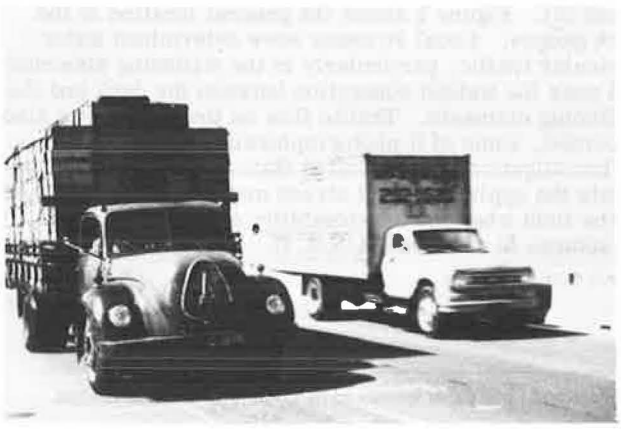

Figure 5. Stress range distribution (a) at gauge 5, measured parallel to stiffener and adjacent to web of floor beam 17, (b) at gauge 21, measured transverse to stiffener and on deck plate, and (c) at gauge 33, measured parallel to stiffener and 25 mm from edge of splice plate.

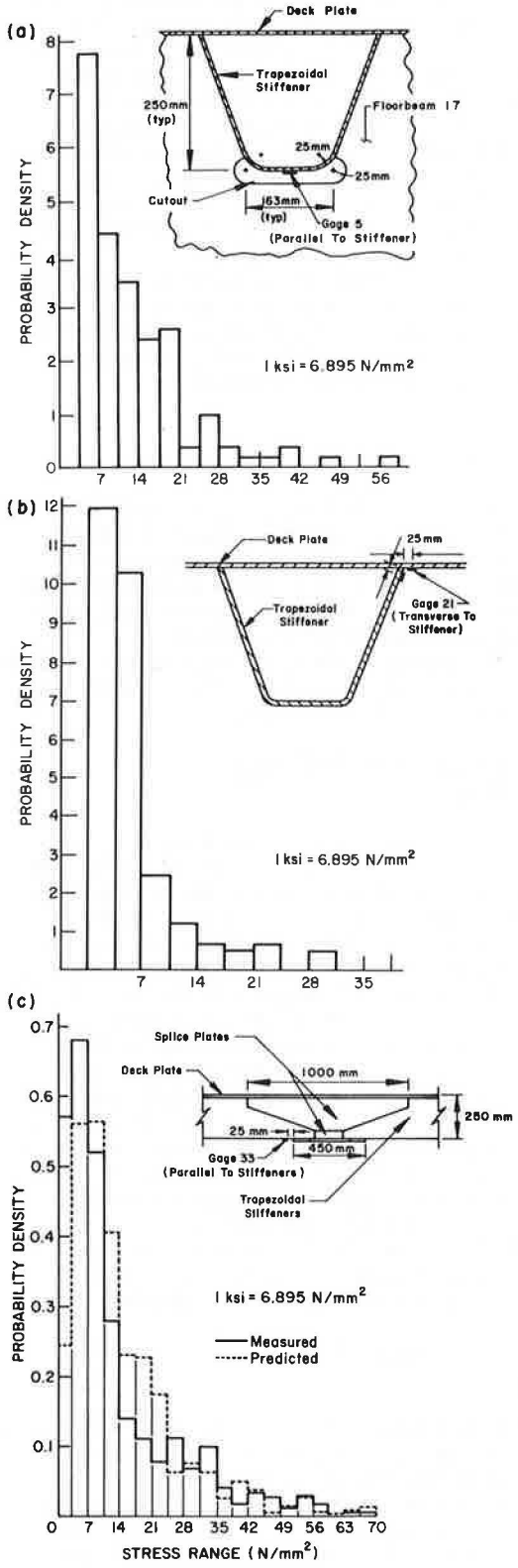

Figure 6. Distribution of axles for (a) 642 trucks, May 30 to June 5, 1974, and (b) 570 525 trucks, March 4, 1974, to May 31, 1975.

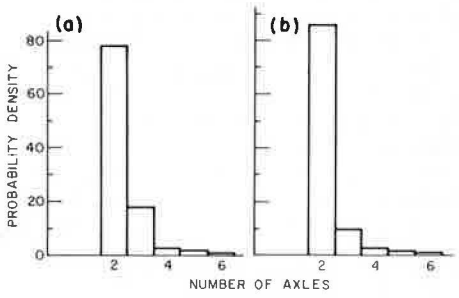

Figure 7. Maximum crawl and speed run stress ranges as a function of the lateral position of the front right tire of the test truck.

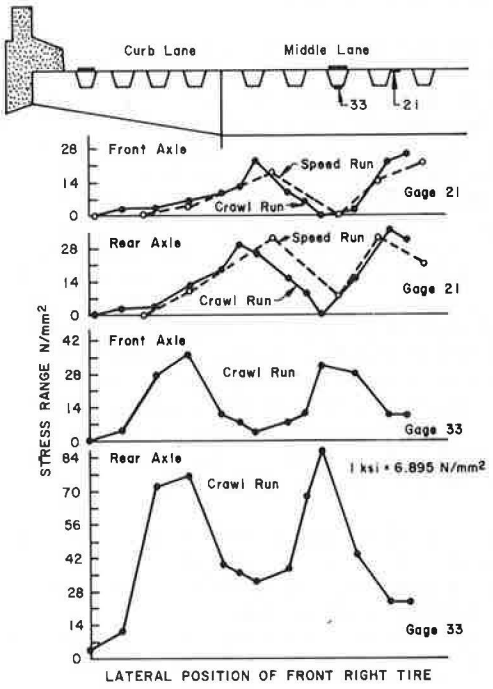

Figure 8. Distribution of axle and gross vehicle weights of (a) 128 axle groups and (b) 64 vehicles.

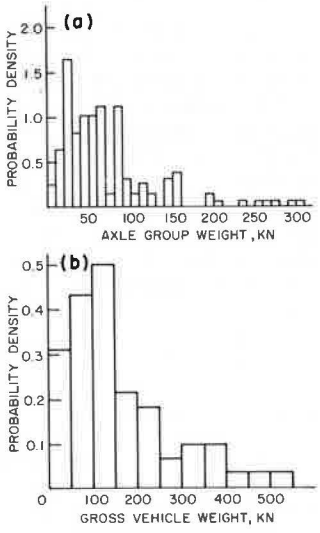

In Figure 8b, the gross vehicle weight distribution essentially exhibits two peaks (bimodal), indicating that a number of multiple-axle trucks at 300 to 400 kN (67 500 to 90 000 lbf) and a larger number of buses and two-axle trucks at 50 to 150 kN (11 200 to 33 700 lbf) may be expected. In Brazil, at present truck traffic at the higher load levels is not so frequent as it is in the United States. However, the observed frequency distribution can be used together with U.S. experience to estimate the probable future distribution of truck traffic over the bridge. Figure 9 shows the estimated average daily truck traffic (ADTT), both observed and projected volume. A rate of increase of 1.5 percent is assumed based on Fisher's experience (8), described in a paper in this Record. If all the main arteries leading to the bridge are assumed to be complete by 1984, a higher rate of increase (3 percent) should then be assumed.

ANALYSIS OF WELDED DETAILS FOR FATIGUE SUSCEPTIBILITY

The results of the field stress measurements were used to evaluate the fatigue behavior of several welded details in the orthotropic deck. To examine the adequacy of the measured stress range histograms (for example, Figure 5c), the lateral (lane) positions of trucks were used together with the axle group weight probability density (Figure 8a) and the influence line for stress range at gauge 33 (Figure 7) to construct the probability density function for stress range at gauge 33. The computed results shown in Figure 5c are in reasonable conformity with the measured stress range spectrum for gauge 33 shown by solid lines in the figure. This comparison indicates that the measured stress range spectra at all gauge locations are a reasonable estimate of the expected stress ranges generated by the truck traffic on the bridge deck.

An examination of the orthotropic deck showed three major details requiring investigation:

1. The end weld of the splice plate on the bottom of the trapezoidal stiffeners (near gauge 33),
2. The weld connecting the trapezoidal stiffeners to the floor beams (near gauge 5), and
3. The partial-penetration rib-to-deck weld between the deck plate and the trapezoidal stiffeners (near gauge 21).

End Weld of Splice Plate

The splice plate constitutes an attachment plate more than 30 cm (12 in) long, which places it in category E of the 1974 AASHTO fatigue provisions (8, 11).

Two methods were used to evaluate cumulative damage due to random application of stress range and its frequency of occurrence. One is the root mean square method (10, 12) in which the root mean square (RMS) of the stress ranges in a spectrum becomes the equivalent constant cycle stress range and is correlated directly with the number of stress cycles in the spectrum. The RMS stress range S_{rRMS} is defined as

$$S_{rRMS} = \sum(\alpha_i S_{ri}^2)^{1/2} \quad (1)$$

where α_1 is the frequency of occurrence of stress range S_{ri}.

An RMS stress range of 22 MPa (3200 lbf/in^2) was computed for the spectrum shown in Figure 5c. This value is shown in Figure 10 and compared with the constant cycle stress range data (S-N curve) from laboratory studies (10). Figure 10 shows that the (99 percent survival) fatigue strength will be reached in about 40 000 000 cycles. If, at this detail, a truck is assumed to produce one stress cycle, this corresponds to about 70 years if the current ADTT is maintained.

Two conditions suggest that the fatigue strength may be reached earlier. First, the ADTT probably will increase with time (Figure 9). Second, the frequency of occurrence of heavier trucks will probably increase. The latter will cause S_{rRMS} to increase over the life of the structure. If the ADTT increases at a constant annual rate of 1.5 percent, the fatigue strength will be approached in about 50 years; if the rate of increase is 3.0 percent after 1984, it will occur in about 40 years. Higher rates of growth will obviously decrease the time required to reach the fatigue strength.

The stress range histogram in Figure 5c can also be evaluated by using Miner's hypothesis for cumulative damage (13). By combining the relationships provided by constant cycle data and Miner's rule, an equivalent stress range S_{rMINER} can be estimated as

$$S_{rMINER} = \left(\sum \alpha_i S_{ri}^3\right)^{1/3} \quad (2)$$

This results in an equivalent stress range of 26 MPa (3800 lbf/in^2), which corresponds to about 20 000 000 cycles of constant cycle stress range as shown in Figure 10. This number of cycles will be reached in about 30 years based on the present frequency of truck traffic and an annual increase rate of 1.5 percent.

Based on the assumed rate of increase in truck traffic, both methods suggest that fatigue cracks might develop in about 30 to 40 years at this detail.

Connection of Trapezoidal Stiffeners to the Floor Beam

The trapezoidal stiffeners pass through the floor beams with cutouts as shown in Figure 5a. The floor beam web is fillet welded to the sloping sides of the stiffener. This detail is directly analogous to a transverse stiffener attached to the web of a girder. It constitutes a non-load-carrying connection and is classified as a category C detail by the current AASHTO fatigue specification (11).

As shown in Figure 5a, the highest recorded stress range in the bottom flange of the trapezoidal stiffener is about 59 MPa (8600 lbf/in^2). The RMS stress range of the stress spectrum is 17 MPa (2500 lbf/in^2); the Miner's equivalent stress range S_{rMiner} is 20.7 MPa (3000 lbf/in^2). The critical point for fatigue is the weld toe termination at the top of the cutout 25 mm (1 in) above the bottom surface. The stress range at this point is even lower. Since both values above are considerably less than the fatigue limit of 82.7 MPa (12 000 lbf/in^2) for category C details, no fatigue damage is expected at this connection, even with substantial increases in truck weights.

Connection of Trapezoidal Stiffeners to Deck Plate

Work in England on experimental orthotropic bridge deck panels showed that high compressive cyclic stresses transverse to the trapezoidal stiffener occur in the deck near the connection welds (3). This work led to an experimental program reported by Maddox (14). Studies were also made in the United States because of differing opinions on the requirements for the deck-to-stiffener connection. The resistance of full and partial penetration welds was examined (15).

The results of these studies are shown in Figure 11 where the bending stress range at the weld root is plotted

Figure 9. Estimated average daily truck traffic.

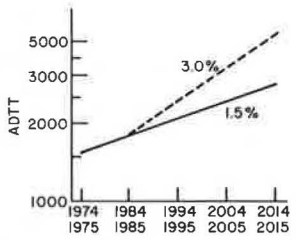

Figure 10. Fatigue strength estimated at end weld of splice plate near gauge 33.

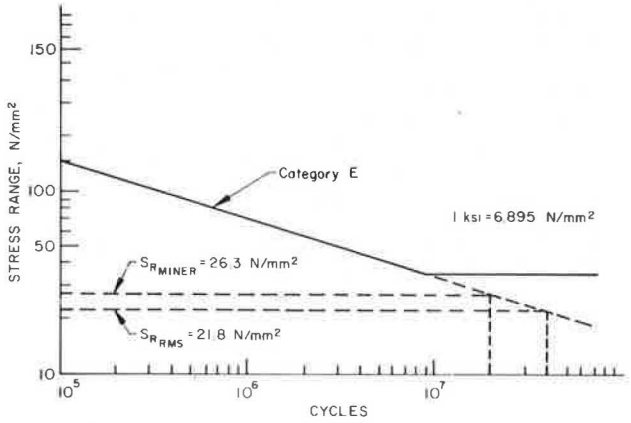

Figure 11. Fatigue strength estimate at connection of trapezoidal stiffener to deck plate at gauge 21.

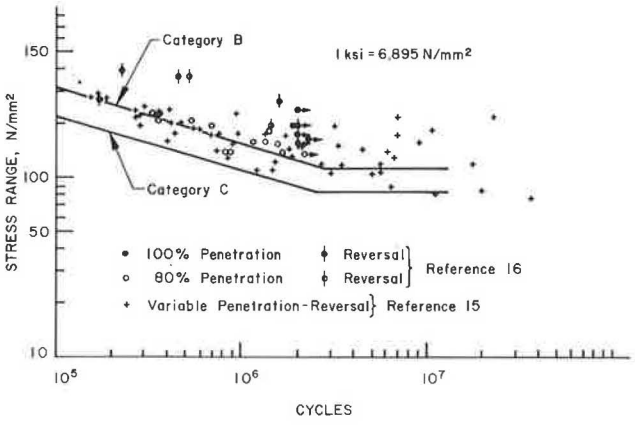

Figure 12. Enlarged etched cross sections of trapezoidal stiffener web to deck plate connection.

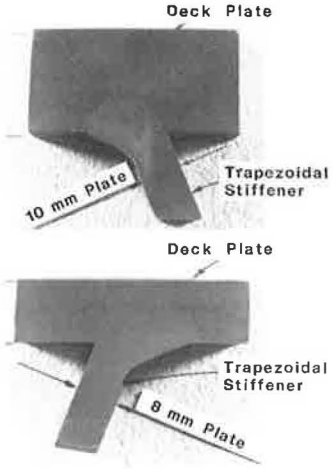

as a function of fatigue life. A comparison of the data points with current AASHTO design curves indicates that category C provides a reasonable lower bound to the test data. Maddox noted that results providing higher fatigue strength generally result from compressive stress at the weld root or the absence of tensile residual stress. This is particularly noticeable with the reversal specimens reported by Seim and Ferwerda (15). It is apparent that the full stress range is not effective in these specimens. The residual tensile stresses in the orthotropic deck of the Rio-Niteroi bridge should be high enough that the category C fatigue strength should realistically model the expected fatigue behavior.

Figure 12 shows etched cross sections of the stiffener to deck plate connection near floor beam 17 showing partial penetration welds. The average ratio of weld throat thickness to the sloping web plate thickness is 0.83. Hence, for bending moment about an axis parallel to the weld, flexural stress in the weld throat is about $(1/0.83)^2 = 1.45$ times greater than the web plate stress. Because of flexural stress gradient in the stiffener web between the weld and the bottom of the stiffener, the stress recorded at gauge 21 (Figure 6a) must be adjusted upward to provide the stress range at the weld. Because only a single gauge was attached to the surface of the stiffener, the stress gradient cannot be adjusted to account for stress gradient through the web plate thickness. However, based on the gauge location and the plate geometry, the stress at the weld was estimated to be about 15 percent higher than that at gauge 21. The weld throat stress therefore is about $1.15 \times 1.45 = 1.67$ times the stress in the stiffener at gauge 21.

The stress range spectrum for gauge 21 shown in Figure 5b is typical for stiffener webs in the vicinity of floor beam 17. In Figure 5b, the maximum stress range is about 32 MPa (4600 lbf/in^2) and S_{rRMS} is about 18 MPa (2600 lbf/in^2). At all locations of measurement, the maximum stress range seldom exceeded 33.8 MPa (4900 lbf/in^2); a single measured stress was 42 MPa (6100 lbf/in^2). Thus, on the average the adjusted maximum stress range on the weld throat is about 69 MPa (10 000 lbf/in^2), which is less than the fatigue limit shown in Figure 11. No failure should occur at any of the stiffener-to-deck plate connections because of transverse stress range. Even if heavier vehicles in the future generate occasional stress ranges exceeding the fatigue limit of the connection, the low value of RMS stress range (less than 40 MPa or 5800 lbf/in^2) suggests that no fatigue damage should occur throughout the life of the structure.

CONCLUSIONS AND RECOMMENDATIONS

A study of the stresses at selected locations of the orthotropic steel deck of the Rio-Niteroi bridge under a test truck of known weight and under random truck traffic indicates that the deck should provide satisfactory service throughout its life. However, the splice detail on the trapezoidal stiffener may have the potential for fatigue crack growth.

Specific conclusions developed from this study follow.

1. The observed stress range spectra at the welded details exhibited the same basic characteristics of those at welded details of many other highway bridges. The stress range spectra are highly skewed, which is comparable to the axle group load spectrum.
2. The strains developed in the orthotropic steel deck are essentially the same under static and moving traffic.
3. The bimodal distribution of truck and bus traffic exhibits the same characteristics as truck traffic in the

United States although the frequency of heavier trucks is currently not so great in Brazil.

4. Given the lateral position of traffic, the frequency and loading of trucks, probably only one stress cycle is significant in the fatigue analysis.

5. End welds of the trapezoidal stiffener splice plates are subjected to stress cycles that exceed the fatigue limit. At the current rate of loading visible fatigue damage may occur in about 30 to 40 years. If the frequency of heavier loads increases, such cumulative damage may occur at an earlier date.

6. There is little probability of fatigue damage to the partial penetration stiffener-to-deck plate welded connections. When fatigue cracks are detected then retrofitting by welding (16) could be effected. Very few of the random stress cycles exceed the fatigue limit.

7. There is little probability of fatigue damage to the stiffener-to-floor beam connections.

ACKNOWLEDGMENTS

The field study described in this report was performed in Brazil by the staff of Fritz Engineering Laboratory, Department of Civil Engineering, Lehigh University. L. S. Beedle is director of the laboratory. D. A. Van Horn is chairman of the Department of Civil Engineering. The study was originally financed by S. A. Empresa de Construção e Exploração da Ponte President Costa e Silva, later renamed Empresa de Engenharia e Construção de Obras Especiais.

The authors wish to thank H. T. Sutherland for preparing all instrumentation, W. C. Herbein and R. P. Batcheler for assistance in preparing the manuscript, Antoinette Larkin for typing the manuscript, and J. M. Gera and R. N. Sopko for preparing the figures.

REFERENCES

1. Steel Box Girder Bridges: Ultimate Strength Considerations. Journal of Structural Division, Proc., ASCE, Vol. 100, No. ST12, Proc. Paper 11014, Dec. 1974.
2. A. Ostapenko and others. A Study of the President Costa e Silva Bridge During Construction and Service (Steel Structure). Fritz Engineering Laboratory, Lehigh Univ., Bethlehem, Penn., Rept. 397.6, 1976.
3. D. E. Nunn and S. A. H. Morris. Trials of Experimental Orthotropic Bridge Deck Panels Under Traffic Loading. U.K. Transport and Road Research Laboratory, Crowthorne, Berkshire, England, TRRL Rept. LR 627, 1974.
4. J. W. Fisher and I. M. Viest. Fatigue Life of Bridge Beams Subjected to Controlled Truck Traffic. International Association of Bridge and Structural Engineering, 7th Congress, Preliminary Publ., 1964.
5. G. R. Cudney. The Effects of Loading on Bridge Life. HRB, Highway Research Record 253, 1968, pp. 35-71.
6. C. F. Galambos and C. P. Heins, Jr. Loading History of Highway Bridges: Comparison of Stress-Range Histograms. HRB, Highway Research Record 354, 1971, pp. 1-12.
7. F. Moses. Truck Loading Model for Bridge Fatigue. Proc., Specialty Conference on Metal Bridges, ASCE, Nov. 1974.
8. J. W. Fisher. Guide to 1974 AASHTO Fatigue Specifications. American Institute of Steel Construction, 1974.
9. J. W. Fisher, P. A. Albrecht, B. T. Yen, D. J. Klingerman, and B. M. McNamee. Fatigue Strength of Steel Beams With Transverse Stiffeners and Attachments. NCHRP, Rept. 147, 1974.
10. J. W. Fisher, K. H. Frank, M. A. Hirt, and B. M. McNamee. Effect of Weldments on the Fatigue Strength of Steel Beams. NCHRP, Rept. 102, 1970.
11. Interim Specifications—Bridges. Subcommittee on Bridges and Structures, AASHTO, 1974.
12. C. G. Schilling, K. H. Klippstein, J. M. Barsom, and G. T. Blake. Fatigue of Welded Steel Bridge Members Under Variable-Amplitude Loading. NCHRP, Research Results Digest 60, April 1974.
13. M. A. Miner. Cumulative Damage in Fatigue. Journal of Applied Mechanics, Vol. 12, Sept. 1945.
14. S. J. Maddox. The Behavior of Trapezoidal Stiffener to Deck Plate Welds in Orthotropic Bridge Decks. U.K. Transport and Road Research Laboratory, Crowthorne, Berkshire, England, TRRL Rept. SR 96 UC, 1974.
15. C. Seim and R. Ferwerda. Fatigue Study of Orthotropic Bridge Deck Welds. Division of Highways and Division of Bay Toll Crossings, California Department of Public Works, Rept. M&R 666473, 1972.
16. J. W. Fisher, M. D. Sullivan, and A. W. Pense. Improving Fatigue Strength and Repairing Fatigue Damage. Fritz Engineering Laboratory, Lehigh Univ., Bethlehem, Penn., Rept. 385.3, Dec. 1974.

Design of the Rio-Niteroi Bridge

H. J. Graham, Howard, Needles, Tammen and Bergendoff, Jacksonville, Florida

A brief overview is presented of the design of the highway bridge linking Rio de Janeiro and Niteroi, which was completed and opened to traffic in 1974. The main navigation spans contain a record girder span of 300 m in length. Inasmuch as the design of long span bridges cannot be separated from their erection, a brief description of the bridge erection is also included.

The cities of Rio de Janeiro and Niteroi, on the eastern coast of Brazil, are separated by the Guanabara Bay (Figure 1). The bay, bordered by mountains rising precipitously from the beaches, forms both an excellent harbor and a formidable barrier to transbay commerce and the expansion of Rio. Before the bridge crossing was completed in 1974, motorists had to choose either a lengthy wait for a vehicular ferry or a 90-km drive skirting the bay.

Serious planning for a crossing of Guanabara Bay was started in 1963. In 1967-68 a feasibility study sponsored by the U.S. Agency for International Development was carried out by a consortium of Brazilian and American engineers. This work included studies of location, tunnel crossings, alternative bridge types, traffic and revenue projections, and cost estimates. A toll project was recommended.

The crossing adopted was a six-lane high-level 13.3-km-long bridge (Figures 2 and 3). Of this length, 8.8 km is over water, and, at the location of the main spans, it is 22 m deep.

Opened to traffic in March 1974, the bridge forms an important link in Brazil's National Highway BR101 that will connect its principal coastal cities and ultimately will extend from Osorio to Natal. Traffic and revenues have thus far substantially exceeded projections.

OVER-WATER APPROACHES

The over-water approach spans consist of twin precast posttensioned concrete box girders (Figure 4). A constant span length of 80 m is used for the continuous spans. Expansion joints are provided 20 m from the piers in every fifth or sixth span. The structure depth is 4.7 m.

The piers for the approach structure are of cellular reinforced concrete and rest on footing blocks near the water surface and on 2-m-diameter reinforced concrete piles reaching to competent founding strata below water.

Precast concrete segments were cast in a yard, barged to the site, and lifted to the final position. Three basic types of precast elements were used: support sections over the piers, normal sections, and hinge sections at the expansion joints.

Segments were erected in pairs by traveling gantries and posttensioned in place; the sequence was repeated until the span projected 40 m on each side of a pier axis. The gantries then moved to the next span and the process was repeated. Concrete was added at the midspan joints; positive moment tendons were inserted, stressed, and grouted; and the span was made continuous. Four traveling gantries were used in the erection of the approach spans.

MAIN NAVIGATION SPANS

Site Constraints

Sited in 22 m of water, the main spans were required to provide 60 m of vertical clearance for navigation without encroaching into the aviation space for aircraft approaching the international and domestic airports at Galleao and Santos Dumont. Because of the 72.4-m maximum height of the fixed structure above sea level and the necessary vertical clearance, only a girder type of bridge was considered.

The selected structure is a three-span continuous steel box girder with spans of 200, 300, and 200 m (Figures 5 and 6). The 300-m main span is the longest unstayed girder span in the world, surpassing the length of its nearest rival by 39 m. The 30-m end cantilevers and 44-m suspended spans complete the 848-m-long steel structure, which makes a smooth transition to the concrete approach spans. The depth of the structure varies from 4.75 m at the juncture with the concrete structure to 13 m at the main piers to 7.5 m over the navigation

Publication of this paper sponsored by Committee on Steel Bridges.

channel. For erection, the superstructure was divided into pieces of 44, 292, 176, 292, and 44 m.

Main Piers

The main channel piers (Figure 7) are supported on forty 1.8-m-diameter reinforced concrete piles that are drilled into bedrock 50 to 60 m below sea level. Under each end pier, 32 piles are used.

Figure 1. Location plan.

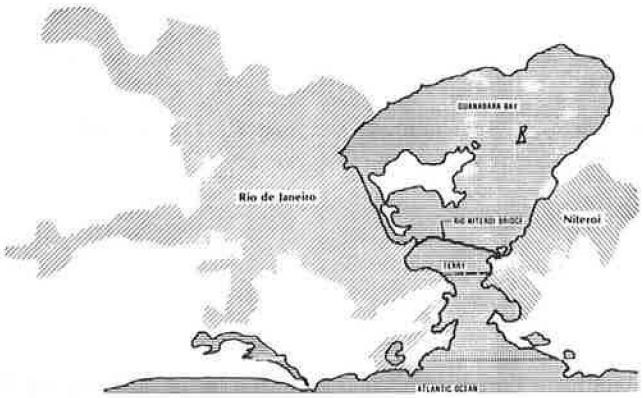

Figure 2. Northwest view of Rio-Niteroi bridge.

Figure 3. East view of Rio-Niteroi bridge.

Design loads for the piles were 650 Mg per pile for dead plus live load and dead load plus 118 Mg of horizontal load at ultimate (4700 Mg per main pier for ship impact).

Massive reinforced concrete footing blocks, extending from 2.5 m below to 2.5 m above sea level, rest on the large piles and support twin tapered hollow box pier shafts. The top of the end pier shafts is 59.96 m above sea level while the top of the main channel piers is at an elevation of 56.44 m.

The twin hollow pier shafts are each a constant 6.86 m wide (transverse to the bridge) and have variable thickness (parallel with the bridge). The walls, which are uniformly 65 cm thick, were constructed with slip forms. The piers are capped with solid blocks 3 m deep.

The depth of the bay at the main piers varies between 21 and 22 m. The 1.8-m-diameter piles were constructed by using large jack-up islands incorporating floats manufactured in Brazil, legs manufactured in Holland, tubes and drills manufactured in Germany, and large-capacity cranes manufactured in the United States. Each island

Figure 4. Main spans.

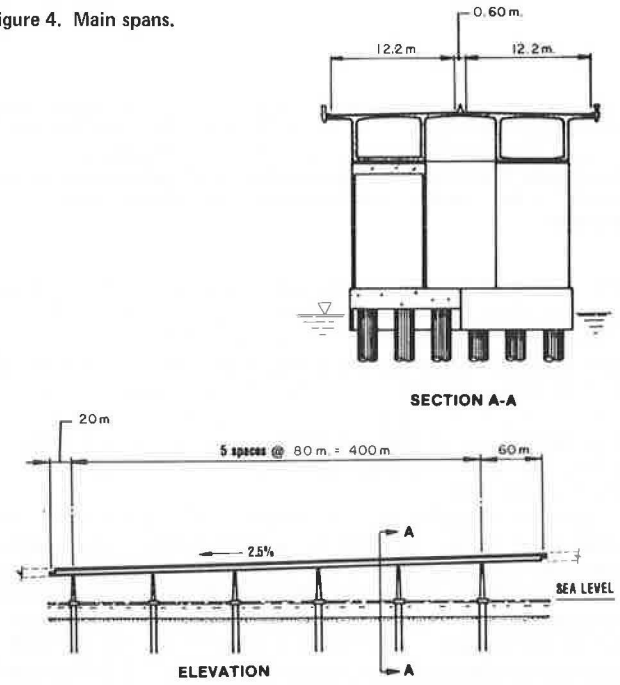

Figure 5. Prestressed box girder approach spans.

was equipped with two drills and ancillary equipment so that two piles could be constructed simultaneously. The procedure for constructing a pile is described below.

1. The 2.2-m inside diameter oscillating tube and 2.0-m outside diameter drill were advanced into the sea bottom until the cutting teeth of the tube reached refusal in residual soil or decomposed rock. Cuttings were removed by reverse circulation of water through the drill stem.
2. Drilling was continued until it penetrated about 1 m into solid rock.
3. The hole was cleaned out by reverse circulation of water through the drill stem, and then it was inspected by a diver.
4. A 10-mm thick, 1.8-cm inside diameter casing was lowered through the tube until its lower edge was about 60 cm above the bottom of the hole. The casing was held in this position from above.
5. Reinforcing cages were lowered into the casing, supported from above, and the casing was filled with high-quality tremie concrete. Concrete was added to well above the bottom of footing.
6. To remove it, the tube was oscillated while sand was placed in the space between the outside of the casing and the inside of the 2.3-m hole formed by the tube.

When all the piles were complete for a pier, concrete boxes made of cast-in-place bottom slabs and precast walls were lowered over the piles, sealed, and pumped out. The casings were removed to an elevation -2.4 m, concrete in the piles was removed to sound concrete, reinforcing was placed, and concrete was added to footing blocks in the dry (generally in three lifts). The pile reinforcing extended 4.8 m into the footing so that the pile heads would be rigidly fixed in the footings and the pier would have added stability.

Figure 6. Elevation of main spans.

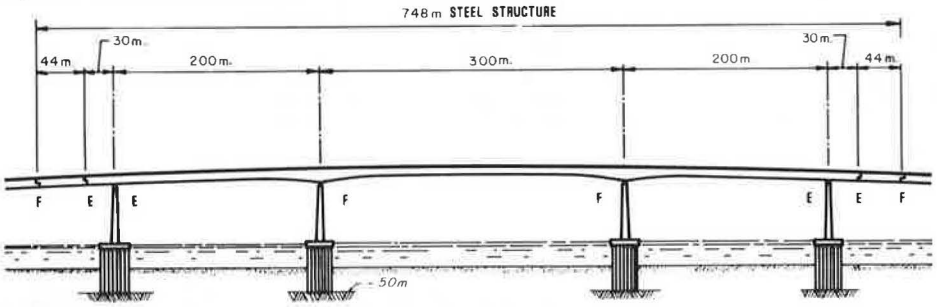

Figure 7. Main channel piers.

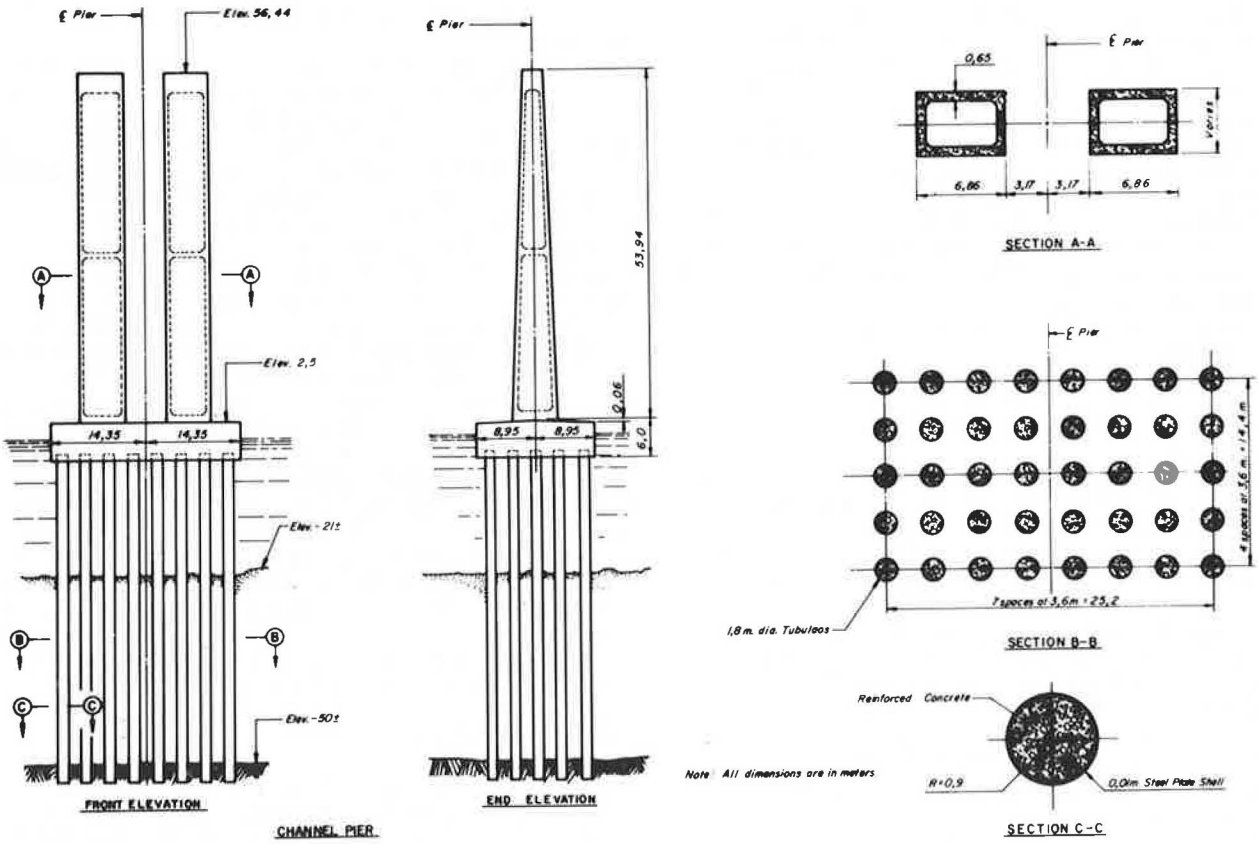

Figure 8. Navigation spans: cross section and typical details.

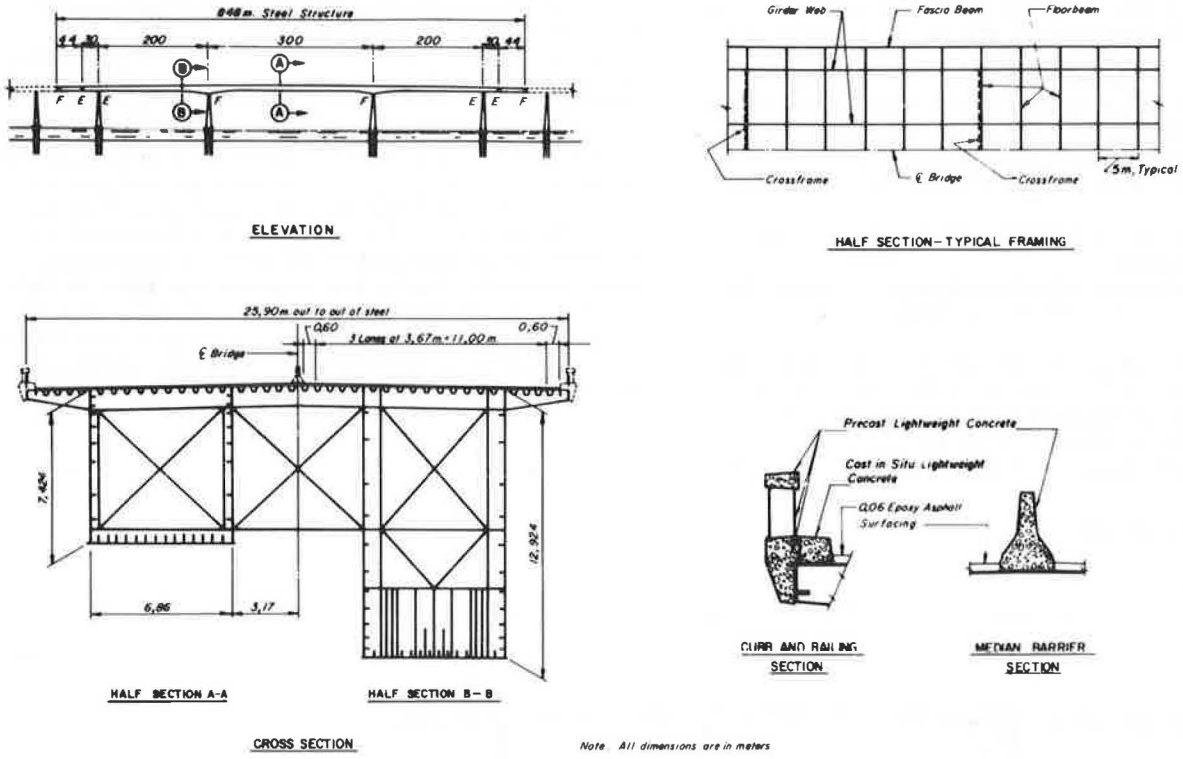

Main Superstructure

The two 12.2-m-wide roadways are supported on a pair of steel boxes centered 13.2 m apart (Figure 8). A central barrier, curbs, railings, and an epoxy asphalt wearing surface complete the traffic roadways.

The orthotropic steel deck is comprised of plates varying between 10 and 25 mm thick and is stiffened with 25-cm-deep trapezoidal ribs 8 to 12 mm thick spaced on about 60-cm centers.

Lower flanges varying from 10 to 45 mm thick are 6.89 m wide and are stiffened by steel plates or bulb flats on 46-cm centers. Stiffener size varies as required by stress or buckling stability or both.

Vertical webs vary between 12 and 18 mm thick and are stiffened with 20-cm-deep bulb flats whose number and spacing are as required for buckling stability.

Transverse floor beams and vertical stiffeners are spaced at 5-m intervals. Cross frames, internal and between boxes, are provided at 30-m spacings.

Three grades of weldable steels, conforming to British Standard 4360 (1968), were used. Yield strengths were 250, 350, and 440 N/mm^2 for grades 43A, 50, and 55 respectively.

The steel superstructure was designed to accommodate the contractor's fabrication and erection scheme. The steel was fabricated in England in 15 by 3.5-m modules, shipped to Brazil, and assembled into full-size boxes in a zero stress cambered shape on cribbing on land.

The two 172.6-m boxes composing the center (pontoon) unit were fabricated side by side, connected together, skidded sideways over storage jetties, and ultimately lowered into the water to form a transport barge for the side span pieces. These units were provided with several watertight bulkheads for safety against sinking and for control of water ballasting during subsequent erection uses.

Next, the two Niteroi side span boxes, each 293.71 m long, were assembled side by side on cribbing, and the centerline connections were fitted. They were jacked up off the cribbing and skidded one box at a time out on the storage jetties. This operation was repeated for the identical Rio side span pieces.

The 44-m spans were assembled on a slipway, fitted with end bulkheads, and launched into the water as pontoons.

Temporary jacking columns were erected alongside the pier shafts, and large temporary ring girders were assembled on top of the pier footings. The side span pieces were floated out (one box at a time) on the pontoon unit and set on the ring girders. They were then jacked to the top of the piers by using twelve 450-Mg jacks, skidded laterally on Teflon skids on the ring girders over the tops of the piers, and placed on the shoes. The total weight lifted, including erection gear, was about 5280 Mg. The jacking operation required 3½ days for the Niteroi side spans and 3 days for the Rio side spans.

The center span was hoisted by using 8 of the 12 jacks and four of the six jacking columns. For this operation the columns were in tension whereas the side spans were in compression. The weight of the center piece was about 3200 Mg (3600 Mg including erection gear).

The 44-m end spans weighing 225 Mg/box were floated to the site and lifted one box at a time by using jacking frames and wire rope tackle.

Precast curb and parapet and median sections of lightweight concrete match the dimensions of those on the approach spans. These are securely anchored to the steel work.

The 6-cm-thick surfacing for the steel deck was of epoxy-asphaltic concrete and was placed in two lifts.

DESIGN CRITERIA

The concrete elements of the bridge were designed to conform to the applicable Brazilian norms. Because no specifications existed for the design of orthotropic steel

deck girders, special criteria were developed. In general, these criteria resulted from a combination of the recommendations of the American Institute of Steel Construction (1) and European practice. The specified theoretical margins of safety against yielding and buckling were slightly higher than those contained in Brazilian and European steel design norms (in accordance with AASHTO specifications).

Design traffic live load was class 36 as given in Brazilian Norm NB-6. For the main steel spans, this loading of 4.26 Mg/m/box resulted in main girder live load moments about 1.8 times as large as those from AASHTO HS-20 loading.

Because no applicable Brazilian norms existed for designing for fatigue in steel highway bridges, AASHTO specifications and loadings were used.

DESIGN METHODS

Concrete Elements

Ultimate design methods were used in the design of the reinforced and prestressed concrete elements of the bridge.

Steel Structure

For the main steel superstructure a working stress design was performed, although some elements, e.g., girder webs and vertical stiffeners, were checked for ultimate strength.

Local traffic stresses in the stiffened deck plate, longitudinal ribs, and transverse floor beams were computed by methods given by Troitsky (2), Sievers (3), and Pelikan and Esslinger (4).

In the design of stiffened plates subjected to compressive or shearing stresses, the buckling stability was investigated for each element in the assembly as well as for the complete assembly. In general, the computations of plate stability were based on the classical elastic plate buckling theories as specified by German Industrial Norm 4114.

When the computed buckling stress of a given element or assembly exceeded the elastic limit of the material, the critical stress was reduced so as not to exceed the yield stress.

In the evaluation of the elastic buckling stresses of the multiple stiffened plate panels of the main girder flanges and webs, extensive use was made of the charts and tables given by Kloeppel and coauthors (5, 6).

Stresses in the intermediate cross frames due to asymmetrical transverse loads were calculated by Homberg's method and checked by the Guyon-Massonet-Sattler method as described by Kuzmanovic (7).

Checks were made for variations in temperature of 15°C below and 30°C above a normal temperature of 24°C. Further, the difference in temperature between a structural member exposed to sunlight and another in shade was assumed as 15°C.

Erection Forces

The contractor's planned erection methods were known at the time of the actual final design. Thus, the moments and shears in each major piece were computed for each stage of its erection, and the structural stability was investigated for the critical stages.

For the 172.58-m-long center span section, the stages investigated were

1. When supported on swan necks at the site fabrication yard thus spanning 192 m while loaded with its own dead load and distributed erection gear;
2. When serving as a floating pontoon and loaded with its own dead load, the weight of erection gear, ballast water, and the weight of a 293.7-m-long side span piece; and
3. While being lifted into final position.

The 293.7-m-long side pieces were investigated for the following stages:

1. While spanning 192 m between the jetties on Caju Island and loaded with dead load plus erection gear,
2. While spanning 110 m between the trestle supports on the pontoon unit,
3. While spanning 200 m between piers, and
4. While spanning 200 m between piers and supporting the weight of the pontoon unit and erection gear during the lifting of the center span.

In addition, the stability of the pontoon-side span combination was investigated for wind and waves when the pieces were floated out.

Although, in general, the dimensioning of the structure was controlled by in-service stresses, additional stiffening for erection was provided at all temporary support points, and additional cross frames were provided between the pontoon boxes to distribute the concentrated reaction of a side span piece to both boxes of the pontoon.

Camber

The computed deflection of the center span under the full design live load (4.26 Mg/m/box) is 0.82 m while that of a 200-m side span is 0.56 m downward and 0.47 m upward. The computed maximum live load deflection at the joint between the 44-m-long suspended span and the 30-m-long cantilever is 0.30 m downward and 0.32 m upward.

The main steel girders were fully cambered throughout their length for dead load deflections. During erection, a substantial weight of erection gear was acting at the end of the 63.7-m temporary cantilevers in the 300-m spans. So that the end slopes of each piece would match at the bolted splices, the structure was cambered in space so that these slopes would match when the girders were resting on the piers and erection gear was in place. By this means excessive temporary raising or lowering of girder ends during closure of the bolted splices was precluded and built-in angle breaks were avoided at the splices.

ACKNOWLEDGMENTS

The Rio-Niteroi bridge, now called Ponte Presidente Costa e Silva in honor of a former Brazilian president, is a project of the Brazilian Ministry of Transport administered through the National Highway Department (DNER) and S. A. Empresa de Construção e Exploração da Ponte Presidente Costa e Silva (ECEX). Mario Andreazza was minister of transport; Eliseu Resende was director of DNER; and Joao Carlos Guedes was director-president of ECEX.

REFERENCES

1. Design Manual for Orthotropic Steel Deck Bridges. American Institute of Steel Construction, 1963.
2. M. S. Troitsky. Orthotropic Bridges—Theory and Design. The James F. Lincoln Arc Welding Foundation, Cleveland, 1967.
3. H. Sievers. Vereinfachte Berechnung der orthotropen Fahrbahnplatte mit Hohlrippen. Der Stahlbau, No. 10, 1968.

4. W. Pelikan and M. Esslinger. Die Stahlfahrbahn Berechnung und Konstruktion. Maschinenfabrik Augsburg-Nuernberg AG, Augsburg, West Germany, 1957.
5. K. Kloeppel and J. Scheer. Buelwerte ausgesteifter Rechteckplatten. Verlag von Wilhelm Ernst und Sohn, Berlin-Wilmersdorf, West Germany, 1960.
6. K. Kloeppel and K. H. Moeller. Buelwerte ausgesteifter Rechteckplatten, Volume 3. Verlag von Wilhelm Ernst und Sohn, Berlin-Wilmersdorf, West Germany, 1968.
7. B. O. Kuzmanovic. Some Design Problems of Large Box Girder Bridges. Journal of Structural Division, Proc., ASCE, Sept. 1972.

Rio-Niteroi Bridge: Thermal Field Studies

A. Ostapenko, Lehigh University

One side span of the three-span (200, 300, 200 m) continuous steel box girder bridge in Rio de Janeiro was instrumented for measuring strains and temperature during construction and in service. Electrical, mechanical, and scratch gauges were used. The field measurements, conducted in winter and summer, show that the daily temperature increase is the largest from 6:30 a.m. to 3:00 p.m. The high temperature change in the top flange drops within 0.30 m by as much as 13 to 15°C and then remains essentially constant in the rest of the cross section. A computer program was developed for generating a complete thermal field in the bridge from the temperatures specified at two cross sections and for performing thermoelastic analysis. The highest thermal stress was found to be 14.2 MPa. Recommendations are made for a temperature change pattern to be used in design of steel bridges under the Rio de Janeiro conditions and for the intensification of research in the United States on thermal effects in bridge structures.

Most commonly the effect of temperature on bridge girders has been considered by providing adequate travel at the expansion joints and bearings. The temperature gradient from the top of the roadway to the bottom fiber of the girder has generally been considered to be linear. Most specifications permit greater allowable stresses when the effect of temperature is included (1). Probably the most important consequence of temperature effects is the deformations, which must be accurately considered in construction. It is only recently that engineers have begun to give attention to the thermal phenomena and that a worldwide trend has developed toward better understanding of the behavior and strength of bridges.

Field measurements of temperature distribution have been conducted mainly on prestressed concrete bridges but also on some steel and composite bridges (2). A theoretical approach has been proposed for computing the temperature distribution in a bridge girder from the ambient conditions (3). These studies have shown that the temperature in a bridge cross section may deviate considerably from the linear pattern usually assumed in design. Reactions of a continuous concrete girder were measured in France as recently as 1975. When a simplified version of the method developed by Emerson (3) was used to calculate thermal stresses from these reactions, the stresses were found to be of potential intensity to induce cracking of concrete (4). Analysis of a small concrete model tested under a thermal load gave good correlation with theory (5). Some sample concrete bridges were also analyzed for thermal conditions in North America (6).

Although the differential equations and principles of thermoelastic analysis are well established, their application to bridge girders is hampered by the complexity of the cross sections, uncertainties of thermal material properties, uncertainty about the surface interaction of the structure, air, and sun rays, and uncertainty about the actual temperature and wind conditions. The problem is unmanageable unless many approximations and simplifying assumptions are made, and therefore the validity of such analyses cannot be accepted unless the results are confirmed by field measurements of the actual temperature distribution in bridge girders. However, only a few and very limited measurements have been conducted so far (2).

The instrumentation program of the Rio-Niteroi bridge (Ponte Presidente Costa e Silva) in Brazil presented an opportunity for obtaining extensive temperature and strain data on a steel box girder bridge of unprecedented dimensions (7, 14).

RIO-NITEROI BRIDGE AND SCOPE OF FIELD STUDIES

The Rio-Niteroi bridge joins the cities of Rio de Janeiro and Niteroi over the Guanabara Bay and has an overall length of 13 km with 8.5 km over water. Most of the bridge is composed of 80-m prestressed concrete spans of segmented construction. Portions continuous over five spans are provided with expansion joints. Except in the overland approaches, the bridge has a uniform twin-box cross section. The main shipping channel is bridged by a three-span continuous steel box girder of a matching twin-box cross section but of a variable depth. This steel girder has two 200-m side spans and a 300-m center span, which is the longest in the world for unstayed box or plate girder bridges.

Publication of this paper sponsored by Committee on Steel Bridges.

Figure 1. Location of instrumented sections in Rio de Janeiro side span.

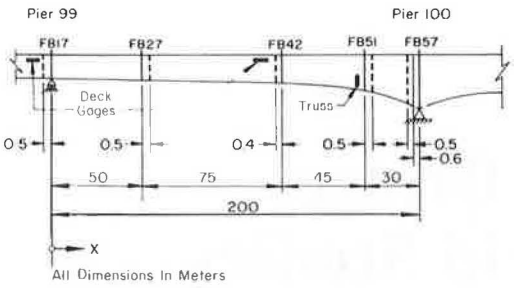

Figure 2. Wiring system for static readings on completed bridge.

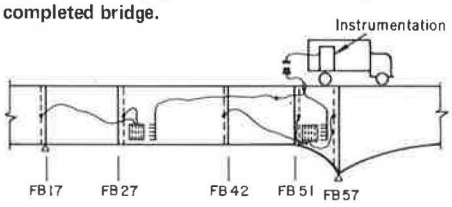

A special bridge authority, S. A. Empresa de Engenharia e Construção de Obras Especiais (ECEX), originally named S. A. Empresa de Construção e Exploração da Ponte Presidente Costa e Silva, was charged by the Brazilian department of highways (DNER) with the planning and construction of the whole bridge (7). As described by Graham in a paper in this Record, structural design and construction supervision of the steel part of the bridge were carried out by an American engineering firm (8). The steel girders were fabricated in large panels in Great Britain and then shipped to Rio de Janeiro. There, the panels were assembled and erected by the joint venture of three companies, two of Great Britain and one of Brazil (9, 10, 11).

Many novel aspects of both the concrete and the steel portions of the bridge made it advisable to conduct a field investigation during and after construction. Laboratorio Nacional de Engenharia Civil (Portugal) was contracted for the concrete portion and Lehigh University for the steel portion (7, 12).

The principal parts of the field study on the steel bridge were as follows:

1. Monitoring of some selected stress points during construction for deviations from computed values,
2. Measurement of stresses during construction over full cross sections,
3. Measurement of stresses under test loads on the completed bridge,
4. Study of stresses in the orthotropic deck under regular traffic conditions, and
5. Study of the temperature distribution and its effects on the bridge.

The thermal study (item 5) is reported here.

INSTRUMENTATION OF STEEL STRUCTURE

Location of Instrumented Sections

The instrumentation on the steel portion of the bridge consisted of electric resistance gauges (strain and temperature), a mechanical gauge, and scratch gauges. The instrumentation was installed in the Rio de Janeiro side span primarily because of the logistics of construction at the time when the field work on instrumentation was started in September 1973.

Figure 1 shows the location of the instrumented sections. The view is from the south with the 300-m center span adjoining on the right. The five instrumented cross sections are indicated by the vertical dashed lines positioned to the right or left of the cross sections labeled FB17, FB27, FB42, FB51, and FB57 (the floor beams in the orthotropic deck). The sections at FB27 and FB57 have strain and temperature gauges; the sections at FB17, FB42, and FB51 have only strain gauges. Strain gauges were also placed in the north box on the components of the orthotropic deck at FB17 and FB42 (labeled deck gauges in Figure 1) and on the truss reinforcing the bottom flange at FB51.

Electric Resistance Gauge System

The electric resistance gauges consisted of (a) 52 longitudinal strain gauges parallel to the girder axis, (b) 82 transverse strain gauges prependicular to the girder axis, mainly for measuring bending strains in the transverse stiffeners and floor beams, (c) 57 three-gauge strain rosettes 45 deg to each other for measuring shearing and principal stresses ($57 \times 3 = 171$ single-gauge equivalents), and (d) 52 temperature gauges. Thus, total single-gauge equivalents were 422. This number included 8 longitudinal gauges, 36 transverse gauges, and 7 rosettes (21 single-gauge equivalents) used for the dynamic strain readings in the orthotropic deck (13). The remaining 357 single-gauge equivalents were read statically in four groups by using an automatic data acquisition unit with 100 channels.

A schematic of the wiring system used for making the static readings of the 357 strain and temperature gauges on the completed bridge is shown in Figure 2. The cables leading from the gauges at FB17 and FB27 were assembled on a switching panel at FB27 and from FB42, FB51, and FB57 on a switching panel at FB51. For taking readings, one-quarter of the gauges at each switching station were connected to the cables leading to a set of plugs housed in a special junction box installed in the concrete curb near FB51. The data acquisition unit was housed in a truck and plugged into the junction box.

To minimize inaccuracies, the switching from one group of gauges to another was accomplished by soldering. When it was desirable to take readings in quick succession, as many as 76 strain and 14 temperature gauges were left connected continuously.

Sections Instrumented for Temperature Readings

The cross sections chosen for mounting temperature gauges were at FB27 and FB57. As shown in Figures 1 and 2, the section at FB27 has an average depth of 6.34 m, is within the span, and thus is subjected to the cooling effect of wind. The other section at FB57 is the deepest one in the bridge (13.04 m), has a large mass, and is partially shielded from the direct effect of wind by the turbulence created by the pier shafts below it. Thus, the thermal conditions at these two sections were expected to be most contrasting.

The temperature gauges were of the electric resistance type and were read by using the same equipment as used for strain gauges. In addition to temperature gauges, a few thermocouples were also installed in the girder, but essentially all of them were damaged during construction and no systematic readings could be taken.

Mechanical Gauge System

Mechanical and scratch gauges provided alternate backup systems to the electric resistance gauges and supplied some additional information on the behavior of the bridge.

In the mechanical gauge system, the distance between two small target holes predrilled at a series of locations in the bridge girder was measured by means of a special mechanical gauge. The difference between two readings taken at different times at a particular location divided by the distance between the two target holes gave the strain change produced by a change in loading and temperature between the readings. A total of 83 locations were prepared for these readings.

By using a standard temperature-stable reference bar, the errors that may have been introduced by the variation in the adjustment of the mechanical gauge were eliminated, and two sets of readings taken at a considerable time interval—days, weeks, or months apart—could be directly compared. Thus, unlike the electric gauges, the mechanical gauge provided a means for measuring strain changes over long periods of time.

The three sets of mechanical gauge readings on the completed bridge, taken in March 1974, June 1974, and January 1975, confirmed the gross elongation or shortening of the girder produced by the seasonal temperature changes and indicated that no unexpected strain changes had taken place.

Scratch Gauges

Eight scratch gauges with 1-m gauge length (initially, 0.305 m) were installed in the Rio-Niteroi Bridge. They were an important backup system during construction. On the completed bridge, their principal function has been to record the stress fluctuations caused by the diurnal temperature changes and unexpected occurrences. Although not so accurate as the electric or mechanical gauges, the scratch gauges can provide a permanent and continuous record of stress changes for several months or even years.

TEMPERATURE READINGS

The temperature gauges were read concurrently with strain gauges. However, because construction and test load readings for the most part were taken at night when the temperature in the bridge was essentially uniform, these readings are not discussed here. After the bridge was completed, the following three sets of readings were taken specifically to study the thermal behavior of the bridge: (a) in February 1974 for finding the temperature distribution on a summer day, (b) in June 1974 for determining the temperature variation at some selected locations with respect to time and (c) in January 1975 for finding the total diurnal temperature change.

Additional information on the thermal behavior of the bridge was obtained from scratch gauge targets.

Temperature Distribution in Cross Section

The readings on February 27, 1974, were taken to establish the temperature distribution in bridge cross sections on a typical hot summer day. The temperature was measured around noon (Figure 3). The heavy solid circles and solid ordinates indicate the places where particular gauges were located. A small circle with a dashed ordinate gives the value transferred from an adjoining plate where the gauge was actually located. The readings show some scatter, but this can be readily ascribed to the later recognized fact that the temperature-time gradient from 11 a.m. to 1 p.m. during which the readings were taken is quite steep and can readily account for discrepancies of 3 to 4°C.

The following observations can be made from the figure:

1. The temperature on each of the four webs is essentially constant over the full depth except for a very sharp increase at the top to the temperature of the top flange;
2. The temperatures in the two outside webs are equal to each other and are approximately 4°C higher than in the two inner webs;
3. The air temperature in the boxes at the lower levels, as measured by the gauges on the bracing diagonals, is equal to the temperature of the outside webs, and, at the top, it is higher and equal to the air temperature outside between the boxes;
4. The temperature in the top flange plate is the highest in the middle of a box (up to more than 42°C) and then drops a few degrees at the webs because of their heat-sink function;
5. The flange tips have markedly lower temperatures than the rest of the flange (more than 10°C lower) because of the concrete curb and railing over them; and
6. Comparison of Figure 3 with a similar plot for FB27 showed no recognizable difference between the temperature distributions that could be ascribed to the different locations along the girder.

Variation of Temperature Distribution With Time

Temperature variation in the bridge cross section with respect to time was determined on June 10 and 11, 1974. No soldering switchings were made, and the same group of 12 temperature and the accompanying 76 strain gauges were read over and over at short time intervals. The selection of gauges was based on the fact that the sun at this time of the year (Brazilian winter) is low in the north (to the left of the cross sections in the figures).

The temperature readings of June 10, 1974, at FB27 were plotted against time (Figure 4). The temperature in the section is essentially uniform and equal to the air temperature at about 9 a.m.; it reaches the highest value at about 2 to 3 p.m. and then decreases toward 5 p.m. The gauge on the inner web gave somewhat lower overall readings than other gauges, apparently because of a malfunction.

Although the air temperature changed through the day by only 5°C, the bridge temperature increased by as much as 14°C. The observation, relevant to the readings made in February 1974, is that the temperature rose quite rapidly between 11 a.m. and 1 p.m. and developed the greatest difference between individual points in the cross section only later, at 2 to 3 p.m.

Figure 5 shows the temperature variation at FB57 on the same day. The pattern is very similar, but it exhibits some additional characteristics. The gauge at the bottom of the north web (hollow circles) shows a very rapid temperature increase under the early exposure to sun rays. At 9 a.m., when the temperature of the top flange was equal to the air temperature, the temperature of the bottom of the web had already risen 5°C and was increasing faster than in other components. Gradually, the temperature in the web leveled off and started decreasing at 2 p.m., that is, before the other points reached their maxima. The gauge at the left tip of the top flange (hollow triangles) hardly warmed up, and its temperature differed from that of the flange itself by about 10°C—the same as was observed in February 1974.

Although the temperature difference in Figures 4 and 5 between the points on the flange and those immediately under it on the web is only about one-third or one-half of

that observed in February, the patterns are in good agreement.

Maximum Diurnal Temperature Change

A diurnal temperature change needed for thermoelastic stress analysis of the bridge could not be properly established either in February or in June 1974, and the January 1975 readings were designed to accomplish this. The readings were taken from 11 p.m. on January 16, 1975, until 5 p.m. the next day to determine not only the temperature variation at certain locations but also the full temperature distribution at times several hours apart.

Figure 6 shows the maximum diurnal temperature change at FB57 between 6:30 a.m. and 3 p.m. on January 17, 1975. The pattern is very similar to the temperature distribution pattern in Figure 3 for February 1974, except that the distribution in the top flange is less accurately defined, inasmuch as many gauges had been damaged in the interim.

Given the symmetry about the vertical axis and the equivalence of temperatures at FB57 and FB27 (not shown here), all the readings of the January 1975 temperature change are shown in Figure 7 on the outline of the north box (the flange tip is on the left side). A pattern of the maximum temperature change was then approximated from the composite plot as shown in the figure by the dashed line. This pattern is also superimposed on the cross section of Figure 6 for a direct comparison with the readings on it.

Inasmuch as meteorological records indicate that air temperature on January 17, 1975, was the highest since 1973, the pattern of the diurnal temperature change in Figure 7 was accepted as a typical maximum pattern.

Scratch Gauge Records of Thermal Stresses

After the completion of the bridge, a typical scratch gauge record was in the form of a continuous zigzag trace, indicating periodic stress changes. Because a day-by-day correlation could be established between the zigzags of the scratch gauge traces and of the meteorological temperature record, these stress changes were ascribed to daily temperature fluctuations. The effect of traffic had to be excluded because the stresses computed for the current traffic level were found to be much lower than those recorded, and also they fluctuated many times rather than once during the day.

Figure 8 shows two example segments of scratch gauge traces in which the highest stress changes were recorded during 1974. One is from the gauge on the bottom of the web at FB27, and the other is from the gauge on the bottom of the web at FB42. The daily stress change of approximately 52 MPa shown by these traces is much higher than the thermal stress computed for the daily temperature changes measured in the bridge. This discrepancy can be plausibly and approximately quantitatively explained by the temperature difference between the gauge and the girder metal produced by the insulating effect of the paint and the air clearance between them. Thus, the temperature in the gauge was much closer to the temperature of the air inside the box than that of the plate to which the gauge was attached. Consequently, the much slower temperature changes of the inside air through the day had a significant magnifying effect on the scratch gauge trace (14). Only a 5 to 9°C difference was sufficient to explain the discrepancy.

THERMOELASTIC ANALYSIS

General thermoelastic analysis of bridges requires that two problems be resolved: (a) the determination of the temperature change pattern and (b) the actual stress analysis. The temperature change pattern can be computed theoretically, but at present only a few simple cases could be successfully analyzed (3, 4, 5, 6). Or the pattern can be measured on the actual structure as was done in this study.

If the commonly made assumptions about the linearity of stress-strain and temperature-strain relationships and about the planar nature of deformations of a cross section are valid, two types of normal stress develop in a girder cross section subjected to a nonplanar temperature change. One represents the self-balancing stress field resulting from the nonplanar nature of the temperature change, and it is affine to the temperature pattern. The other type of stress is produced by the redundant forces of the statically indeterminate structure, is planar, and is zero for statically determinate girders (5, 6). In equation 1, these two types of stresses are given by the first and second bracketed terms.

$$\sigma(y,z) = \Big[-\alpha E T + (1/A)\int\int E\alpha T\, dy dz + (y/I_z)\int\int E\alpha T y\, dy dz + (z/I_y)\int\int E\alpha T z\, dy dz \Big] + \big[(1/A)(\|n_i\|^T \|X_i\|) + (y/I_z)(\|m_{iz}\|^T \|X_i\|) + (z/I_y)(\|m_{iy}\|^T \|X_i\|)\big] \quad (1)$$

where

- a, E, T = coefficient of thermal expansion, modulus of elasticity, and temperature change (each may be a function of the coordinates in the cross section),
- A, I_z, I_y = area and moments of inertia of the cross section,
- n_i, m_{iz}, m_{iy} = axial force and banding moments produced by the ith redundant $X_i = 1$,
- X_i = final value of the ith redundant, and
- T = transpose of the $\|n_i\|$, $\|m_{iz}\|$, and $\|m_{iy}\|$ column matrices.

Method Developed for the Rio-Niteroi Bridge

The method used for thermoelastic analysis of the Rio-Niteroi bridge was based on the above principles. The bridge is a three-span continuous girder with 5 deg of indeterminacy, three in the vertical plane (two vertical reactions and one horizontal, at the center pier) and two in the horizontal plane (the four piers are treated as elastic supports for twisting and horizontal bending of the girder produced by an unsymmetrical variation of temperature across the width). Longitudinally, the girder is subdivided into thirty-five 20-m segments.

Each midsegment cross section is broken down into 171 elements as shown in Figure 9 for a section near FB57. The flange and web plates consist of relatively wide elements except at the top of the webs, where, in anticipation of a steep temperature gradient, the elements are only 0.10 m wide. Each longitudinal stiffener is treated as an individual element. The numbering system of shallower sections is kept the same, but the dimensions are modified by reducing the width of or completely eliminating the lowest web elements.

The temperature distribution is taken in the computer program to be symmetrical about the midlength of the bridge although it does not have to be symmetrical in the cross section. The temperature values for all the seg-

ments are generated from the temperatures at FB27 and FB57, which are used as input data.

Although the computer program was developed primarily for the Rio-Niteroi bridge, it can be modified for other three-span, four-web box or plate girder bridges.

Thermal Stresses

Thermoelastic analysis of the bridge girder was performed for a number of temperature change patterns. The thermal stresses computed at FB42 for the January 1975 pattern (Figure 7) are shown in Figure 10. The maximum compression in the top flange and at top of the webs is 11.6 to 14.2 MPa. The tension in the web below the top flange is about 11.6 MPa and in the bottom flange 7.5 MPa.

The stresses at the section of FB42 are representative of the higher stresses obtained for other sections along the girder. Yet, for this bridge, the stress levels are quite low; they can be readily covered by the 25 to 33 percent increase in allowable stresses generally permitted when thermal effects are added to the effects of dead and live loads.

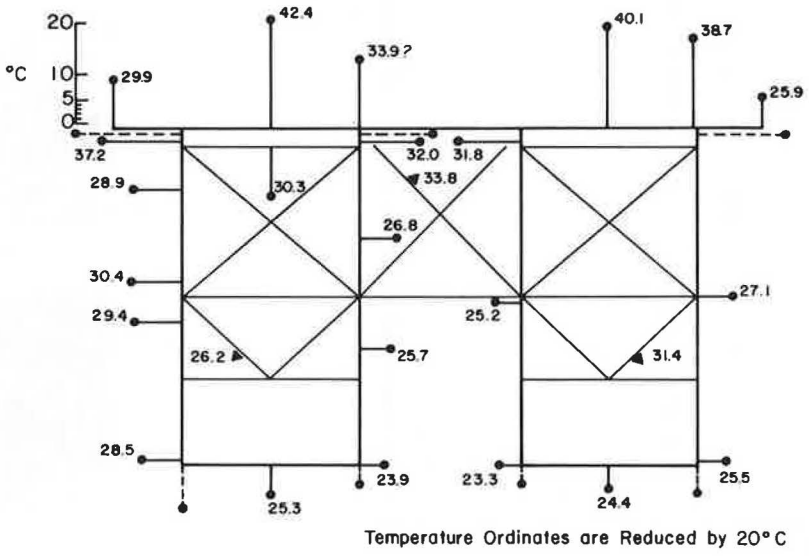

Figure 3. Temperature distribution at FB57 on February 27, 1974.

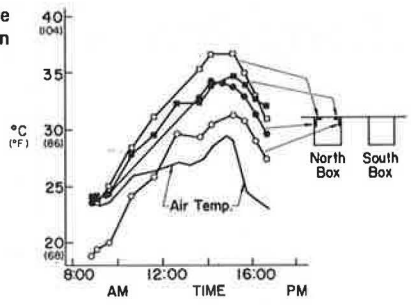

Figure 4. Temperature versus time at FB27 on June 10, 1974.

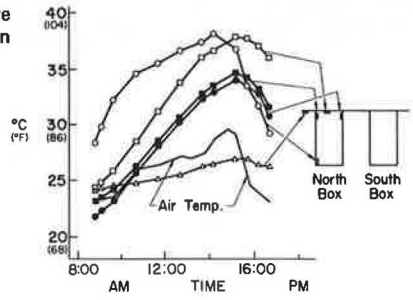

Figure 5. Temperature versus time at FB57 on June 10, 1974.

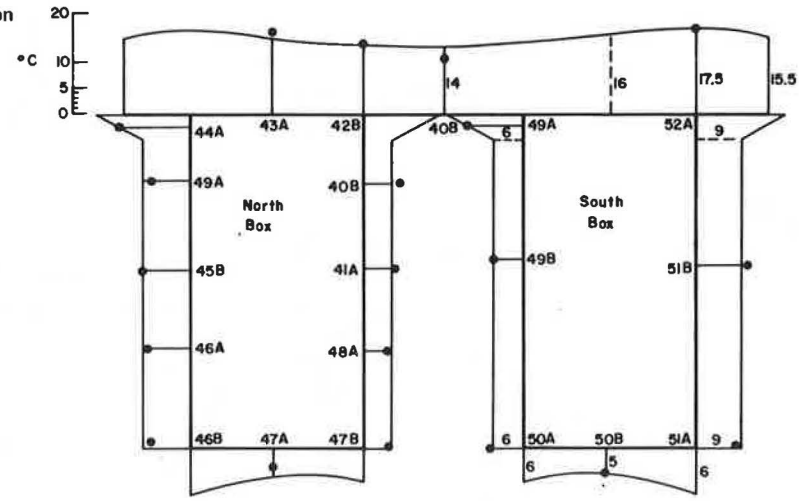

Figure 6. Diurnal temperature change at FB57 on January 16 and 17, 1975.

Design Recommendations for Diurnal Temperature Change in Steel Bridges

This thermal study leads to the conclusion that the diurnal temperature change pattern observed is typical of steel girder bridges under the climatic conditions of Rio de Janeiro. A simplified and conservative version of the recommended pattern is shown in Figure 11.

Figure 7. Composite temperature changes at FB57 for January 16 and 17, 1975.

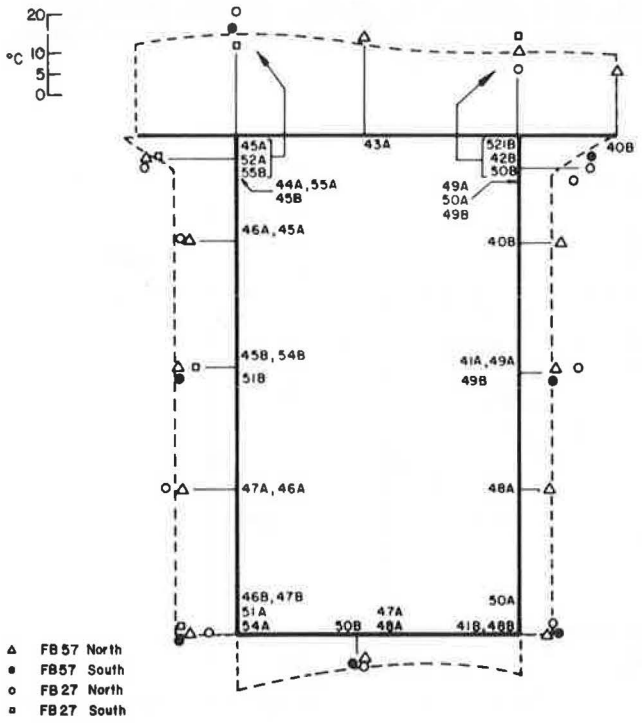

CONCLUSIONS AND RECOMMENDATIONS

The following conclusions can be made from this work.

1. The temperature distribution in the cross section

Figure 8. Scratch gauge traces with diurnal stress changes 235X; 0.305-m gauge length.

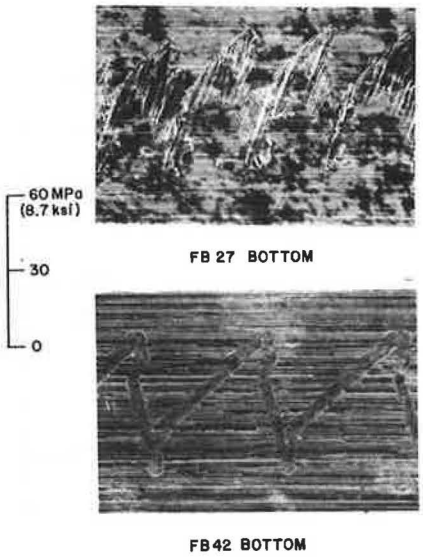

Figure 9. Breakdown at FB57 for thermoelastic analysis.

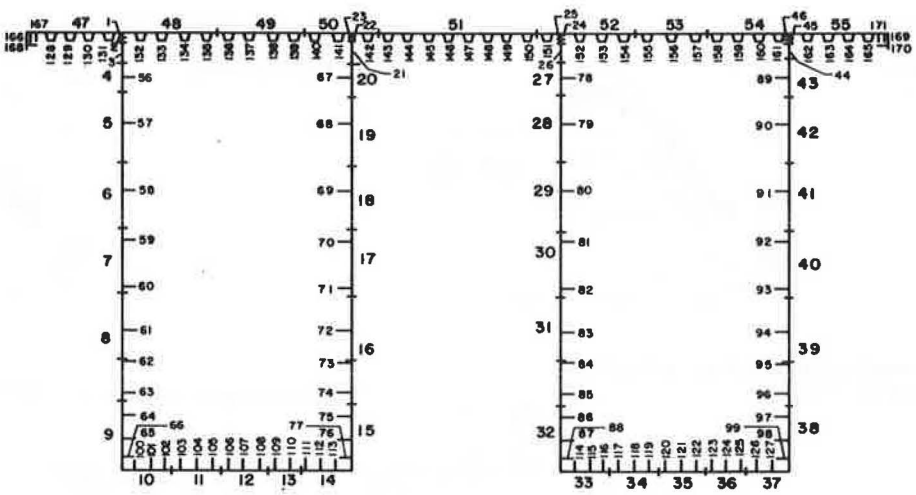

Figure 10. Thermal stresses at FB42 during January 1975.

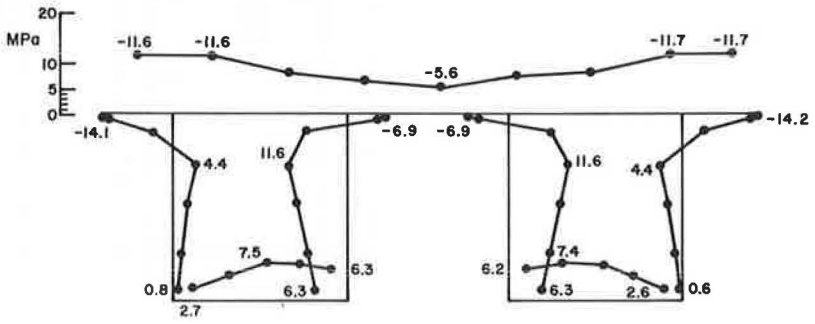

Figure 11. Temperature change recommended for climatic conditions of Rio de Janeiro.

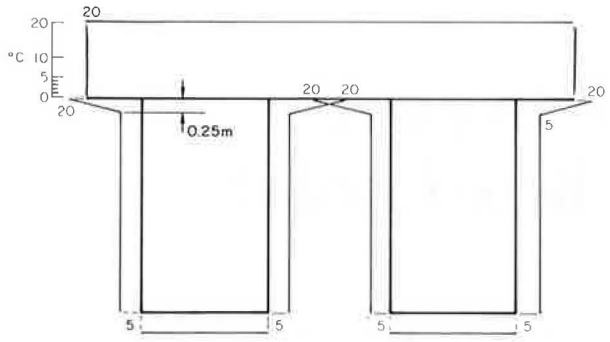

showed a sharp gradient at the very top of the webs and an essentially constant temperature for the rest of the web.

2. The greatest change in temperature took place between 6:30 a.m. and 3 p.m.

3. There was no detectable difference in temperature distribution between a deep section at the pier and a shallow section at midspan.

4. The greatest normal stress due to a diurnal change of temperature was found to be only 14.2 MPa. However, a girder of different proportions may develop much higher stresses.

5. Scratch gauges were effective in recording stresses, but they require very good insulation from the outside air if they are to have the same temperature as the structure and measure thermal stresses accurately.

6. A prudently conservative temperature change to be considered in design of similar steel bridges under the climatic conditions of Rio de Janeiro is recommended as shown in Figure 11.

The lessons learned in this field study conducted under the conditions in Rio de Janeiro point to the need for similar investigations in the United States so that the AASHTO design recommendations can reflect more realistically the true field conditions. Specifically, the following recommendations are made.

1. Conduct extensive theoretical and field studies on concrete and steel bridges under at least two extreme climatic conditions in the United States.

2. Install a few temperature measuring and recording devices in some bridges in the vicinity of meteorological stations. Information gathered should help in the correlation of theoretical and short-term experimental work recommended above.

ACKNOWLEDGMENTS

The work described represents a portion of a research project directed by J. W. Fisher and conducted at Fritz Engineering Laboratory, Department of Civil Engineering, Lehigh University. The project was sponsored by S. A. Empresa Construção e Exploração da Ponte Presidente costa e Silva (ECEX), with J. C. Guedes and F. Valle the consecutive presidents. The author appreciates the support and interest given this project by directors of the Technical Division of ECEX, first, the late J. P. Ferreira and, currently, J. B. S. Corrêa, and the assistance by many of the ECEX staff, especially the staff of SEOBES with P. S. da Costa.

Gratitude is due to G. F. Fox, H. J. Graham, and E. P. Rausa of Howard, Needles, Tammen and Bergendoff International, Inc., and to their resident staff in Rio de Janiero. The author also thanks the following of the Fritz Engineering Laboratory staff: H. T. Sutherland, J. E. O'Brien, D. H. DePaoli, M. E. Bhatti, and D. P. Erb.

REFERENCES

1. J. C. Reynolds and J. H. Emanuel. Thermal Stresses and Movements in Bridges. Journal of Structural Division, Proc., ASCE, Vol. 100, ST1, Proc. Paper 10275, Jan. 1974, pp. 63-78.
2. J. D. Mortlock. The Instrumentation of Bridges for the Measurement of Temperature and Movements. Transport and Road Research Laboratory, Crowthorne, Berkshire, England, TRRL Rept. LR641, 1974.
3. M. Emerson. The Calculation of the Distribution of Temperature in Bridges. Great Britain Transport and Road Research Laboratory, Crowthorne, Berkshire, England, TRRL Rept. LR561, 1973.
4. P. Leger. Influence of Temperature Gradients on the Bearing Reactions of a Structure. Colloquium on Bridge Loading, International Association for Bridge and Structural Engineering, Cambridge, England, April 1975.
5. B. Hunt and N. Cooke. Thermal Calculations for Bridge Design. Journal of Structural Division, Proc., ASCE, Vol. 101, No. ST9, Proc. Paper 11545, Sept. 1975, pp. 1763-1781.
6. M. Radolli and R. Green. Thermal Stresses in Concrete Bridge Superstructures Under Summer Conditions. TRB, Transportation Research Record 547, 1975, pp. 23-36.
7. Ponte Presidente Costa E Silva. Empresa de Engenharia e Construção de Obras Especiais, Rio de Janeiro, March 1974.
8. G. F. Fox. Rio-Niteroi Bridge Construction. Howard, Needles, Tammen and Bergendoff, 1975.
9. A. Cottrill. Rio-Niteroi Bridge: First Major Lift Gives Head Start to Tight Completion Program. New Civil Engineer, August 9, 1973.
10. Long Box Girders Lifted for Record Span. Engineering News-Record, Nov. 1973, pp. 28, 29.
11. I. J. Upstone. Rio-Niteroi Bridge. Building With Steel, No. 18, Sept. 1974, pp. 31-36.
12. A. Ostapenko. Rio de Janeiro to Niteroi. Lehigh Research Review, Vol. 5, No. 2, May 1974, pp. 1-3.
13. J. H. Daniels, B. T. Yen, and J. W. Fisher. Rio-Niteroi Bridge: Stresses in Orthotropic Deck Under Traffic. Paper presented at the 55th Annual Meeting, TRB, 1976.
14. A. Ostapenko and others. A Study of the President Costa e Silva Bridge During Construction and Service (Steel Structure). Fritz Engineering Laboratory, Lehigh Univ., Bethlehem, Penn., Rept. 397.6, March 1976.

Studies of Skewed Concrete Box-Girder Bridges

Mark R. Wallace, Division of Structures, California Department of Transportation

Analyses of 51 mathematical models using the finite element analysis program CELL were undertaken to describe the behavior of common skewed, concrete box-girder bridges. An assessment was made of effects on structural behavior of varying superstructure width to span length (aspect) ratio, number of cells, skew angle, type of loading, and depth. Span length and skew angle were found to be the most significant parameters influencing girder shear distribution. Aspect ratio and skew angle affected longitudinal bending moments to the largest extent. Based on the results of this study, methods for shear and bending design of skewed bridges are presented.

Bridge engineers have recognized several peculiarities in skewed concrete box-girder bridge behavior. Shear cracks have developed in exterior girders near obtuse support corners. Transverse cracks have developed at midspan of certain highly skewed, prestressed bridge decks. Tendencies toward uplift at acute support corners of long span bridges have been noted.

Although skewness produces analysis and design complications, it also affords design advantages. Since support reactions tend to concentrate at obtuse corners, reductions occur in effective structure spans. The thick end diaphragms act to reduce longitudinal stresses in the superstructure. Hence, possibilities exist for material savings by refining structural analysis.

University of California researchers developed a finite element analysis program CELL for use in performing elastic analyses of box-girder bridges having a constant depth and an arbitrary plan geometry (1). They further used the program for analyzing skewed bridges. Results of the study enabled them to devise methods whereby the stiffening effects of skewed supports could be considered for reducing superstructure design moments (2). Aluminum models were tested for physical verification (8). Dead-load design moments were reduced 19 percent for 30-deg skews and 41 percent for 45-deg skews.

In an analysis of a highly skewed, two-span, two-celled railroad bridge California Department of Transportation researchers found the following skew effects (3, 4):

1. Significant reductions in longitudinal bending moments from those of comparable straight or normal structures on orthogonal bearings,
2. Severe redistribution of reactions and girder shears toward obtuse support corners,
3. Uplift tendencies at acute corners of the longest span abutments under some loading conditions, and
4. No measurable benefits from including intermediate diaphragms in the superstructure.

Similar effects of skew have also been reported by others (5, 6, 7, 9).

OBJECTIVES, CONCEPTS, AND PROCEDURES

The objectives of the study reported in this paper were to describe the behavior of skewed box-girder bridges, and to suggest design criteria. The CELL program was used to study and analyze 51 mathematical models to assess effects of varying superstructure plan geometry, number of cells, skew angle, type of loading, and depth.

Basic Concepts

The obtuse corner reactions for any symmetrical loading condition will exceed acute corner reactions when a simple span, skewed box-girder superstructure on parallel abutments is supported at its corners. Figure 1 shows this concept. A concentrated load P was applied at the center of a skewed plate (Figure 1a). Since the load was applied nearer the obtuse corners, as opposed to the acute corners, the obtuse reactions were larger. In other words, a structure will behave more stiffly between its obtuse corners than between its acute corners. As a commonly accepted design approach, total abutment reaction R is used to establish a moment diagram for a structure having an assumed span length equal to the center girder length (Figure 1b). In California design practice, a "whole-width" design concept is employed, in which the moment of inertia of all girders comprising the superstructure is lumped in one unit.

Publication of this paper sponsored by Committee on Concrete Bridges.

The above procedure, however, leads to a conservative design because the skew itself has the effect of reducing the maximum moment in the structure. One means of demonstrating this effect is to superimpose two conditions that are equivalent to the total left support reaction (Figure 1c). The true reactions on the left may be described as a component that is normal (which sums to R) and a component that is skewed or unbalanced. The normal component affects longitudinal behavior exactly as a normal reaction affects a normal structure. The unbalanced component accounts for the portion of the reaction that is due to skew. It has the effect of applying a couple to the left support that causes a counterclockwise rotation about the moment center (y-axis in Figure 1d), opposing the clockwise rotation caused by the load. Thus, a resisting couple results from the unbalanced longitudinal distribution of support reaction. Its magnitude is calculated as shown at the bottom of Figure 1d. A clockwise couple of the same magnitude occurs at the other end of the span. The magnitude of the couple is a function of the reaction difference, structure width, and skew angle. When the preceding two effects are superimposed, a moment is obtained at midspan that is reduced from the moment of the simple span by the magnitude of the couple as shown in Figure 1e and discussed elsewhere (9).

The above concepts also apply to box-girder bridges; however, they must be modified according to the following indeterminate complexities of box-girder behavior.

1. The end diaphragm contributes measurably to the stiffness of a skewed structure. As its span lengthens, the support rotation increases. When this lengthening occurs, the end diaphragm provides a good mechanism for longitudinal as well as transverse distribution of reaction, carrying an increasingly greater load to the obtuse corner. Increases in skew angle accentuate this redistribution.
2. The unbalanced distribution of support reactions also produces torsional resisting moments at the supports, even under symmetrical loading. If moments are taken about the longitudinal centerline (x-axis) of the structure, a torsional couple is obtained that depends on the reaction unbalance and structure width (Figure 1f).

Most box-girder bridge sections are designed according to the whole-width concept. However, because skewness produces some doubt as to the desirable section for design purposes, the critical moment value had to be determined between that calculated at a total section, normal to the center girder midspan, and that calculated along a nonnormal section, cut somewhere between lines 1 and 2 in Figure 2.

Models and Program Description

The current study was initiated by establishing superstructure width to length (aspect) ratios of the longest spans in each of 395 concrete box-girder structures being designed in California. Based on those data, a range of mathematical models was chosen for assessment of parameter influence and general behavior. Most often, models analyzed were of 4 and 8-celled bridges supported on parallel abutments and containing girders spaced as shown in Figure 3b. Most models were skewed 30 and 45 deg, and all webs were assumed to be vertical.

The support (boundary) conditions used are shown in Figure 4a. Each girder reaction point was restrained against vertical movement. To stabilize each model, transverse movement at center girder reaction points and longitudinal movement at the exact center of the structure were prevented. Figure 4b shows a layout plot of a finite element mesh for a 4-celled box, which is typical of all meshes used in the present study.

Loadings

All model structures were analyzed for dead-load behavior and several for prestress and live-load behavior.

1. Structure dead-load was calculated and applied internally by using the CELL program.
2. Live-load behavior was studied through application of loads appropriate to span lengths. Uniform lane loads and concentrated midspan loads (riders) were applied to spans exceeding 48.8 m (160 ft). Short span behavior was studied through application of one truck (HS 20-44) or the maximum number of trucks a particular structure would be designed to carry.
3. Effects of prestress loads were studied to relate results obtained by using the usual analysis and by using the CELL analysis. Skewed bridges having parallel supports are currently designed by assuming normal supports; therefore, working prestressing forces were calculated for the normal condition. Figure 5 shows the procedure. The forces were assumed to be applied through cables draped as shown in Figure 5a. Equivalent loadings, comprising a combination of concentrated loads at the girder ends and an upward load acting over the deck area, were applied. The equation in Figure 5b was used to calculate the uniform load to balance the dead load.

RESULTS AND OBSERVATIONS

Moment Reduction

Results indicate that substantial savings can be realized by taking advantage of the reduction of design stresses produced by the effects of skew. Figure 6 shows moment-reduction design curves that could be used for arriving at more economical designs for simple span, reinforced concrete, box-girder bridges. These curves represent envelopes of data from the models previously mentioned. The dotted lines indicate extrapolation beyond most of the data.

Initial studies show that similar reductions would exist for multiple span structures. The relative amounts carried by various spans depend on several factors, such as span unbalance and intermediate support conditions. Varying superstructure depth-to-span length (D/L) ratio within the range of 0.0475 to 0.0615 has little influence on moment reduction values.

The curves in Figure 6a could be used to reduce the dead-load design moments in box girders having 6 to 10 cells and spans ranging from 17.1 to 33.5 m (56 to 110 ft). These limits encompass most simple span, reinforced concrete structures. Similar reduction curves for structures having 2 to 5 cells appear in Figure 6b. The curves would be used as follows:

1. Calculate the midspan dead-load moment by assuming that the structure is supported on normal abutments;
2. If the abutment skews are within 15 deg of one another and the cross section is prismatic, proceed to find a reduction factor;
3. Enter Figure 6a or 6b and use the smaller of the two skew angles;
4. Read a factor from the ordinate axis, using the curve for the appropriate girder (normal) span length; and
5. Reduce the dead-load design moment according to the formula $M_D = F \times M_N$, where M_D = design moment and M_N = normal moment.

Aspect ratio was found to be the most significant

Figure 1. Total moment at midspan due to skew.

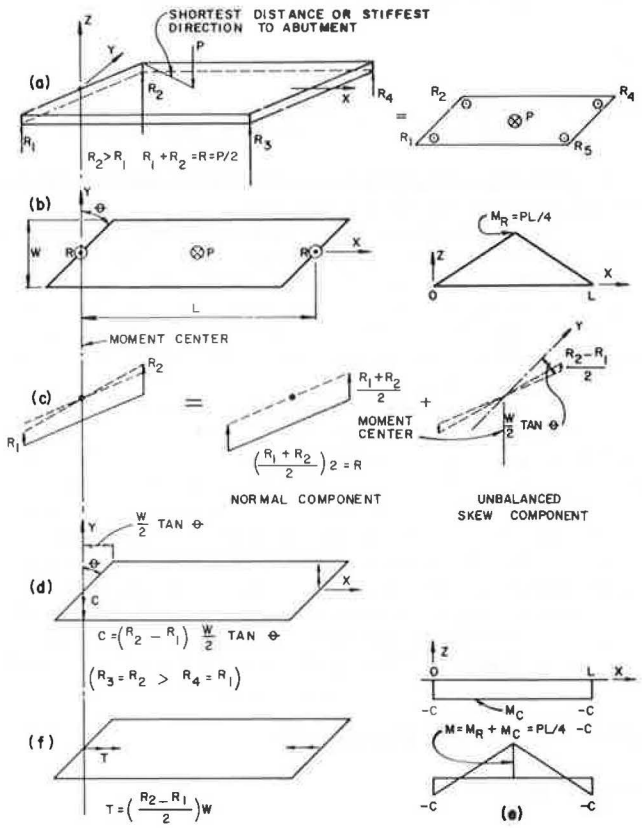

Figure 2. Location of maximum longitudinal stress.

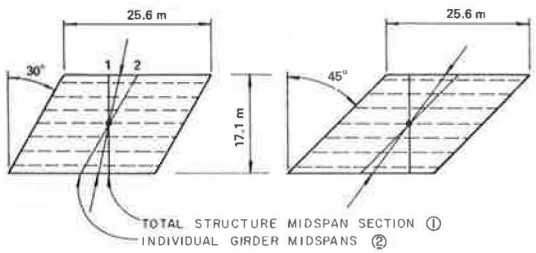

Figure 3. Shear distribution locations and loadings of a typical box girder.

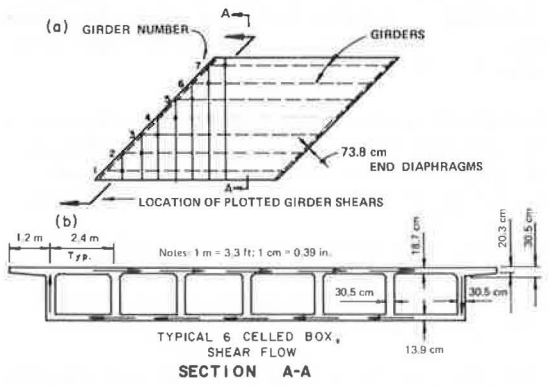

Figure 4. Support conditions for finite element mesh used in models.

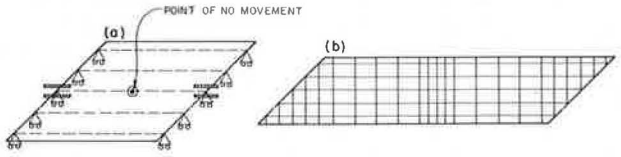

Figure 5. Prestress loading.

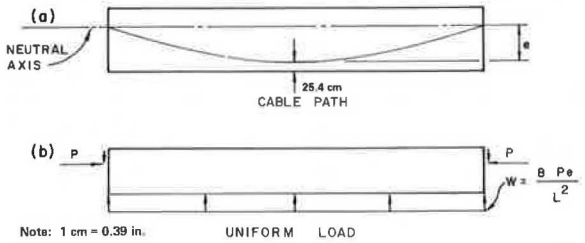

Figure 6. Moment reduction curves.

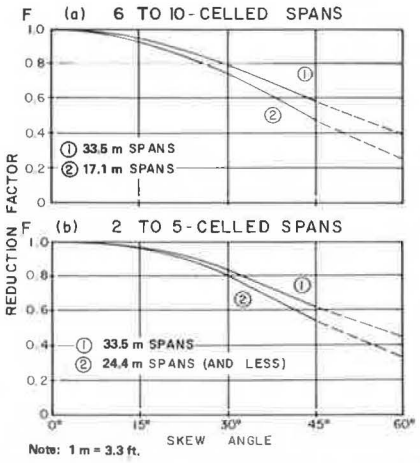

Figure 7. Dead-load deflection.

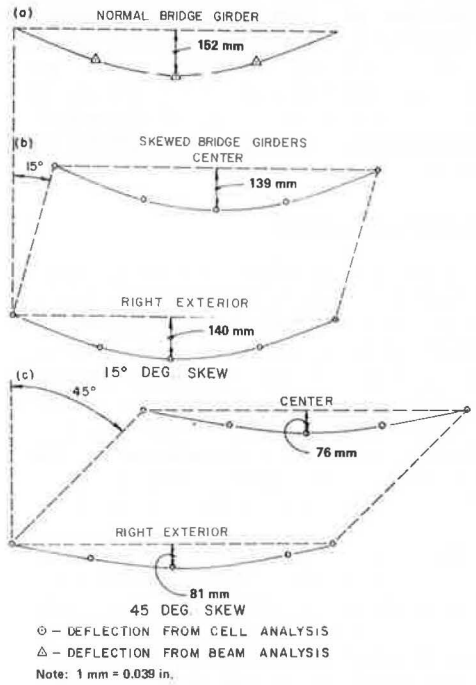

parameter influencing overall bending behavior. Although aspect ratio is not referred to in the plots themselves, it is reflected in the curves in Figure 6. Notice that the factors decrease with decreasing span length and with an increase in the number of cells. As a general rule, transverse distribution of girder moments for structures skewed less than 45 deg and having aspect ratios of 0.5 and less can be considered the same as that of comparable structures on normal supports. Six to ten-celled structures that have 1:1 aspect ratios and are skewed 45 deg exhibit ratios about 10 percent larger between exterior and center girder moments than do their normally supported counterparts. To verify the analyses, statics checks were made by comparing external and internal moments at midspan. In most cases, moments checked to within 1 percent and vertical forces summed exactly to zero.

Moment Derivation

Figure 2 shows the migration of the maximum longitudinal stress location in various exterior girders. The maximum stress in each individual girder of the structural section is indicated near the lines that are designated by arrows. The largest moment value obtained by summing individual girder moments along any such line was used for establishing reduction curves. The total moment for each skewed structure was divided by the maximum moment value calculated for a normal maximum structure of the same span and section. The result was the reduction factor F.

Deflections

Dead-load deflection data for a CELL model having a 54.9-m (180-ft) span, a 21.9-m (72-ft) width, and 9 girders are presented in Figure 7. This example typifies the study's results. Figure 7a shows the theoretical, elastic, deflected shape of a bridge girder with orthogonal bearings found from simple beam analysis. Results for center and right exterior girders obtained by using CELL analyses are plotted for 15 and 45-deg skews respectively. The following information was noted:

1. A significant reduction in deflection due to skew is evidenced at 15 deg,
2. Deflections are only half as great as normal for 45-deg skews,
3. The discrepancy between exterior and center deflections is larger at 45 deg than at 15 deg, and
4. Narrower structures of the same span as that shown in Figure 7 exhibit smaller discrepancies between exterior and center deflections.

Shear Behavior

The girder shears were calculated at the CELL mesh node locations nearest the left support. The shear distribution location can be thought of as a section cut parallel to the abutment and as close to it as possible (Figure 3a). Transverse shear distribution results under dead load for the simple span box girder depicted in Figure 3 are presented in Figure 8a. The structure is 25.6 m (84 ft) in span length, 17.1 m (56 ft) wide, and skewed 45 deg at each support. In this case, and for all the dead-load analyses, it was evident that the exterior girder framing the obtuse support corner of a structure would carry a much greater portion of the total structure shear than would any other girder. The interior girders carry about the same amounts of shear as they would if the structure were normally supported. Such behavior might be expected because a greater contribution is made to torsional rigidity (shear flow) by the deck and exterior girders than by the interior girders (Figure 3b).

Statics checks indicate a 7 to 9 percent violation of vertical equilibrium between external reactions and internal girder shears. Although this error is tolerable, it could be reduced by mesh refinement. Shear behavior at acute corners is opposite to that at obtuse corners. The acute corner exterior girder carries but a small amount of shear. In some long span and highly skewed structures, the shear at the acute corner girder actually reverses in sign, indicating an uplift tendency.

Six separate live loadings were applied to each of four structural models. Figure 9 shows a plan for live loads 1 and 5. Figure 8b shows that live load 5 is more critical for shear in the obtuse exterior and first interior girders than is live load 1. Live load 1 is resisted by a more uniform shear distribution among the five girders nearest the obtuse corner. Much of live load 1 travels directly to the end diaphragm.

The data indicate that shear distribution depends primarily on span length and that an approximate linear increase occurs in the exterior girder shear as skew angle increases because of relative support rotation. If other parameters are held constant, the longer the span is, the greater is the redistribution of reaction toward the obtuse corner of a skewed support. [These box-girder study results are in agreement with a previously stated theory (9).] Therefore, ranges of design shear factors based on span length were developed from the data. For example, the dead-load shear factors for obtuse corners of a reinforced concrete box girder are shown in Figure 10. The factors were calculated by taking the ratios of the shear results for exterior and first interior girders of skewed and of comparable straight or normal structures ($F = V_s/V_N$). Interpolation within these ranges should lead to acceptable designs, that is, ±5 percent.

The range of shear factors for exterior girder design in multiple span structures is likely to be lower than the comparable range for simple spans. How much lower depends on various factors such as span unbalance, number of spans, and number of columns. Preliminary analyses of a model having two spans of 30.5 m (100 ft) and 24.4 m (80 ft) and skewed 30 deg produced factors for the exterior girder range in the long span about 25 percent lower than those for a simple span of the same length. The short span shears were almost uniformly distributed across the section.

The shear factor range for an exterior girder would be about 13 percent higher for a combined dead and live loading than for a dead loading alone because live load 5 produced a more critical condition in the obtuse exterior girder than live load 1. A converse effect occurs at acute corners and girder shears are also effectively reduced. By interpolating within ranges, one may use the shear factor curves to obtain a factor for a particular structure; depth-to-span length ratio (D/L), span length, and skew are used to obtain a factor to increase design shears from those of identical structural sections supported on normal abutments. The following example illustrates the process. For a bridge that has a span length of 24.4 m (80 ft), a D/L of 0.052, and abutment skews of 30 and 40 deg, find the design shear factors for the exterior and first interior girders at the obtuse corners. The steps in the solution are as follows:

1. Enter the exterior girder range in Figure 10 and interpolate between the 0.045 and 0.060 D/L lines, for a 33.5-m (110-ft) span to establish a line for the desired value of 0.052;
2. Using the span length of 24.4 m (80 ft), interpolate between the new line for a 33.5-m (110-ft) span, D/L of 0.052 and the lower limit line [L = 17.1 m (56 ft)] to es-

tablish the factors of 1.63 for the 30-deg skew and 1.83 for the 40-deg skew;

3. Establish factors of 1.09 and 1.12 for the first interior girder by interpolating within the lower range; and
4. Increase the design shears in the exterior and first interior girders by the appropriate factor F, according to the formula $V_D = F \times V_N$, where V_D = design shear and V_N = normal shear.

High reaction concentrations at the obtuse corner cause about 3 to 6 percent of the total structure dead-load shear to be carried by the end diaphragm as structure aspect ratio increases from 0.5 to 1.0. Most of this dead-load shear is concentrated near the obtuse corner.

Figure 8. Transverse shear distribution.

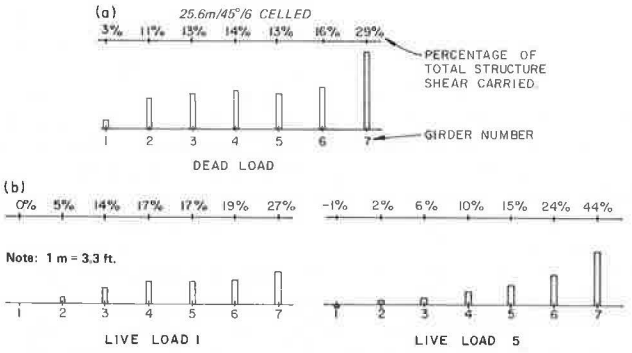

Figure 9. Plan for live loads 1 and 5.

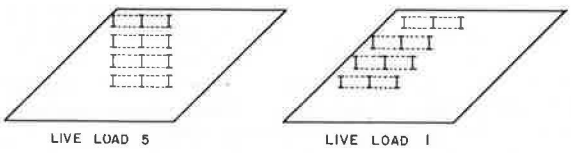

Figure 10. Dead-load shear factors for obtuse corners of a simple span box girder.

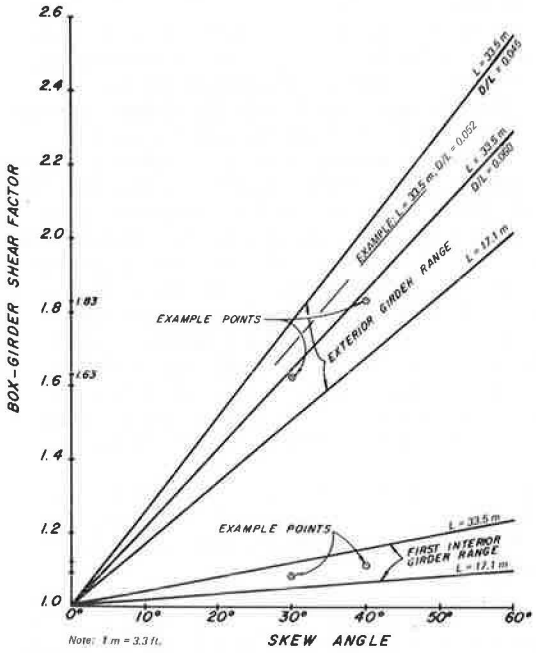

Prestress Behavior

Longitudinal stress results indicate that reductions in prestressing forces are possible in wide structures having skews over 45 or 50 deg. For example, a bridge skewed 50 deg, and having 13 girders and an aspect ratio of 0.675, was analyzed by using the CELL program. Results indicate a possible reduction in prestressing forces of 11 percent. This reduction may have occurred because dead-load torque peaks at 45 or 50 deg and tends to reduce dead-load moments most highly at those skews, as discussed by Kollbrunner and Basler (9). However, present design procedures for designing a prestressing system to counteract dead- and live-load stresses in individual girders appear realistic and effective, as far as the total structure is concerned. In producing an effective, uniform, upward load, prestressing has overall effects that oppose the dead load. Since end moments produced by skewed supports resist downward movement under dead loading, they should also resist upward movement due to prestressing. Analysis results for prestress loadings support this notion. Distribution of shear in the models under prestress loading was almost identical to dead-load distribution, though opposite in sign. Thus, draping the cable parabolically with maximum eccentricity at each girder midspan, which is current practice, is the proper general approach. However, a larger torque is produced in the superstructure by dead loadings than that produced by the lower uniform load due to prestressing. Therefore, support design should provide for a larger relative settlement at the obtuse corners resulting from rotations due to combined loading.

Live-Load Bending Behavior

Results indicate that live-load reductions of lesser magnitude than those for dead load can be realized in simple spans. As a structure widens in relation to its length, the indicated live-load reduction lessens relative to the dead-load reduction. The smaller reduction is due to a more localized spanning effect occurring in the individual girder than would exist in a corresponding girder of a narrow bridge. However, the load case studies were not extensive enough to provide general behavioral guidelines.

SUMMARY

This study of skew parameters of simple spans provided the following information.

1. General knowledge regarding the effect of skew on transverse shear distribution to individual girders near abutments of concrete box-girder bridges;
2. A more accurate method for designing shear reinforcement than previously used heuristic methods;
3. Some insight into the overall structural behavior gained from deflection results;
4. Evidence that aspect ratio and skew are the significant parameters influencing bending behavior and that span and skew are significant in affecting shear behavior (depth-to-span length ratio changes within the usual ranges of 0.040 to 0.062 do not appreciably influence overall structural behavior);
5. A proposed method that allows reduction in dead-load design moments in simple span, reinforced concrete bridges and leads to savings in concrete or steel quantities;
6. Illustration that substantial savings are possible in multiple span, reinforced concrete bridges and would far offset the added design expense involved in finite element analyses with the CELL program; and
7. Evidence that shows that prestress forces can be reduced in certain highly skewed structures.

The study did not provide comprehensive live-load analyses, general multiple span design criteria, or refined criteria for prestressing forces required in skewed bridges.

RECOMMENDATIONS

In the design of skewed, simple span, concrete box-girder bridges, the shears in the exterior and first interior girders should be modified according to factors obtained from design charts such as those shown in Figure 10. In the design of abutment bearing pads and end diaphragms for shear, the effects of the high obtuse corner reactions should be considered. Simple span, reinforced concrete bridges should be designed for longitudinal bending according to the following procedure:

1. Analyze each structure for dead loading by assuming that it behaves like a beam on normal supports;
2. If the abutment skews are both greater than 15 deg and within 15 deg of each other and the section contains 2 to 10 cells, proceed to reduce dead-load design moments according to Figure 6;
3. Apply live load to the structural section by analyzing the superstructure as if it were on normal supports (this conservative approach is required because information is limited regarding live-load behavior);
4. Use established methods for designing longitudinal reinforcement but base the design on the reduced dead-load moment obtained in step 1 (the bars should be extended farther toward the obtuse corners than is current practice); and
5. Accept the CELL program for general use in design practice.

ACKNOWLEDGMENTS

This research was performed and financed by the California Department of Transportation. Assistance was provided by A. C. Scordelis of the University of California, Berkeley, and is gratefully acknowledged. The contents reflect the views of the author, who is responsible for the facts and the accuracy of the data presented. The contents do not necessarily reflect the official views or policies of the California Department of Transportation. This report does not constitute a standard, specification, or regulation.

REFERENCES

1. K. J. Willam and A. C. Scordelis. Computer Program for Cellular Structures of Arbitrary Plan Geometry. Univ. of California, Berkeley, UC-SESM Rept. 70-10, Sept. 1970.
2. C. D. Comartin and A. C. Scordelis. Analysis and Design of Skew Box-Girder Bridges. Univ. of California, Berkeley, UC-SESM Rept. 72-14, Dec. 1972.
3. H. D. Nix and E. E. Evans. Analysis of a Skewed Concrete Box-Girder Railroad Bridge (Floral Park Underpass). Bridge Department, California Division of Highways, Research and Development Rept. 4152-73-8.
4. M. R. Wallace. Floral Park Underpass. Office of Structures Branch, California Department of Transportation, Research and Development Supplemental Rept. 0002-1-73-10.
5. R. G. Sisodiya, A. Ghali, and Y. K. Cheung. Diaphragms in Single and Double-Cell Box-Girder Bridges With Varying Angle of Skew. ACI Journal, Proc., Vol. 69, 1972, p. 415.
6. D. W. Funkhouser and C. P. Heins. Skew and Elevated Support Effects on Curved Bridges. Journal of Structural Division, ASCE, July 1974, p. 1379.
7. Suite of Bridge Design and Analysis Programs: Volume 2— MOT/CIRIA Finite Element Package for the Analysis of Reinforced Concrete Slab Bridge Decks. New Zealand Ministry of Transport, May 1969.
8. W. G. Godden and M. Aslam. Model Studies of Skewed Box-Girder Bridges. Univ. of California, Berkeley, UC-SESM Rept. 71-26, Dec. 1971.
9. C. F. Kollbrunner and K. Basler. Torsion in Structures. Springer-Verlag, Berlin and Heidelberg, 1969, pp. 62-95.

Fatigue Damage in the Lehigh Canal Bridge From Displacement-Induced Secondary Stresses

John W. Fisher, Ben T. Yen, and J. Hartley Daniels, Fritz Engineering Laboratory, Lehigh University

Strains were measured at several structural steel details on one of the Lehigh Canal bridges under normal traffic. Inasmuch as these bridges have several fatigue cracks in the tie plates connecting the floor beams to the outrigger cantilever brackets, the primary focus was on the tie plates and the cause of fatigue cracking. Strain gauges were mounted on five tie plates, on a stringer, and on the longitudinal girders. An automatic computer-controlled data acquisition system was used to record the strain range occurrences. In addition, an analog trace recorder was used to determine the live load strain variations with time. Stress ranges in the stringer and girders were comparable to those observed by others in girder bridges. However, the horizontal in-plane bending stresses in the tie plates were found to be two to three times as high. The higher stress range was attributed to differential displacements between the deck-stringer system and the girders, which were transmitted through the tie plates. The strain measurements on the tie plates and the volume of truck traffic during the structure's life were used to estimate the cumulative damage in several tie plates. Good correlation was obtained with the root mean square stress range and constant cycle laboratory fatigue test results. Miner's rule was also found to provide a good correlation.

Fatigue cracks have recently been detected at steel bridge details such as the ends of cover plates, web or flange attachments, and tie plates connecting transverse floor beams and brackets across the main girders. Among bridges that have sustained some of these cracks are the Yellow Mill Pond Bridge on the Connecticut Turnpike (1), the Lehigh River and Lehigh Canal bridges in Pennsylvania, and the Allegheny River bridge on the Pennsylvania Turnpike. All of these bridges carried large volumes of truck traffic.

Recent laboratory studies on the fatigue strength of beams with cover plates or welded attachments indicate that the stress range under live loads controls the fatigue behavior of structural details (2, 3). To further examine the fatigue behavior of several steel bridge details under traffic loading and correlate the stress range history of these details with laboratory fatigue data, pilot field tests of one of the Lehigh canal bridges were undertaken. This paper summarizes the results of these pilot studies.

Publication of this paper sponsored by Committee on Dynamics and Field Testing of Bridges.

DESCRIPTION OF BRIDGES

The Lehigh Canal bridges consist of twin bridges that carry the eastbound and westbound lanes of US-22 near Bethlehem, Pennsylvania. Each bridge is continuous for three spans and has small haunches at the interior piers (Figure 1). Each bridge has two riveted longitudinal girders with a floor beam-stringer system and a noncomposite concrete deck. The 44-m (144-ft) end span of the eastbound bridge was chosen for testing because of its accessibility. A typical cross section of the two-lane bridge is shown in Figure 2a. The details of tie plates, which connect the outrigger brackets to the floor beams and girders, are shown in Figure 2b. The bridges were constructed in 1951 to 1953 and opened to traffic in November 1953.

Inspections by Pennsylvania Department of Transportation personnel revealed several cracks in the tie plates in spring of 1972. The approximate location and length of these tie plate cracks in the test span are shown in Figure 3. Throughout the length of the Lehigh Canal bridges and the Lehigh River bridges, most of the tie plate cracks were at or near the outside edge of the longitudinal girders. Several of the plates had cracked across their entire width; some had only fine hairline cracks. All observed cracks appeared to be through the thickness of the tie plates as shown in Figure 4. All cracks started at the edge of the tie plates from a tack weld that was used to connect the tie plates to the outrigger bracket during fabrication.

STRAIN DATA ACQUISITION

Strain gauges were mounted on the tie plates, the longitudinal girders, and a stringer. Most of the gauges were placed on the tie plates parallel to the edges of these plates and above the cutoff point of the top flange of the cantilever brackets (shown in insert to Figure 5). All gauges were 6.4-mm (¼-in) electrical resistance foil gauges.

Strain variations due to traffic were recorded by using the FHWA automatic data acquisition system and an analog trace recorder. The FHWA system consists of an amplifier, an analog-to-digital signal converter, and a

computer (4). The computer was connected to a teletype machine for input-output. In this study the strain range frequencies at the gauge points were sought. As each vehicle traveled over the bridge, the magnitudes of strain ranges were recorded. After a period of time, the number of strain range excursions (occurrences) from predetermined values (levels) was printed. Very low strain ranges due to vibration and automobile traffic were excluded.

Analog traces were recorded periodically. The analog recorder used the amplifiers of the FHWA system so that strain variations of several gauges could be monitored by the two systems simultaneously.

Traffic on the bridge was correlated with recorded strains in the tie plates and girders by visually observing traffic flow and by recording the number and types of trucks for short periods of time. The standard FHWA truck classification was used to identify truck traffic. Altogether 170 h of strain data were acquired for statistical evaluation and stress analysis.

STRESSES AND DISPLACEMENTS

Stress History Measurements

From analog traces of strain variation and observations of the traffic on the bridge, it was evident that each truck crossing the bridge caused one primary stress range at all gauge points. This is true of the tie plates and the girders (Figure 6).

The recorded live load stress distributions in the tie plates with gauges are shown in Figure 3 for a given instance. The stress distribution indicates that the tie plates were subjected to bending in the horizontal plane. The gauges at the centerline of the tie plates had low stress magnitudes, implying that truck loading caused little axial elongation or vertical bending of the plates.

It is also apparent from Figure 3 that the maximum live load horizontal bending stresses in a tie plate depended on the location of the tie plate in the bridge span. Maximum stresses were higher in the tie plates near the abutment and toward the pier. This distribution agrees with the crack pattern observed in the tie plates.

Live load stresses in the longitudinal girders and in a stringer of the bridge were low compared to those observed in the tie plates. The magnitudes of maximum live load stresses in the girders were about 55 MPa (8000 lbf/in^2). These values are stress ranges resulting from stress reversal in continuous girders and are slightly higher than the maximum stresses recorded by other investigators in main longitudinal members (4, 5, 6, 7, 8).

In-Plane Bending of Tie Plates

The time variation of stresses shown in Figure 6 was the sum of the static response to a truck and the vibrational stresses. The static stress response at a point on a girder flange is analogous to the stress influence line for that point. All stress-time response records shown in Figure 6 for a gauge on a girder are typical stress influence lines for a point in the side span of a three-span continuous beam.

For tie plates, the stress-time response records (Figure 6) indicate that the pattern of stress variation was the same for all types of trucks; only the magnitude of the stress range changed. Furthermore, the relationship between the stress variation in the tie plate and those in the girder was the same for all trucks. This suggested that the stress variation in the tie plates was directly related to the behavior of the longitudinal girders. Preliminary analysis indicates that longitudinal displacement at the top flange of the girder causes horizontal bending in the tie plates (Figure 7). Because the longitudinal displacement of a point on the top flange of the girder is the product of the slope of the deflection curve and the distance from the neutral axis to that point, the strain influence line for the tie plates is analogous to the influence lines for slope in the girder at the tie plate. Figure 8 shows a comparison of the strain variation at gauges 5 and 10 on tie plates C4S and C6N and the influence lines for the slopes of the girder at the corresponding points. The similarity is apparent.

Effect of Tie Plate Geometry and Connection of Plate to Girder

Horizontal in-plane bending stresses in the tie plates and the longitudinal displacements of the top flanges of the girders were further examined by removing cracked tie plates C0S and C1S (Figure 3). New tie plates of different widths and thicknesses were placed at these locations in different combinations. The plates were bolted to the floor beam and cantilever bracket in all cases but sometimes were not connected to the top flange of the girder. Strain gauges were mounted at middepth on the edge of these tie plates to measure the horizontal in-plane bending strains due to normal truck traffic and a test truck. Simultaneously, the deflections of floor beam-outrigger bracket C0S and girder ES (Figure 5) were measured against the back wall of abutment C with dial gauges. The relative longitudinal displacements between the girder top flange and the outside stringer near floor beams C0 and C1 were also measured. The test truck was a two-axle truck with front and rear axle loads of 47 and 103 kN (10 600 and 23 200 lbf) respectively.

Table 1 gives the average maximum stress range in the tie plates under loading of a test truck and random traffic. The horizontal deflections at floor beam C0S under random truck traffic are given below (location refers to area between abutment wall and component listed):

Location	Maximum Deflection (mm)	East Departure (mm)	West Departure (mm)
Stringer	0.711	0.483	0.229
Outrigger bracket	0.508	0.381	0.127
Girder top flange	1.422	1.143	0.279
Stringer	0.432	0.406	0.025
Girder bottom flange	1.219	0.229	0.991

The results showed that

1. Unbolting the tie plate from the main girder generally decreased the stress range in the tie plates,
2. The stress range was further decreased when narrow plates were used, and
3. Changes in plate thickness did not alter the magnitude of the stress range in the tie plates.

These tests further confirmed the fact that displacements were primarily responsible for the horizontal, in-plane bending stresses in the tie plates.

The average maximum horizontal deflection of floor beam-bracket C0S and girder ES against the back wall of abutment C is given above. The horizontal displacement at the top of the girder was more than twice those occurring at the stringers and the outrigger bracket, indicating a relative displacement. Unbolting the tie plate from the girder flange and reducing the tie plate width increased the relative displacement between the top flange of the girder and the outside stringer slightly because a more flexible connection was generated, which, actually, is compatible with the design

Figure 1. Lehigh Canal bridge (instrumentation installed in left side span).

Figure 2. (a) Cross section of bridge and (b) tie plate detail at floor beam-bracket connection to girder.

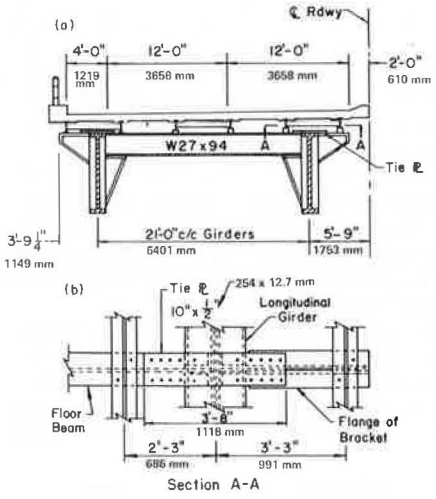

Figure 3. Cracks and stresses in tie plates of test span.

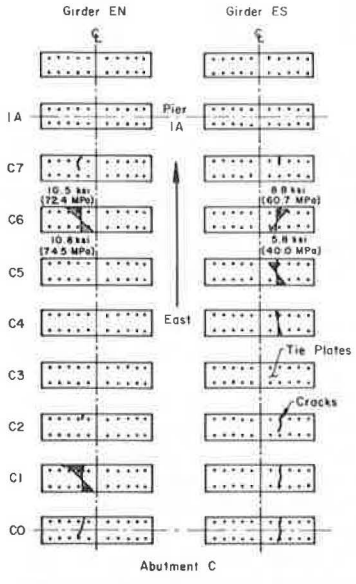

Figure 4. Crack in tie plate originating at tack weld.

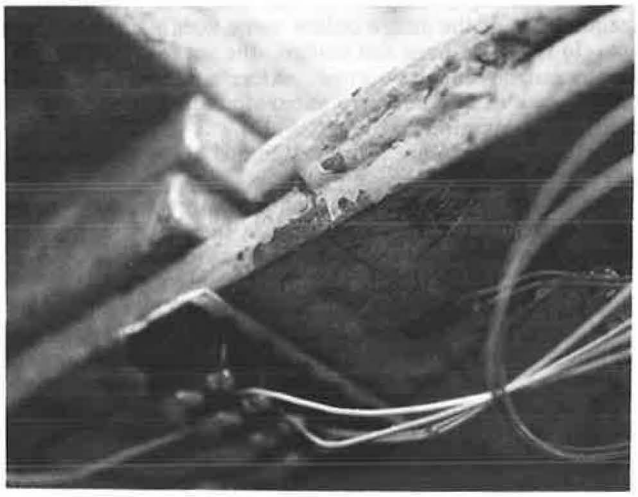

Figure 5. Instrumentation on tie plates and girder.

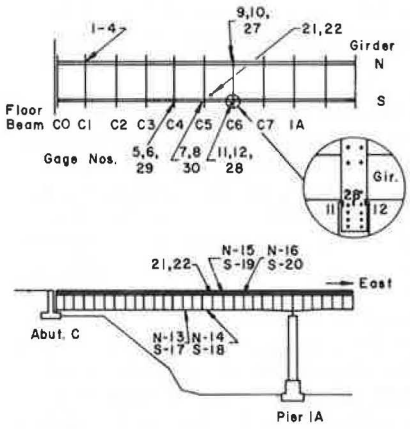

Figure 6. Comparative response of tie plate C4S and south girder under various loads.

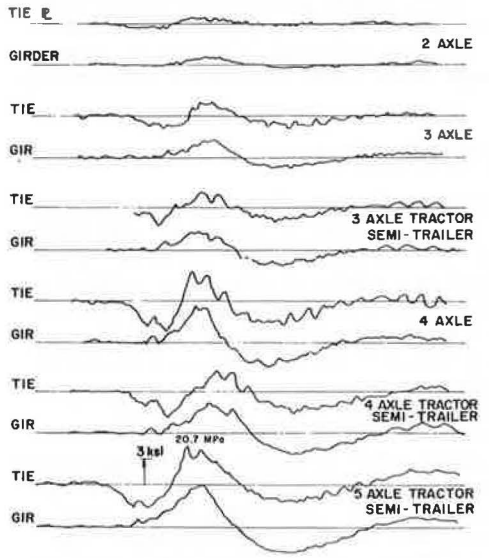

assumptions. Unbolting and reducing tie plate widths, on the other hand, greatly reduce the bending stresses in the tie plates.

STRESS RANGE UNDER RANDOM TRAFFIC

The stress range occurrence data from the FHWA system were plotted as histograms depicting the frequency of occurrence between the stress range levels. Examples are shown in Figure 9 for gauges on tie plates C4S and C6N and on girder EN. The gauge on tie plate C4S was subjected to stress reversal, and the maximum stress magnitudes were smaller than those recorded on other tie plates (Figure 3). A large percentage of the stress range occurrences was at low stress levels. Tie plate C6N was subjected to high maximum stresses, and the stress range was relatively more frequent at higher levels. There was also a tendency for two peaks on the histograms. The gauges on the main girders indicated much lower stress range levels. It was observed that only larger trucks induced stresses of more than 6.9 MPa

Figure 7. Longitudinal displacement at top flange of girder and horizontal bending of tie plate.

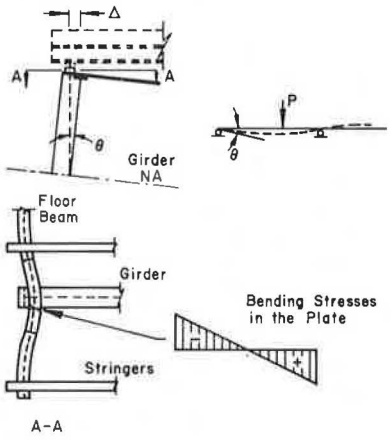

Figure 8. Comparison of measured strain history in tie plates and influence lines for girder slope.

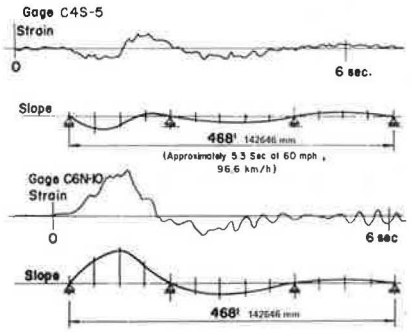

Table 1. Stress range in new tie plates.

Loading	Gauged Section on Tie Plate	Plate Thickness (mm)	Stress (MPa) 254-mm Plate Bolted	254-mm Plate Unbolted	203-mm Plate Bolted	203-mm Plate Unbolted	152-mm Plate, Unbolted
Test truck	Near bracket	25.4	72.4	65.5	—	31.0	24.8
		12.7	72.4	58.6	—	34.5	24.8
	Centerline of girder	25.4	34.5	48.3	48.3	31.0	17.2
		12.7	34.5	34.5	58.6	31.0	25.5
	Near floor beam	25.4	48.3	48.3	—	34.5	13.8
		12.7	64.1	37.9	—	34.5	21.4
Random traffic	Near bracket	25.4	141.0	124.0	—	62.1	58.6
		12.7	148.0	82.7	—	62.1	44.8
	Centerline of girder	25.4	69.0	107.0	55.2	44.8	34.5
		12.7	75.9	62.1	75.9	53.1	37.9
	Near floor beam	25.4	75.9	82.7	—	—	27.6
		12.7	82.7	58.6	—	55.2	31.0

Note: 1 mm = 0.039 in; 1 MPa = 145 lbf/in^2.

Figure 9. Stress histograms.

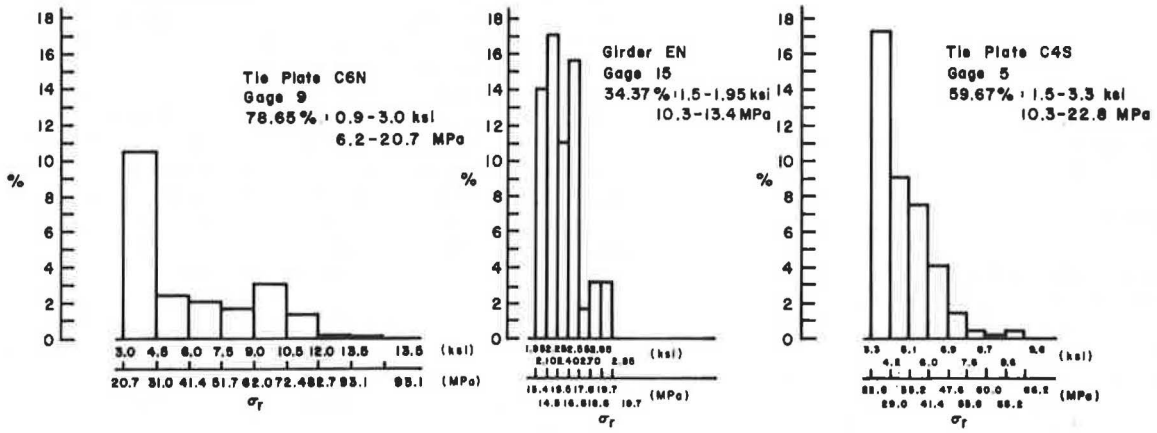

Figure 10. Gross vehicle weight distribution.

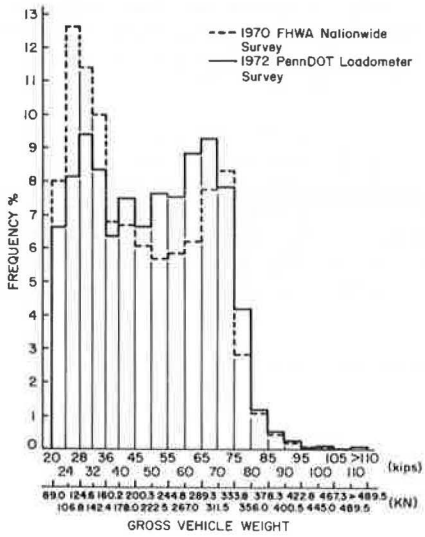

Figure 11. Estimated ADTT at the Lehigh Canal bridge.

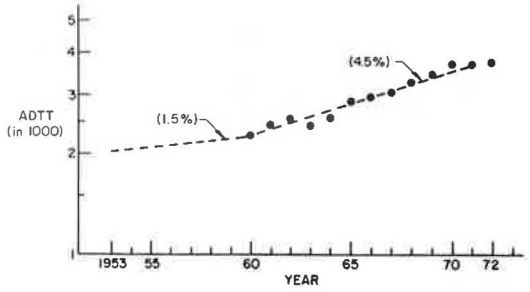

Figure 12. Comparison of estimated equivalent stress range with laboratory test data.

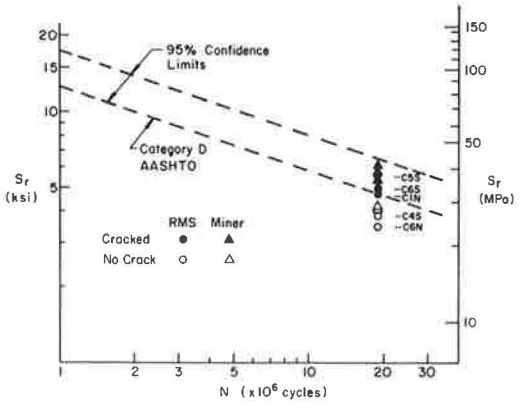

(1000 lbf/in^2) in the girders. The single-peaked histograms reflect this response.

TRAFFIC RECORDS

Traffic counts taken during the in-service testing indicated that the highest volume of trucks consisted of five-axle tractor semitrailers (3S-2). The Pennsylvania DOT provided 24-h traffic counts taken during 1972-73 at a site near the Lehigh Canal bridge. A comparison showed that the 24-h traffic surveys resulted in more two-axle trucks and five-axle tractor semitrailers than were observed at the bridge site during the short sample periods. Overall, the percentages of various types of trucks from the 24-h records were consistent with the observations at the bridge site. Pennsylvania DOT records were also consistent with results from loadometer surveys throughout the state and the nation.

The results of a 1970 FHWA nationwide loadometer survey and the results of a 1972 Pennsylvania DOT loadometer survey for 20 stations on main arteries in Pennsylvania are shown in Figure 10. The relative distributions of truck weight frequencies from the two surveys are comparable. The two peaks in the histograms indicate a large number of loaded trucks of 267 to 334 kN (60 000 to 75 000 lbf) and large numbers of two-axle or unloaded tractor semitrailers of 107 to 160 kN (24 000 to 36 000 lbf).

Inasmuch as the results of traffic counts at the bridge were consistent with traffic counts of the Pennsylvania DOT, which in turn were comparable to results from state and nationwide loadometer surveys, the results of traffic counts at the bridge were considered representative of the normal traffic crossing the Lehigh Canal bridge. Furthermore, the measured stress range histograms were considered to be representative of the stress range spectra due to the truck traffic crossing the bridge.

The total number of trucks that have traveled over the bridge during the 19-year period from 1953 to 1972 was estimated from the Pennsylvania DOT traffic count data. These estimated average daily truck traffic (ADTT) counts are shown in Figure 11 and range from 2038 trucks per day in 1953 to 3709 in 1972. The average rate of increase was about 1.5 percent before and 4.5 percent after 1960 when main arteries leading to the bridge were open to traffic. The total volume from 1953 to 1972 was estimated to be 18.9 million trucks.

CORRELATION WITH FATIGUE TEST RESULTS

Results from beam tests and girder tests in the laboratory have indicated that stress range and the length of welded attachments are controlling factors for fatigue strength (2, 3). Design specifications are derived from available test results (9). Bending tests of tie plates with tack welds (10) showed that category D of the 1974 AASHTO specification is applicable to tack-welded tie plates.

The riveted tie plates of the Lehigh Canal bridge were subjected to horizontal in-plane bending under random truck traffic. Most of the tie plates have 25 to 50-mm-long (1 to 2-in) tack welds connecting the edges of the tie plates to the top flange of the bracket as shown in Figure 4. Load transfer between the flange of the outrigger bracket and the tie plate was provided by both the rivets and the tack welds. Because the tack welds were at the end of the joint, which is the most highly stressed region (11), the stress concentration at the end of the tack weld appears to be as severe as the condition at short attachments to beam flanges as was confirmed by the pilot studies (10). In comparisons of laboratory fatigue test results and measured stresses at the bridge, adjustments must be made to the measured stresses because cracks occurred at the edges of the tie plates where stresses were higher. Furthermore, the measured stresses were not of constant magnitude.

One procedure to account for the stress range spectrum is the root mean square (RMS) method (2, 12, 13). In this method, the RMS of the stress ranges in a spectrum is considered equivalent to a constant cyclic stress range and is correlated with the number of stress cycles corresponding to the spectrum. The RMS stress range is defined as

$$S_{rRMS} = \left(\sum \alpha_1 S_{ri}^2\right)^{1/2} \quad (1)$$

where α_1 is the frequency of occurrence of stress range S_{ri}.

The stress range occurrences of the gauges of the tie plates were used to determine the RMS values of stress ranges. These values were then adjusted to the plate edges where the crack growth originated.

The S_{rRMS} at the plate edge and the fatigue cycles corresponding to the truck traffic (18.9 million) are shown in Figure 12 and are compared with the constant stress range laboratory data. The data from the Lehigh Canal bridge lie above or near the lower confidence limit for category D. Cracks were observed in tie plates C1N, C5S, and C6S; the data (circles) are on or above the lower confidence limit. Tie plates C4S and C6N had no visible cracks at the time of measurement; the data points for these two plates are below the category D line.

The comparison shown in Figure 12 indicates that, when the RMS stress range is used, the lower confidence limit for category D of AASHTO provides a reasonable lower bound to the fatigue strength of the tack-welded tie plates of the Lehigh Canal bridge. Tie plates that plotted above this limit could be expected to exhibit visible fatigue cracking. The plates C4S and C6N can be expected to develop fatigue cracks under additional truck traffic.

Another procedure to account for cumulative damage is Miner's hypothesis (12). Tie plates C1N, C5S, and C6S had cracks; the cumulative damage ratio based on Miner's hypothesis was close to or higher than 1.0. No visible cracks were detected at tie plates C4S and C6N, which had damage ratios less than unity.

By combining the relationship provided by constant cycle data (2) and Miner's rule (12), an equivalent stress range S_{rMiner} was estimated (13) as

$$S_{rMiner} = \left(\sum \alpha_i S_{ri}^3\right)^{1/3} \quad (2)$$

The S_{rMiner} values of the tie plates are also shown in Figure 12. The results demonstrate that by using Miner's rule the lower confidence limit for category D of AASHTO 1974 specifications also provides a reasonable estimate of the fatigue strength of the tie plates of the Lehigh Canal bridge.

SUMMARY AND CONCLUSIONS

From the pilot field studies and the analysis of results of the Lehigh Canal bridges, the following conclusions can be reached.

1. The live load stresses in the main longitudinal girders were similar to those observed in longitudinal members of other bridges. The maximum live load stresses (stress ranges) were 55 MPa (8000 lbf/in^2).
2. The live load stresses in the tie plates connecting the outrigger brackets and floor beams were much higher than those observed in the longitudinal members. The distribution of these stresses in the plates indicates that horizontal in-plane bending was occurring with little axial extension or twisting of the plates.
3. The development of live load stress in the tie plates was related to displacements caused by longitudinal strain of the main girder under bending. The relative longitudinal movement of the top flange of the main girder with respect to the stringers, brackets, and concrete slab caused a horizontal bending of the tie plates.
4. Unbolting the tie plates from the girder and reducing the tie plate width both decreased the magnitude of the in-plane bending stresses in the tie plates. Bridges using this system in the future should avoid connecting the tie plate to the girder.
5. The crack pattern in the tie plates agreed with the measured strain ranges.
6. The measured stress history for short time periods was compatible with the frequency distribution of trucks reported by the Pennsylvania DOT and FHWA on comparable roads.
7. The RMS stress range and an estimated traffic volume for 1953 to 1972 indicated that category D of 1974 AASHTO interim specifications provides good correlation with crack occurrence on several tie plates.
8. Miner's hypothesis also showed that category D provides a reasonable estimate of the damage that had occurred in the tie plates.

It is apparent that care should be taken to minimize displacement-induced moment and stresses such as those occurring in the tie plates. Very short distances between the first stringer on a bracket and a longitudinal girder result in high displacement-induced moments in the tie plates. These moments are reduced when this distance is increased.

On the Lehigh Canal bridge, more comprehensive studies are being undertaken to develop more complete knowledge of the stress range-life relationship as the bridge provides a unique opportunity to relate laboratory studies to the random loading and corresponding bridge response.

ACKNOWLEDGMENTS

This investigation is a part of a research project being conducted at Fritz Engineering Laboratory, Lehigh University. The project is sponsored by the Pennsylvania Department of Transportation and the Federal Highway Administration, U.S. Department of Transportation.

Thanks are due to Hugh T. Sutherland, Fritz Laboratory Instruments associate, and H. Latz, FHWA, for their assistance in acquiring the data. The assistance of the Fritz Engineering Laboratory staff is also acknowledged.

REFERENCES

1. D. G. Bowers. Loading History of Span 10 on Yellow Mill Pond Viaduct. HRB, Highway Research Record 428, 1973, pp. 64-71.
2. J. W. Fisher, K. H. Frank, M. A. Hirt, and B. M. McNamee. Effect of Weldments on the Fatigue Strength of Steel Beams. NCHRP, Rept. 102, 1970.
3. J. W. Fisher, P. A. Albrecht, B. T. Yen, D. J. Klingerman, and B. M. McNamee. Fatigue Strength of Steel Beams With Transverse Stiffness and Attachments. NCHRP, Rept. 147, 1974.
4. C. F. Galambos and W. L. Armstrong. Loading History of Highway Bridges. Bureau of Public Roads, U.S. Department of Transportation, Jan. 1969.
5. G. R. Cudney. The Effects of Loading on Bridge Life. HRB, Highway Research Record 253, 1968, pp. 35-71.
6. W. T. McKeel, Jr., C. E. Maddox, Jr., H. L. Kinnier, and C. F. Galambos. Loading History Study of Two Highway Bridges in Virginia. HRB, Highway Research Record 382, 1972, pp. 27-37.
7. W. L. Armstrong. Dynamic Testing of Curved Bridge—Huyck Stream. Journal of Structural Division, Proc., ASCE, Vol. 98, No. ST9, Sept. 1972.
8. F. Moses and R. Carson. Probability Theory for

Highway Bridge Fatigue Stresses. Case Western Reserve Univ., Cleveland; Ohio Department of Transportation, Final Rept., SMSMD No. 50, July 1973.

9. J. W. Fisher. Guide to 1974 AASHTO Fatigue Specifications. American Institute of Steel Construction, 1974.
10. D. P. Erb. Fatigue Strength of Tack Welded Tie Plates. Lehigh Univ., Bethlehem, Penn., MS thesis, Sept. 1975.
11. J. W. Fisher and J. Struik. Guide to Design Criteria for Bolted and Riveted Joints. Wiley Interscience, 1974.
12. M. A. Miner. Cumulative Damage in Fatigue. Journal of Applied Mechanics, Vol. 12, No. 1, Sept. 1945.
13. C. G. Schilling, K. H. Klippstein, J. M. Barsom, and G. T. Blake. Fatigue of Welded Steel Bridge Members Under Variable Amplitude Loading. NCHRP, Research Results Digest 60, 1974.

Abridgment

Replacement or Repair of Old Truss Bridges

Conrad P. Heins, University of Maryland
William S. Fout and Raymond Y. Wilkison, Frederick County Roads Board, Frederick, Maryland

Throughout Frederick County, Maryland, and possibly many other counties in Maryland, there are many steel truss bridges that were built in the late nineteenth century. Most of these truss bridges are on secondary roads and carry a single lane of local traffic. Their importance, however, cannot be minimized, for they supply a great need to the local community.

All of these bridges have been inspected and rated. In many instances the ratings are so low that only passenger cars are permitted to cross the bridge. School buses, farm equipment, and trucks must find an alternate route, or the bridge must be replaced or repaired to upgrade its capacity. Because the cost of replacing these bridges is prohibitive, the solution is to repair and strengthen the bridges. The actual strength of the bridges can only be determined if the bridge is examined under a typical truck loading.

This paper presents the results of tests on six such steel truss bridges and the effects that strengthening of the deck had on the floor system. Also presented are the results of laboratory tests on stringer beams when the beams are stiffened with nailers and planking. The results yield a distribution factor that is less conservative than that of AASHTO.

PROBLEM

The useful carrying capacity of bridge elements can be determined by analytical methods or experimental tests. When the structural system is highly indeterminant, simplified analytical methods can greatly underestimate the load-carrying capacity. In the instance of bridge structures, which are highly indeterminant systems, the ultimate load capacity may be 15 times the elastic capacity.

Six truss bridges throughout Frederick County, Maryland, were examined, and the allowable load capacity was determined by simplified analytical techniques. These results recommend a severe lowering of the carrying capacity of the bridges. These results may be reasonable at face value. However, from field observations it has been noted that the bridges have supported much greater loads without any noticeable detrimental effects to the structure. Therefore, there is some disagreement between the analysis results and what is actually occurring in the structure under load.

This discrepancy was overcome by testing six selected bridges and certain components in the laboratory under a known load and proper instrumentation. The results of the testing and the rating of the bridges are presented.

PROGRAM DETAILS

The objectives of the study were to

1. Select six bridges that had been inventoried, inspected, and rated for test purposes;
2. Examine and study the bridge inspection and rating reports for each bridge, and locate critical members;
3. Determine the location of strain gauges for each bridge;
4. Determine the field truck loading position;
5. Instrument the bridge with strain gauges;
6. Test the bridge, i.e., position a loaded truck at various locations on the bridge and read gauges;
7. Reduce data, and develop rating;
8. Test in the laboratory typical floor beams with and without nailers;
9. Compare field and laboratory test results with analytical data; and
10. Prepare recommendations for the rating of the bridges.

BRIDGE FIELD TEST STUDY

Bridge Description and Gauge Locations

The six truss bridges that were field tested consist of single-lane steel pinned, jointed truss structures approximately 4.6 m (15.0 ft) wide with spans 18 to 27 m (60 to 90 ft) long. With the exception of the Gapland Road bridge, the other five bridges have wooden decks. These

Publication of this paper sponsored by Committee on Dynamics and Field Testing of Bridges.

Table 1. Rating of Long Mills Road bridge over Owens Creek.

Member	Gauge	Dead Load Stress (MPa)	Live Load Stress (MPa)	Allowable Stress (MPa)	Rating
Floor beam	1	20.7	82.8	69.0[a]	H8.8
Diagonal	2	0	32.4	86.3	H40
Diagonal	3	0	-33.8	86.3	H12.8
Stringer	4, 5	—	68.3	86.3	H18.9
Bottom horizontal	6	33.1	18.6	86.3	H42.8
Bottom horizontal	7	33.1	22.8	86.3	H35

Note: 1 MPa = 145 lbf/in^2.
[a]Corrosion of member.

Table 2. Rating of Daysville Road bridge over Israel Creek.

Member	Gauge	Dead Load Stress (MPa)	Live Load Stress (MPa)	Allowable Stress (MPa)	Rating
Stringer	1	6.9	72.5	86.3	H16.4
Bottom horizontal	2	27.6	20.7	86.3	H42.5
Top horizontal	3	-19.3	-43.5	32.4	H4.5
Top horizontal	4	-19.3	-35.2	32.4	H5.6
Floor beam	5	24.2	147.0	82.8	H6
Vertical	6	0	12.4	86.3	H104

Note: 1 MPa = 145 lbf/in^2.

Table 3. Rating of Water Street bridge over Israel Creek.

Member	Gauge	Dead Load Stress (MPa)	Live Load Stress (MPa)	Allowable Stress (MPa)	Rating
Diagonal	1	23.5	60.0	75.9	H13
Bottom horizontal	2	37.3	33.1	86.3	H22
Stringer	3	8.3	51.8	86.3	H22.6
Diagonal	4	58.0	49.7	—	—
Floor beam	5	14.5	18.6	43.1	H23
Top horizontal	6	-24.8	-31.1	58.7	H16

Note: 1 MPa = 145 lbf/in^2.

Table 4. Rating of Gapland Road bridge over Broad Run.

Member	Gauge	Dead Load Stress (MPa)	Live Load Stress (MPa)	Allowable Stress (MPa)	Rating
Stringer	1	5.7	45.5	86.3	H26.7
Floor beam	2	20.0	66.2	86.3	H11.5
U-bolt	3	—	70.4	—	—
Vertical[a]	4	12.4	33.1	43.1	H14
Vertical[a]	5	12.4	2.1	43.1	H225
Bottom horizontal	6	31.1	24.8	86.3	H33
Diagonal	7	33.8	66.2	69.0	H8

Note: 1 MPa = 145 lbf/in^2.
[a]Corrosion of member.

Table 5. Rating of Old Hagerstown Road bridge over Little Catoctin Creek.

Member	Gauge	Dead Load Stress (MPa)	Live Load Stress (MPa)	Allowable Stress (MPa)	Rating
Bottom horizontal	1	35.9	10.4	86.3	H73
Diagonal	2	26.9	51.8	86.3	H17
Stringer	3	13.1	134.6[a]	86.3	H8
Stringer	4	13.1	117.3[a]	86.3	H9.4
Stringer	5	13.1	183.5[a]	86.3	H6.5
Floor beam	6	29.0	86.9	86.3	H9.9

Note: 1 MPa = 145 lbf/in^2.
[a]Without lateral support. With lateral support through new nailers, the live load stress would be 69 MPa and the ratings would be H15.9.

decks are nailed to nailing strips attached to the steel stringers. The deck members are generally wooden (7.6 by 25.4 cm or 3 by 10 in) and the nailers are wooden (7.6 by 25.4 cm or 3 by 10 in), either of pine or oak. The Gapland Road bridge deck consists of steel grating.

Each of the six bridges was instrumented with SR-4 strain gauges at various positions.

Loading

The truck load that was applied to each bridge consisted of a gravel loaded 2D truck. The rear axle weight of 10.2 Mg (22.5 kips) was positioned along the bridge at various locations, as dictated by the influence lines, to institute maximum effects. These trucks are similar to the design H15 vehicle, which has a rear axle weight of 10.8 Mg (24 kips) and front axle weight of 2.7 Mg (6 kips). This type of vehicle represents the worst possible load a bridge can be subjected to.

Test Results

The test truck was placed on each bridge at various positions, and the induced strains on the various members were recorded. In some instances, the strain gauges were monitored for both static and dynamic loading.

The resulting induced stresses are given in Tables 1 through 6 for each of the six bridges. The gauge numbers refer to the gauge locations on the bridge. The tabulated stresses were obtained by converting the strain readings from an assumed elastic modulus of 2.07 GPa (30 million lbf/in^2).

BRIDGE DESIGN STUDY

As mentioned previously, each of the six bridges was rated based on a complete analytical study. The ratings were obtained after computing the probable induced dead and live load stresses and the allowable stresses. The allowable stresses were selected from the AASHTO specification in the Manual for Maintenance Inspection of Bridges and field observations; the design value of certain members was reduced if the member was noted to be distorted or corroded. With these criteria and field observations of the various members, the rating of each bridge was computed. The ratings correspond to H15 truck with an appropriate reduction.

Those members of each bridge that govern the rating are as follows:

Bridge	Member	Gauge	Rating
Longs Mill Road	Stringers	4, 5	H0
Crum Road	Floor beam	2	H2
Water Street	Diagonal	1	H1.2
Daysville Road	Stringer, floor beam	1, 5	H3
Old Hagerstown Road	Stringer	3, 4, 5	H1
Gapland Road	Diagonal	7	H5

If the dead load stresses computed are accurate, it remains to establish the accuracy of the live load stresses. Such stresses were obtained through tests (Tables 1 through 6). These field live load stresses, in conjunction with the computed dead load stresses, were used to reevaluate the bridge ratings.

LABORATORY STUDY

As described, the ratings of three of the six bridges are governed by the strength of the stringers. In most instances, these low ratings are due to the fact that no lateral bracing of the compression flange is assumed. To rectify this condition, the county engineer devised a

Table 6. Rating of Crum Road bridge over Israel Creek.

Member	Gauge	Dead Load Stress (MPa)	Live Load Stress (MPa)	Allowable Stress (MPa)	Rating
Top chord	1	-22.1	-39.3	86.3	H9.9
Floor beam	2	42.8	107.6	86.3	H6
Stringer	3	6.2	58.0	86.3	H20.7
Vertical	4	10.4	26.9	86.3	H42
Bottom horizontal	5	35.2	43.5	86.3	H17.6
Bottom horizontal	6	31.0	39.3	86.3	H21
Top chord	7	26.2	20.7	86.3	H44

Note: 1 MPa = 145 lbf/in^2.

method of providing continuous lateral bracing by attaching wooden (7.6 by 20.3-cm or 3 by 8-in) nailing strips to each stringer. The top deck is then nailed to the nailing strips to provide continuous lateral support.

To determine the effectiveness of this type of bracing, a series of laboratory tests was conducted to accurately evaluate the strength of the stringer members and thus provide an alternate rating.

Model Descriptions

Two models were constructed for test purposes. One model consisted of three 6I12.7, 3.1-m-long (10.0 ft) steel girders spaced 0.9 m (3.0 ft). The three girders were welded at each end to 7.6 by 7.6-cm (3 by 3-in) steel angles. The other model consisted of the same members but had nailing strips bolted to the side of each stringer. Attached to each strip were 7.6 by 25.4-cm (3 by 10-in) wooden planks.

Each model was instrumented with SR-4 strain gauges attached on the top and bottom flanges at midspan. Vertical deformation at midspan of the models was also measured during each test.

The models were subjected to two loads applied on the top flange of the center girder. The model without the nailing strips had similar planking laid across the model width.

Results

The resulting stress data indicate that the average distribution is 14, 72, 14 percent for the model without nailers and 22, 56, 22 percent for the model with nailers for the exterior, center, exterior girders. Based on this information, the load distribution factors are S/4.2 and S/5.2 for the decks without and with nailers respectively.

BRIDGE RATING

Each of the six bridges had been rated previously; however, these ratings were revised by using the observed field live load stresses and computed dead load stresses. A summary of these results (Tables 1 through 6) yielded the following new bridge rating:

Bridge	Rating	Bridge	Rating
Longs Mill Road	H10	Gapland Road	H8
Daysville Road	H5	Old Hagerstown Road	H10
Water Street	H10	Crum Road	H6

For the Water Street and Old Hagerstown Road bridges new floor systems are required. The Daysville and Gapland Road bridges, which have ratings less than H10, are governed by the truss elements. The Crum Road bridge rating is governed by the floor beam. A comparison of these new ratings and the analytical ratings, as listed previously, shows a substantial increase in the load capacities of the six bridges.

Field Testing of a Reinforced Concrete Highway Bridge to Collapse

James L. Jorgenson, Department of Civil Engineering
Wayne Larson,* Solien Engineering

A three-span reinforced concrete slab bridge was loaded to collapse. The slab was 9.75 m (32 ft) wide and 30.5 cm (12 in) thick, and on each edge was cast a 92 by 25.4-cm (34 by 10-in) curb. Loading was produced by hydraulic rams that were reacted to by overhead steel beams attached to the piers by tension rods through the slabs. The load was increased at intervals, and at each interval deflection and strain on the concrete surface were measured. The strength of the concrete and steel materials was more than the design minimum values; average cylinder strength was 47.33 MPa (6865 lbf/in^2) compared with a design value of 20.68 MPa (3000 lbf/in^2), and average steel coupon yield strength was 365.77 MPa (53 050 lbf/in^2) compared with a design value of 275.79 MPa (40 000 lbf/in^2). The results indicate that (a) the measured concrete stresses were lower than the calculated values; (b) the load causing first permanent set was accurately predicted by calculating the yield moment in the slab; (c) the collapse load was accurately predicted by considering the formation of yield moments along the centerline and over the piers of the bridge for a channel section loaded around its weak axis; and (d) based on the line load for the center span, it would take 8 HS20-44 trucks placed in the center of the bridge to cause any permanent deflection and 20 HS20-44 trucks to cause collapse.

This paper reports on the field testing to failure of a 10-year-old reinforced concrete highway bridge that was taken out of service when the highway was realigned. The test results are to be used to determine the magnitude of overload permitted on similar bridges. Seldom is a full-sized bridge available for testing to destruction, and, when it is, seldom can an economical loading system be devised for the tests. Most of the literature on strength of highway bridges is based on laboratory tests on small-scale beams and slabs, although Burdette and Goodpasture recently reported on testing to destruction of four highway bridges in Tennessee (1).

The testing program had the following objectives:

1. To compare the design stress with stresses measured on the bridge slab,
2. To determine the stresses caused by a four-wheel load pattern placed at the center of the middle span,
3. To find the load at which the first permanent set occurs and to compare this with the computed value, and
4. To compare the measured and computed ultimate strengths of the bridge.

DESCRIPTION OF BRIDGE

The bridge was on ND-18 located 1.6 km (1 mile) south of Casselton. It was a three-span, cast-in-place, reinforced bridge with a two-lane roadway (Figure 1). The slab was 9.75 m (32 ft) wide and 30.5 cm (12 in) thick, and on each side was cast a 92 by 25.4-cm (34 by 10-in) curb. The spans were 6.1, 7.6, and 6.1 m (20, 25, and 20 ft). The direction of the drainage ditch below the bridge required that the piers and abutments be on a 25-deg skew. Also, the bridge was located on an 8-deg horizontal curve that required a superelevation of the roadway surface on a slope of 1 to 16.

The curb on each side of the roadway was not cast monolithically with the slab; however, it was keyed into the slab, and tie bars were extended from the slab to the curb. A reinforced concrete guardrail and posts existed above the curb. The guardrail was removed before the bridge was tested. The bridge was constructed with No North Dakota State Highway Department class AE-1 1/2 concrete requiring a concrete cylinder strength of 20.68 MPa (3000 lbf/in^2). The reinforcing was intermediate grade with a minimum yield of 275.79 MPa (40 000 lbf/in^2).

TESTING PROGRAM

Application of Loads

The wheel load pattern used by a vehicle causing an overload is unknown; hence, two load patterns were approximated. The first loading was a four-wheel pattern placed at the center of the span and used only for stresses within the linear range. The wheels were 1.8 m (6 ft) apart transversely and 1.2 m (4 ft) apart longitudinally. The second loading was placed linearly across the center of the center span and used to destroy the bridge.

The framing used for the test loads is shown in Figure

Publication of this paper sponsored by Committee on Dynamics and Field Testing of Bridges.

*Mr. Larson was a graduate assistant at North Dakota State University when this research was performed.

Figure 1. Plan and longitudinal section of bridge.

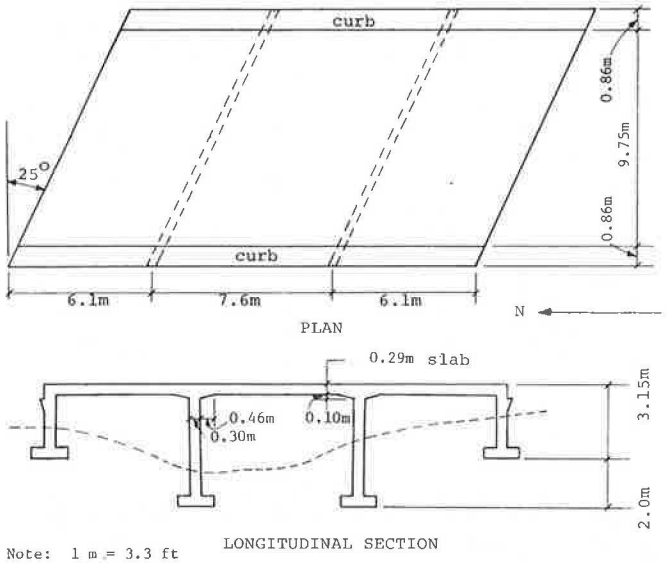

Note: 1 m = 3.3 ft

Figure 2. Framing used to provide test loads.

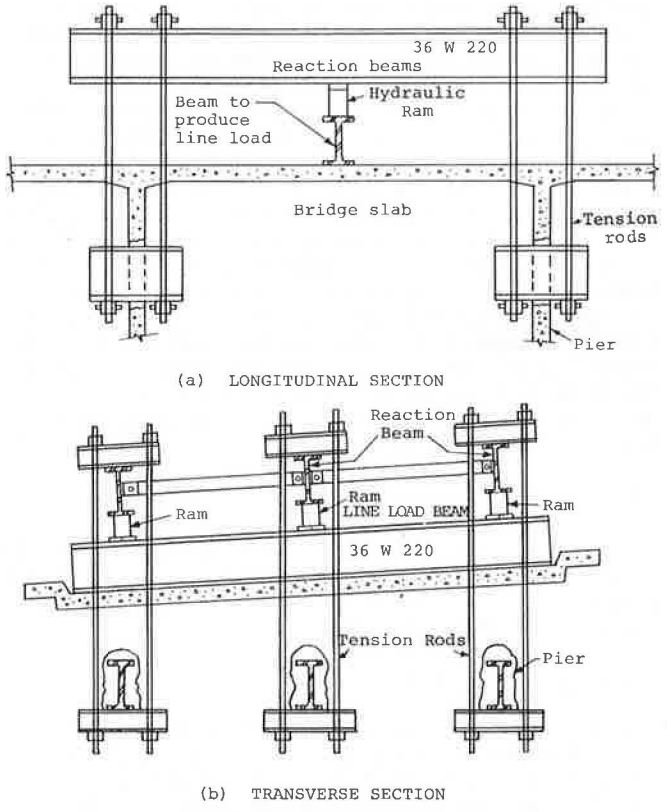

2. The wide flange beam at the center of the span was used to produce the line load on the bridge and was loaded by three hydraulic rams. The reaction to the rams was provided by three reaction beams, each end anchored to the pier by four tension rods running through 10-cm (4-in) diameter cored holes in the slab. The same framing arrangement was used for the four-wheel load pattern except that the line load beam was replaced with a small frame, which produced the four-point load from the single ram at the center of the bridge.

Bearing plates 20 cm (8 in) square simulated the wheel contact area. The line load beam had a 30-cm (12-in) wide lower flange. Plywood, 1.6 cm (58 in) thick and 46 cm (18 in) wide, was used to provide a more uniform load at the contact surface. When the three-jack arrangement shown in Figure 2b did not produce failure of the bridge, one additional ram was placed at each end of the line load beam.

Loading Procedure

The first loading applied to the bridge was the four-wheel load pattern. The hydraulic rams were activated by a Riehle hydraulic pumping and indicating unit having a 68.95-MPa (10 000-lbf/in^2) pressure capacity. The pumping unit was transported to the site and stored in an enclosed truck. Since the line load beam and jack weight on the bridge was 40 kN (9000 lbf), all ram loadings were increased by this amount. However, this load was not included in deflection or strain measurements inasmuch as all gauges were zeroed when the beam and jack were already in place.

The four-wheel load pattern was loaded to a total of 293 kN (66 000 lbf) in four approximately equal load increments. This load was believed to be well below the load that would cause permanent deflection. After each load increment, when "equilibrium deflection" was reached, deflection dial and strain gauge readings were taken. The equilibrium deflection was arbitrarily established as the deflection at which the deflection rate at midspan was less than or equal to 25.4 μm/min (0.001 in). After the final loading was applied and all strain gauges and deflection measurements were taken, the pressure on the hydraulic ram was released and zero ram load readings were taken.

The line loading pattern was then carried out. The first loading increment was 334 kN (75 000 lbf), and each subsequent load was raised by 222 kN (50 000 lbf). After each loading increment, strain and deflection readings were taken at all locations. To detect the presence of any permanent deflection, the load was removed when a total load of 1001 kN (225 000 lbf) was reached. The same procedure was used at a total load of 2113 kN (475 000 lbf) and again when the load reached 3225 kN (725 000 lbf). The limit of the initial loading system was reached at 3670 kN (825 000 lbf). Although there was a deflection at the center of the span equal to 3.81 cm (1½ in) at this loading, complete failure had not been achieved. The loading was removed and final strain and deflection readings were taken.

Two weeks later, the testing resumed and two additional hydraulic rams were used. For this loading only deflection readings were taken, for many of the strain gauges were broken because of the cracking of the concrete. The loading was applied in 445-kN (100 000-lbf) increments up to a total load of 3114 kN (700 000 lbf), after which 222-kN (50 000-lbf) increments were used until the total load reached 4003 kN (900 000 lbf). At this time the midspan dial reading was reset to zero and read at every 0.6 cm (¼ in), a safe distance away from midspan. After 7.6 cm (3 in) of dial guage had expired, the loading was controlled by transit readings on one of the scales attached to the bottom surface of the bridge slab.

Strain Measurements

Strain measurements were taken at various points on both the upper and lower surfaces of the bridge. These strains were measured with both an electrical resistance strain guage [with a 15-cm (6-in) guage length] and a mechanical strain guage. Because approval from the North Dakota State Highway Department was received in December, the strain guages had to be applied in cold weather.

Figure 3. Deflections due to four-wheel load of 254 kN (57 000 lbf).

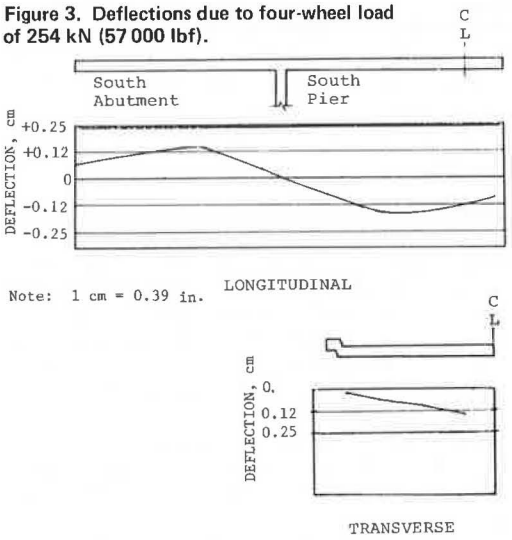

Figure 4. Line load versus deflection.

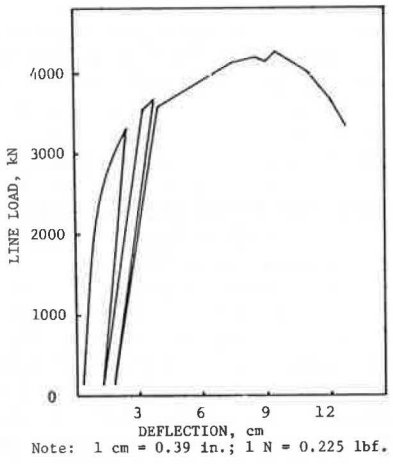

An unsuccessful attempt was made to locate a glue that would adhere in a temperature of -23°C (-10°F). Finally, regular epoxy glue was applied after the contact surface was heated to about 15.5°C (60°F) for a 10-hour period so that the glue could set properly.

During the heating process, the entire area below the bridge was enclosed with plastic. A propane burner with a blower was placed below the slab and heated an area on the lower surface of about 30.4 cm (12 in) in diameter to about 15.5°C (60°F). Since the top surface of the bridge was not covered, plywood boxes were built and placed over the location where the strain gauges were to be applied. Holes were cut in the boxes so flame throwers could direct heat toward the area. This procedure maintained the temperature required for the concrete surface. The strain gauges were then glued in place and held firmly by pressure plates. The heat was kept on for 10 h while the glue cured.

The gauges were arranged in a 45-deg rosette pattern, with one of the gauge axes parallel to the longitudinal axis of the bridge. Each gauge location contained electrical resistance strain gauges and three sets of mechanical stops for the mechanical strain gauges. For each strain gauge group located on the upper surface, a group was placed on the bottom surface of the slab in the same pattern.

Deflection Measurements

Twenty dial guages [with 25.4-μm (0.001-in) graduation] were used to measure the slab deflections at different locations on the top surface of the bridge. These gauges were mounted on a light-steel framework supported above the center of the two piers, hence essentially independent of the bridge slab being tested. To provide a smooth contact surface for the gauges, small metal plates were attached to the concrete surface.

Another set of deflections were taken on the underside of the slab during the line loading. Scales were attached to blocks of wood that were glued to the bottom surface of the slab. Taut wires were strung between the pier walls and located next to the scale. These readings were taken from a transit telescope located about 15 m (50 ft) away in the bed of the drainage ditch.

TEST RESULTS

Figure 3 shows the deflections due to the four-wheel loading of 254 kN (57 000 lbf). At this loading the deflection at the center of the bridge was 61.6 mm (0.062 in). However, the deflection 66 cm (2.2 in) south of the bridge center was 1.7 mm (0.066 in).

The line load deflection curve for the center of the bridge is shown in Figure 4. The curve indicates the loading cycles reported earlier and shows an ultimate load of 4226 kN (950 000 lbf). Transverse and longitudinal deflections were similar in shape to those reported for the four-wheel load pattern (Figure 3).

A number of 10-cm-diameter (4-in) cores were taken from the bridge slab and tested (AASHO T-148) by the state highway department. The strength results of 12 cores are as follows: average value of 47.33 MPa (6865 lbf/in^2), value range of 43.54 to 51.85 MPa (6315 to 7520 lbf/in^2), and standard deviation of 2.84 MPa (412 lbf/in^2).

At the conclusion of the bridge testing and before the bridge destruction, specimens of steel reinforcing near the supports were removed and tested (AASHO T-68) at the North Dakota State University for yield strength. The results for seven tests are as follows: average value of 365.77 MPa (53 050 lbf/in^2), value range of 307.09 to 406.51 MPa (44 540 to 58 960 lbf/in^2), and standard deviation of 36.04 MPa (5227 lbf/in^2).

CALCULATIONS

Calculations can be used to predict the performance of the bridge. Calculations are used here to indicate the design load stresses, the load causing permanent set, and the ultimate load on the bridge.

Design Load Stresses

The bridge was designed for an HS20-44 load (2). Moments and stresses used in bridge design are given in Table 1. The moments were calculated on the basis of an elastic analysis for a three-span continuous slab. The stresses are based on a working stress theory; the steel concrete modular ratio is equal to nine.

Load Causing First Permanent Set

Except for the cracking of the concrete in tension, a reinforced concrete section will behave elastically until the steel reaches its yield stress. Beyond yield stress, there will be a permanent deflection in the beam. Therefore, it is important to identify the minimum load that will cause a permanent set in the bridge slab.

For the 27.7 cm^2/m (1.31 in^2/ft) of steel in the lower

face of the 9.75-m-wide (32-ft) slab, the live load moment necessary to produce yielding is 2210 kN·m (1 630 000 lbf·ft). This moment can be converted to a transverse line load along the center of the bridge by the following equation: Moment = coefficient × load × length. If the length of the exterior span of this three-span, simple supported bridge is used, the coefficient is 0.2106. Using the live load moment given above of 2210 kN·m (1 630 000 lbf·ft) gives a line load of 1721 kN (387 000 lbf) that must be applied along the centerline to cause permanent set.

During testing, the curbs and slabs were observed to be acting together, and the moment was thus approximated in two parts. The moment in the slab was 2074.4 kN·m (1 530 000 lbf·ft), and the moment in each curb for 11.6 cm^2 (1.8 in^2) of steel was 223.7 kN·m (165 000 lbf·ft). The slab moment and the two curb moments give a moment of 2521.8 kN·m (1 860 000 lbf·ft) that will cause yielding. Based on the above coefficient, a line load of 1962 kN (441 000 lbf) would be necessary to cause permanent set.

Load Causing Collapse

The first permanent set load causes a yield stress at one point in the bridge. However, before actual collapse can occur, yielding and hinges must form under the load and over the two piers. The moment in the hinge over the two piers is labeled M_1, and the moment at the center of the midspan is labeled M_2. Two methods of determining M_1 and M_2 are presented. In the first method the 9.75-m-wide (32-ft) slab and the curbs are considered separately and added to the total moment.

M_1 is calculated to be 2664.2 kN·m (1 965 000 lbf·ft) as follows: The slab steel area is 9.55 cm^2/m (1.48 in^2/ft), the live load moment is 2139.5 kN·m (1 578 000 lbf·ft), and the moment in each curb for 14 cm^2 (2.7 in^2) of steel is 262.4 kN·m (193 500 lbf·ft). M_2 is calculated to be 2521.8 kN·m (1 860 000 lbf·ft) as follows: Slab steel area is 27.7 cm^2/m (1.31 in^2/ft), live load moment is 2074.4 kN·m (1 530 000 lbf·ft), and the moment in each curb is 223.7 kN·m (165 000 lbf·ft).

The conservation of energy principle was used to develop a relationship between the applied line load and M_1 and M_2. The result was as follows: Line Load = M_1 + $M_2 \times 4 \div$ center span length. Based on the above values for M_1 and M_2 the line load is 3238.3 kN (728 000 lbf).

Combining the slab and curb gives different values for M_1 and M_2. To find M_1, the compression is all taken in the bottom of the slab and the moment is calculated for the steel in the top of the slab and added to the moment calculated for the steel in the top of each curb. The steel areas are the same as those used in the previous calculation for M_1. The moment is 2662.8 kN·m (1 964 000 lbf·ft). To find M_2, the compression is all taken by the portion of the curbs above the slab. The tension steel of the slab and curb is added, and the moment is 4504 kN·m (3 322 000 lbf·ft). Using the previously derived equation to relate the moment to a loading gives a load of 4470.5 kN (1 005 000 lbf) that is needed to produce a collapse.

COMPARISON OF TEST RESULTS

Stresses in Slab

The first objective was to compare the design stresses with those obtained by measuring the strains on the bridge slab. At each location, strains were measured for both the upper and lower surfaces. Based on a straight line strain relationship, the strain at the elevation of the steel was calculated. Then, using the modulus of elasticity for concrete and steel, the concrete/steel stresses were calculated. This stress comparison is given in Table 2 for a line load of 814 kN (183 000 lbf).

The first set of calculated stresses was based on a three-span slab over simple supports. The curbs were neglected in these calculations.

The second set of calculated stresses was based on a slab with curbs, and was computed by using the STRUDL program. For this calculation, the bridge was divided into a gridwork consisting of beams running parallel with the piers and parallel with the direction of traffic. The program permitted a separate input of stiffness for each longitudinal and transverse beam. Each longitudinal beam had a constant stiffness except for the edge beams, which were significantly stiffer because of presence of the curbs. The amount of transverse stiffness was adjusted until the deflections agreed with those observed during testing.

The third set of calculated stresses was based on a channel-shaped section. The slab is the web of the channel while the curbs make up the flanges.

The slab model is often used in design, and the channel model is applicable to the collapse load on the bridge. However, the slab with edge beam model is the best representation of actual behavior since it incorporates both slab and curbs while adjusting the relative stiffness to match measured deflections.

The large difference between the measured and calculated stresses cannot be justified. One factor that might account for the difference is the application of strain

Table 1. Design moments and stresses.

Item	Load	At Midspan	Over Piers
Moment, kN·m	Dead + live	23.85	28.63
Concrete stress, MPa	Dead + live	7.72	8.48
Steel stress, MPa	Dead + live	126.2	141.3
Concrete stress, MPa	Live	5.86	5.07
Steel stress, MPa	Live	95.6	86.2

Note: 1 N·m = 0.738 lbf/ft; 1 Pa = 0.000 145 lbf/in^2.

Table 2. Stress comparison for a line load of 814 kN (183 000 lbf).

	Measured Stresses (MPa)		Calculated Stresses (MPa)					
			Slab		Slab With Edge Beams		Channel-Shaped Section	
Location	Concrete	Steel	Concrete	Steel	Concrete	Steel	Concrete	Steel
Midspan	1.59	15.9	9.17	148.2	6.27	102.0	0.55	77.2
	2.41	31.0	9.17	148.2	4.55	74.5	0.55	77.2
	0.76	12.4	9.17	148.2	6.72	109.6	0.55	77.2
	2.41	6.89	9.17	148.2	6.79	110.3	0.55	77.2
	1.17	11.7	9.17	148.2	5.45	88.9	0.55	77.2
	1.65	14.5	9.17	148.2	6.20	101.3	0.55	77.2
Piers	0.76	6.89	2.36	39.4	2.57	42.7	1.99	28.6
	1.65	6.89	4.34	72.4	3.10	51.7	3.65	52.4

Note: 1 Pa = 0.000 145 lbf/in^2; 1 N = 0.225 lbf.

gauges in cold weather. The glue may not have fully cured and may have been still partially elastic at the time of testing. This would cause strains to be measured; however, they would be considerably below the actual strains that occurred.

Load Causing First Permanent Set

To determine the load causing first permanent set from test results, it was necessary to plot the load deflection curves for each of the points near the midspan of the slab. Each curve was studied to determine the load at which the curves left the straight line relationship. That load for most of these points was 1668 kN (375000 lbf), and thus that value was taken to be the line load causing first permanent set.

Two values for permanent set were calculated. The first, 1721 kN (387000 lbf), was based on using only the moment in the slab, and the second, 1962 kN (441000 lbf), was based on using the moment in the slab and the curbs. A comparison of the values indicates that the test load was within 3 percent of that predicted from the slab moment and 15 percent below that predicted from the curb moment.

Collapse Load

Figure 4 shows that a collapse load of 4226 kN (950000 lbf) was obtained. A plastic collapse model that incorporates the slab and curb beams separately predicted a collapse load of 3238 kN (728000 lbf). To predict a collapse load near the actual failure load, it is necessary to consider slab and curbs as a channel-shaped section loaded about its weak axis so that at the center of the bridge the curbs are in compression and the slab is in tension. A collapse load of 4470.5 kN (1005000 lbf) was predicted and is within 5 percent of the actual collapse load.

Bridge Overloads

What magnitude of truck overloads is represented by the reported line loads? The center span truck load design moment of 59.2 kN·m/m (13000 lbf·ft/ft) on a 9.75-m-wide slab is equivalent to a live load moment produced by a line load of 421 kN (94000 lbf). For each such line load increase, the bridge will carry an additional HS20-44 truck load in each lane. The following table gives the live load safety factors for various numbers of HS20-44 trucks on the bridge.

Number of Trucks		Safety Factor	
In Each Lane	On Bridge	Permanent Set Load	Collapse Load
1	2	3.96	10.03
2	4	1.98	5.02
3	6	1.32	3.34
4	8	0.99	2.51
5	10		2.00
6	12		1.67
7	14		1.43
8	16		1.25
9	18		1.11
10	20		1.00

The safety factor is given for the permanent set load as well as for the collapse load. Extremely high truck loads are necessary to cause permanent set or collapse load; for example, permanent set will not occur until a load of four times the HS20-44 truck load is placed in each lane.

The 1957 AASHO bridge specifications used in this design did not permit an overload for the HS20-44 loading; however, they did permit overloads up to 100 percent for lighter load when the adjacent lane was not loaded (5).

CONCLUSIONS

As a result of testing and calculations on the reinforced concrete bridge, the following conclusions were made:

1. Strength of concrete and steel materials was more than the design minimum values; therefore, the average cylinder strength for concrete was 47.33 MPa (6865 lbf/in^2); the design minimum strength was 20.68 MPa (3000 lbf/in^2). The average yield strength of the reinforcing steel was 365.77 MPa (53050 lbf/in^2); the design minimum value was 275.79 MPa (40000 lbf/in^2).
2. Measured stresses in the concrete and steel for both the line load and the four-wheel load were very close to the calculated stresses. This was partially due to the omission of the curbs in the calculated stresses in the bridge but also may be due to the difficulties of carrying out strain measurements in cold weather.
3. The load causing first permanent set was accurately predicted by calculating the yield moment in the slab and neglecting the moment in the curbs. On this basis the line load causing first permanent set was 168 kN (375000 lbf); the predicted load was 1721 kN (387000 lbf).
4. The collapse load for the bridge was accurately predicted by considering the formation of yield moments along the centerline and over the pier of the bridge. These moments were calculated on the basis of a channel-shaped section loaded about its weak axis. On this basis, the line load causing collapse was 4226 kN (950000 lbf), and the predicted load was 4470.5 kN (1005000 lbf).
5. A line load of 421 kN (94700 lbf) produced the same moment in the center of the bridge as did an HS20-44 truck in each lane. Hence, it would take eight HS20-44 trucks placed in the center of the bridge to cause any permanent deflection in the bridge, and it would take twenty HS20-16 trucks placed in the center of the bridge to cause collapse.

ACKNOWLEDGMENTS

This research project was sponsored by the North Dakota State Highway Department in cooperation with the Federal Highway Administration, U.S. Department of Transportation, and was performed by faculty and staff of the North Dakota State University. Bruce Baily was responsible for the loading system, Satya Keshava was responsible for the deflection measuring system, and Chingmiin Chern was responsible for the strain measuring system. Students assisted in setting up the instrumentation and conducting the testing. The loading frame was constructed by Swingen Construction of Grand Forks, whose assistance and cooperation are acknowledged. We would also like to acknowledge the cooperation of Allen Anderson, Clair Rice, and Earl Nelson of the North Dakota State Highway Department.

The opinions, findings, and conclusions in this report are those of the authors and not necessarily those of the North Dakota State Highway Department or the Federal Highway Administration.

REFERENCES

1. E. G. Burdette and D. W. Goodpasture. Full-Scale Bridge Testing: An Evaluation of Bridge Design Criteria. Department of Civil Engineering, Univ. of Tennessee, Dec. 31, 1971.
2. Design Calculations for Bridge Under Test. Bridge Division, North Dakota State Highway Department,

Bismarck, 1958.
3. Interim Specification 1972. AASHO Committee on Bridges and Structures, AASHO, Washington, D.C., 1972.
4. W. C. Boyer and J. I. Abrams. Influence Lines for Continuous Beams. Johns Hopkins Press, Baltimore, 1954-56.
5. Standard Specifications for Highway Bridges, 8th Ed. AASHO, Washington, D.C., 1957.

Rigid Frame Highway Bridge Study

H. L. Kinnier and F. W. Barton, Virginia Highway and Transportation Research Council

This report describes the experimental and analytical study of a rigid frame highway bridge (on Interstate 64 near Charlottesville, Virginia). Experimental data included strains and deflections at midspan of the girders and strain data in the vicinity of one of the haunches. These data, along with calculated values of bending moment based on the measurements, provided a basis for evaluation of the design and for comparison with subsequently calculated analytical data.

The test structure shown in Figures 1 and 2 is 65.8 m (216 ft) long and consists of five, three-span, welded rigid frames. The two interior supports are inclined I-shaped columns framed integrally with the welded haunched girders and supported on concrete footings with anchor bolts attached to the web in such a manner as to allow free rotation. The ends of the bridge are simply supported on shelf abutments with allowance for longitudinal movements. The structures (Figure 2) were designed for an HS20-44 live load by using A-36 structural steel in accordance with the 1965 AASHO specifications. Construction was completed in late 1969, and testing took place in September 1972.

TEST PROCEDURE AND INSTRUMENTATION

The test vehicle was a three-axle diesel tractor semitrailer loaded to simulate an HS20-44 loading. A total of 35 test runs were made. Ten crossings (two runs in each of the five lanes) were made at a crawl speed of 4.8 to 8 km/h (3 to 5 mph), and one run was made in each of the five lanes at speeds of 24, 48, 64, 80, and 97 km/h (15, 30, 40, 50, and 60 mph).

SR-4 wire strain gauges were placed at flange positions and rosette gauges on the haunch web on the westbound bridge. In addition, deflection gauges were installed at midspan of the five frames (Figure 3). Signals from pneumatic traffic tubes, installed on the approach on either side of the bridge span, provided a means of locating the test vehicle during the interval of testing, relating its position to the resulting stresses and deflections, and calculating the average speed of the test vehicle.

RESULTS

The output of the strain gauges, deflection gauges, and pneumatic tube signals was recorded as continuous traces on oscillograph tapes. Measured strains were converted to approximate stresses from the characteristics of the gauges and an assumed modulus of elasticity of 207 GPa (30 million lbf/in^2).

Midspan stresses and deflections of each frame are given in Tables 1 and 2 for various positions of the test vehicle. Distribution factors corresponding to each loading lane are also included.

ANALYTICAL RESULTS

A theoretical analysis of the rigid frame bridge was conducted to verify the experimental data collected and to provide additional stress and deflection information in regions where experimental data were lacking. Such a theoretical analysis also provides a basis for evaluating the design procedures used and, it is hoped, additional

Figure 1. Test structure on I-64 over US-250 east of Charlottesville, Virginia.

Publication of this paper sponsored by Committee on Dynamics and Field Testing of Bridges.

Figure 2. Partial elevation of test structure.

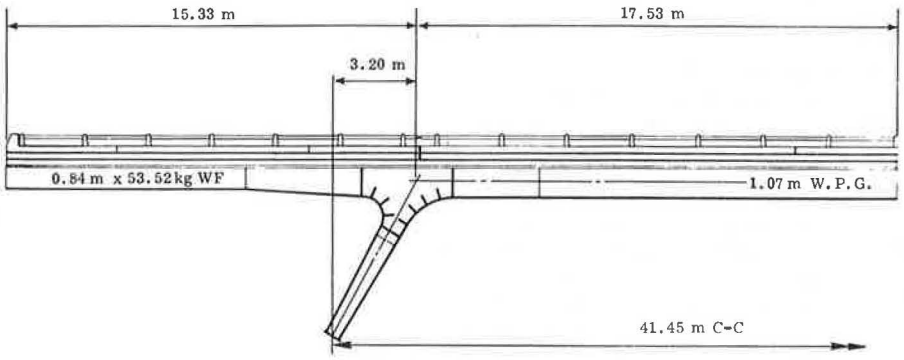

Figure 3. Transverse section and lane locations.

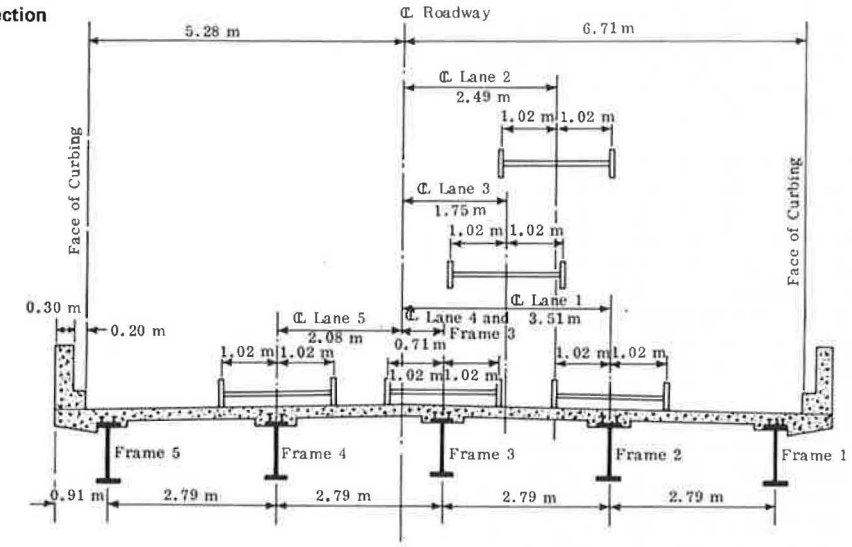

Table 1. Peak midspan deflections and load distribution based on deflections.

	Lane									
	1		2		3		4		5	
Frame	Deflection (mm)	Distribution (%)	Deflection (mm)	Distribution (%)	Deflection (mm)	Distribution (%)	Deflection (mm)	Distribution (%)	Deflection (mm)	Distribution (%)
1	5.75	29.5	4.25	21.5	3.50	16.9	2.00	9.5	0.25	1.2
2	7.50	29.5	5.75	29.1	5.25	25.3	3.75	17.9	1.75	8.3
3	5.25	26.9	6.00	30.4	6.50	31.3	6.50	30.9	5.25	24.7
4	2.50	12.8	3.00	15.2	4.00	19.3	5.50	26.2	7.00	32.9
5	0.25	1.3	0.75	3.8	1.50	7.2	3.25	15.5	7.00	32.9

Note: 1 mm = 0.0039 in.

Table 2. Maximum tensile stresses (lower flange midspan) and load distribution based on stresses.

	Lane									
	1		2		3		4		5	
Frame	Stress (MPa)	Distribution (%)	Stress (MPa)	Distribution (%)	Stress (MPa)	Distribution (%)	Stress (MPa)	Distribution (%)	Stress (MPa)	Distribution (%)
1	10.72	24.5	8.24	19.1	6.24	13.7	2.76	6.1	0.52	1.2
2	17.00	38.9	14.82	34.4	13.72	30.0	9.07	20.1	4.72	10.5
3	10.82	24.8	12.79	29.8	15.34	33.5	15.34	34.0	10.34	23.0
4	4.27	9.8	5.83	13.5	7.69	16.8	12.00	26.6	16.82	37.4
5	0.90	2.0	1.38	3.2	2.72	6.0	5.93	13.2	12.51	27.9

Note: 1 MPa = 145 lbf/in^2.

information regarding stress distribution in the haunch region of the bridge.

The analysis was performed by using a finite-element computer program in which a typical frame was represented as a series of flexural elements. The total rigid frame structure was subdivided into 16 elements, with two elements representing each end span, four elements modeling the center span, one element for each inclined leg, and three elements representing each haunch. The flexural characteristics of the actual structure were modeled as closely as possible. The stiffness matrices were formulated to represent the flexural characteristics of each of the elements by taking into account those elements in which there was a linear variation in depth. Also, modeling of the haunch incorporated the variation in depth and the extremely stiff nature of the central portion of the haunch. The inclined legs were assumed to be pinned at the base, and the bearings at the abutments were treated as roller supports providing no restraint against horizontal motion. Influence lines for deflections and moments at critical locations were determined.

The calculated deflection at midspan, using a theoretical loading based on the measured lateral load distribution, was determined to be 6.8 mm (0.27 in), and the experimental midspan deflection was measured to be 7.1 mm (0.28 in). Midspan moment due to the vehicle loading was calculated to be 473 kJ (350 thousand ft·lbf), and the experimentally determined midspan moment was approximately 454 kJ (335 thousand ft·lbf).

Variations in support conditions had negligible effects on the midspan moment but significantly affected moments in the haunch region. For example, permitting the deck to move horizontally may increase the positive moment in the haunch region by as much as 400 percent. Moments and deflections were also calculated for various haunch representations. Whereas differences in assumptions of haunch stiffness do have an effect on moments and deflections, the effect is not significant.

SUMMARY AND CONCLUSIONS

The conclusions drawn from this study are summarized below.

1. Midspan flexural stresses and deflections in the five frames were sensitive to the transverse position of the test vehicle on the concrete deck. As has also been demonstrated in studies of simple beam composite deck and steel stringers, live loads on the decks are by no means carried equally by the several components of the superstructure. However, AASHTO specifications for lateral distribution to stringers are highly conservative as design guides.
2. The live load stresses as experimentally determined were small compared to live load stresses calculated in the design.
3. The estimated values of the ratio of moduli of elasticity of steel to concrete and the effective width of the composite concrete slab have only a small effect on the section modulus of bottom fibers. Any reasonable estimates for these design parameters are very satisfactory for bridges of this type.
4. Influence diagrams for moments and deflections were not appreciably affected by various modelings of the haunch in the finite-element analysis.
5. Influence diagrams for midspan moments and deflections were not appreciably affected by various support condition assumptions at the abutments and slant legs; however, the influence diagrams for moments at either side of the haunch were greatly affected by the above-mentioned support conditions.

Ultimate Load Test of a High-Truss Bridge

F. Wayne Klaiber, Wallace W. Sanders, Jr., and Hotten A. Elleby,
Engineering Research Institute, Iowa State University

As a result of the construction of the Saylorville Dam and Reservoir on the Des Moines River, six highway bridges crossing the river were scheduled for removal. An old pin-connected, high-truss, single-lane bridge was selected for a testing program that included ultimate load tests. The purpose was to relate design and rating procedures currently used in bridge design to the field behavior of this type of truss bridge. The ultimate load tests consisted of testing one span of the bridge, two I-shaped floor beams, and two panels of the timber deck. The theoretical capacity of each of these components is compared with the results from the field tests. This paper examines the portion of the program related to the ultimate load testing of the trusses. The bridge was rated using the 1970 AASHO maintenance manual. The test span ratings of the trusses averaged about 18 percent of actual capacity and were fairly consistent except for the floor beams, where the lateral support conditions for the compression flange caused considerable variation.

In recent years a considerable number of field tests (1) on bridges have been conducted. However, nearly all of these were conducted at or near design loads. The catastrophic collapses of several old bridges, the approval of load factor design for steel bridges by AASHO (2, 3), and the requirement nationwide for rating highway bridges (4) have all generated considerable interest in testing actual bridges to failure. However, only a limited number of tests (1) have been conducted at substantial overloads or near ultimate capacity. Most of these were performed either on laboratory models or on specially designed bridges, as in the AASHO road tests (5, 6).

The exceptions are a 1960 test of the Glatt Bridge in Switzerland (7), four tests recently completed in Tennessee (8, 9, 10, 11, 12), and a special test that was planned for the summer of 1975 on a bridge in southeast Missouri (13). However, all six of these bridges, as well as the AASHO road test bridges, were beam-and-slab bridges. Therefore, no information was available concerning the behavior of old high-truss bridges typical of those found in Iowa and throughout other parts of the country. Thus, a load test program was designed to provide information on the ultimate load-carrying capability of this type of bridge.

As a result of the construction of the Saylorville Dam and Reservoir on the Des Moines River, six highway bridges crossing that river were scheduled for removal. Five of these were old pin-connected, high-truss, single-lane bridges. However, for these bridge types there are no technical data and no field test data up to ultimate capacity; therefore, the capacity must be determined solely from field examinations. The removal of these five bridges created an excellent opportunity for studying the behavior of truss bridges by testing actual prototypes. The general purpose of the load tests was to relate design and rating procedures currently used in bridge design to the field behavior of this type of truss bridge and to provide data on the behavior of this bridge type in the overload range up to collapse.

The purpose of a study (14) conducted several years ago by Iowa State University was to determine the feasibility of conducting these load tests. The findings of the study included a recommendation to conduct a broad range of programs on several of the truss bridges included in this removal program. Because of the construction schedule, only one of the truss bridges became available for testing and was tested during the summer of 1974. Therefore, a research program to conduct several of these recommended tests was developed and undertaken by Iowa State University. In part, the research program consisted of the following phases:

1. Service load testing of the bridge,
2. Ultimate load testing of several steel floor beams,
3. Ultimate load testing of timber deck sections,
4. Ultimate load testing of trusses in an "as is" condition as well as in a "damaged" condition, and
5. Fatigue testing of tension truss members after the trusses were dismantled.

The original test program (14, 15) consisted of load testing two spans of the bridge to failure. One of the spans was to be tested in its "as is" condition while the other one was tested after a major member had been damaged to simulate the effect of vehicular impact. Since the main thrust (member damage) of the proposed second truss test was accomplished while testing the first truss,

Publication of this paper sponsored by Committee on Dynamics and Field Testing of Bridges.

the ultimate load testing of the second truss was modified. The testing program was changed to include ultimate load tests of the floor beams at panel points 4 and 5.

This paper reports on the portion of the testing program related to the ultimate load testing of the trusses of the bridge. A more detailed analysis of the results is given by Saunders and others (16).

TEST BRIDGE

The high-truss bridge selected for testing was the Hubby Bridge (Figures 1 and 2), located over the Des Moines River in an area that will be included in the Saylorville Reservoir, southern Boone County, about 40.2 km (25 miles) northwest of Des Moines. It was built in 1909 and consisted of four 50.3-m-long (165-ft) modified Parker high-truss simple-spans.

The trusses consisted of tension eye-bars that had both square and rectangular cross sections, built-up laced channels for the end posts and upper chord compression members, and laced channels for the other compression members. Square tension eye-bars ranged in size from 1.9 to 2.9 cm ($\frac{3}{4}$ to $1\frac{1}{8}$ in) and were used for truss hangers and diagonals. Rectangular tension eye-bars ranged in size from 1.6 by 7.6 cm ($\frac{5}{8}$ in by 3 in) to 2.1 by 10.2 cm ($\frac{13}{16}$ in by 4 in) and were used for the truss lower chords and diagonals. The eyes for these two types of eye-bars were formed by bending the end of the bar to form a tear-shaped eye. The end of the bar was forged to form a permanent connection with the rest of the bar. The channels ranged in size from 10.2 to 22.9 cm (4 to 9 in) deep and were used for truss compression members. The deck was built of stringers, crossbeams, and floor planks all made of timber. All of the timber members were 7.6 by 30.5 cm (3 in by 12 in), approximately 5.2 m (17 ft) long, and were made from Douglas fir that had been pressure treated with creosote. A typical panel of deck consisted of 15 stringers, 8 crossbeams, and 16 floor planks. The standard I-section floor beams were 30.5 cm (12 in) deep and weighed 45.5 kg/m (30.6 lb/ft) of length. The floor beams were connected to the truss by means of clip angles and 1.3-cm ($1\frac{1}{2}$-in) bolts.

Based on chemical analysis and physical property tests, it was determined that the tension eye-bars were made of wrought iron and the other members were made of steel. These results are given in Table 1. Tensile tests were conducted on coupons from typical members of both wrought iron and steel to obtain material properties; the stress-strain curves indicated behavior typical of the respective material. The results also indicate that the steel used satisfied the requirements for ASTM A36 steel, even though the steel was manufactured around 1900, and that the wrought iron conformed to ASTM A207 specifications.

TRUSS TEST

To test the span 2 trusses, simulated axle loads were applied at joints L_4 and L_5 in the ratio of 1 to 4; the greater load was applied at L_5. This ratio represented the relationship between the axles on an AASHO H15 truck. Although the load spacing in the truss test was 5.03 m (16.5 ft) since it was limited by floor-beam spacing and panel length, the effect of this difference with the actual 4.27-m (14-ft) specified axle spacing would be minimal because of the large load ratio and would not significantly affect the results.

The loads were applied by using hydraulic jacks connected to weights. Two large reinforced concrete mats that were used to supply the needed dead weights were cast under span 2. A concrete pumping system pumped the concrete from the southwest end of the bridge to the locations where the mats were formed. At the same time, two other mats were cast under span 1 and were used for subsequent floor beam tests. The sizes of the concrete mats varied from 0.46 by 1.83 by 7.62 m (1.5 by 6 by 25 ft) to 0.92 by 3.05 by 7.62 m (3 by 10 by 25 ft) These mats ranged from 15.4 Mg (34000 lb) to 50.8 Mg (112000 lb) with soil piled on top of each of the concrete mats to increase its mass.

Rods of 2.5-cm (1-in) diameter were attached to the concrete mats by using concrete inserts and a system of structural tubes (Figure 3). The hydraulic jacks were connected to the rods through a similar system of structural tubes so that the loads could be applied to the truss. Sketches of the loading system are shown in Figure 4.

Truss tests were conducted by applying strain gauges, which were encapsulated and self-temperature compensated for steel, to the truss members (Figure 5). Tension eye-bars were instrumented with one strain gauge on each of the two bar members. Two laced channels or two built-up laced channel members were instrumented with four gauges mounted near the four corners of the member to allow for computing the bending moment in both directions and the axial force for the member. Vertical and horizontal deflection readings were taken at midspan and at the 0.3 and 0.7 points on both sides of the span. For the truss test, 9 deflection indicators were used along with 108 strain gauges on the truss members.

Procedure

The first load was applied in increments of 44.5 kN (10000 lbf) [35.6 kN (8000 lbf) at L_5 and 8.9 kN (2000 lbf) at L_4]. As loading progressed to higher levels, the increments were reduced to 22.2 kN (5000 lbf) [17.8 kN (4000 lbf) at L_5 and 4.4 kN (1000 lbf) at L_4] until failure was reached.

The truss test proceeded as planned up to a total load of 355.9 kN (80000 lbf). While the load was proceeding to 400.3 kN (90000 lbf), yielding took place in one of the hangers at L_5 (downstream side). During the load increment to 489.3 kN (110000 lbf), there was considerable yielding at L_5. When loading proceeded to 578.3 kN (130000 lbf) the rust flaked on the hangers at L_5 (upstream side).

At a total load of 591.6 kN (133000 lbf) [473.3 kN (106400 lbf) at L_5 and 118.3 kN (26600 lbf) at L_4], equivalent to AASHO H66.5 truck, one of the hangers at L_5 (upstream side) failed. When the failure occurred, a portion of the load transferred from L_5 to L_4, resulting in a load of 280.2 kN (63000 lbf) at L_5 and 169.0 kN (38000 lbf) at L_4 at a loading ratio of 1.66 to 1. At this point, the large truss deflection caused the floor beam to move 10.2 cm (4 in) away from the timber stringers at L_5. This occurred because of the continuity of the floor system and the lack of a positive tie between the timber floor and floor beams. After the hanger failure, the load was reapplied and increased to 556.0 kN (125000 lbf) [400.3 kN (90000 lbf) at L_5 and 155.7 kN (35000 lbf) at L_4]. The load was increased to 498.2 kN (112000 lbf) at L_5 and 124.6 kN (28000 lbf) at L_4. At this load, the maximum vertical deflection at midspan was 38.1 cm (15 in), and significant distortion of the bridge was visible (Figure 6).

After readings were taken, the load was removed from L_5 because any further increase in load would cause more distortion of the lower chord at L_5. The load was then applied at L_4 to the capacity of the loading system [349.2 kN (78500 lbf)] without any additional failures resulting to the truss members.

It was decided that further testing of the trusses would

Figure 1. Hubby Bridge.

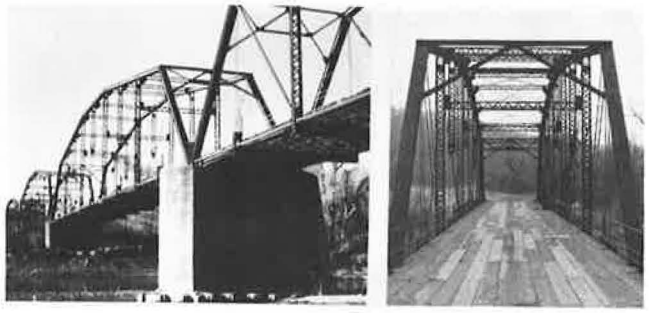

Figure 2. Layout of Hubby Bridge.

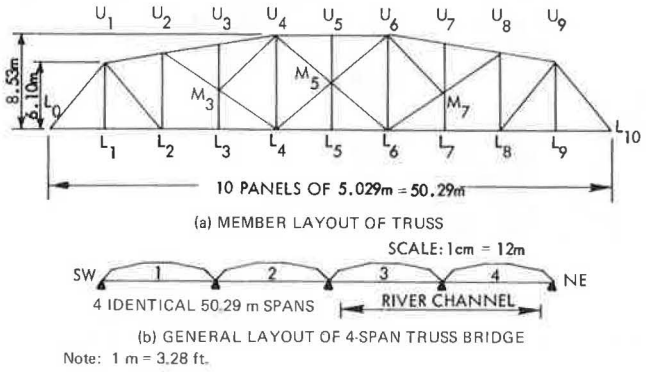

Note: 1 m = 3.28 ft.

Figure 3. System used to attach steel rods to concrete mats.

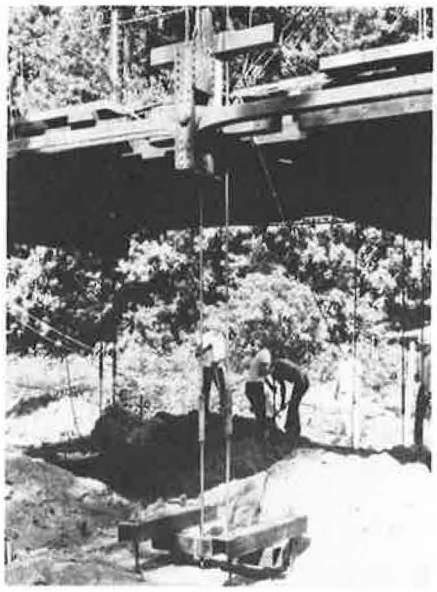

Table 1. Physical properties of wrought iron and steel based on chemical analysis and physical tests.

Properties	Wrought Iron	Steel	Properties	Wrought Iron	Steel
Chemical (%)					
Carbon	<0.03	0.19	Vanadium	<0.01	–
Manganese	<0.05	0.40	Silicon	0.22	<0.05
Phosphorus	0.29	0.012	Cobalt	0.02	–
Sulfur	0.042	0.029	Physical (MPa)		
Nickel	<0.05	<0.05	σ_y	244.8	289.6
Chromium	<0.05	<0.05	σ_{ult}	338.5	404.7
Molybdenum	<0.03	<0.03	ϵ	193×10^5	2.13×10^5
Copper	<0.03	0.03			
Aluminum	0.03	–			

Note: 1 Pa = 0.000 145 lbf/in^2.

not provide any additional information. Therefore, the objectives of the second truss test, to "damage" one of the key members and reload, were pursued. To simulate the damage, member L_2U_2 was cut with an acetylene torch. This member was selected because it was representative of the laced-channel compression members and because an end post would have required an elaborate loading system to be sufficiently damaged and would have resulted in immediate catastrophic failure. Initially, only one of the two channels of the member was cut. Loading was applied at L_4 and was increased to 311.4 kN (70 000 lbf) without any signs of additional distress. Thus, the other channel of member L_2U_2 was cut, leaving only the web of the channel remaining intact. The load at L_4 was again increased to 311.4 kN (70 000 lbf) without any signs of distress. Again, the load was removed from the bridge and one bar of member L_2U_1 was cut. The truss at L_4 was again loaded to 320.3 kN (72 000 lbf) with no apparent signs of distress. After the load was removed, member L_2U_2 was cut through completely leaving a gap of about 10.2 cm (4 in). Loading at L_4 was

Figure 4. Truss loading system.

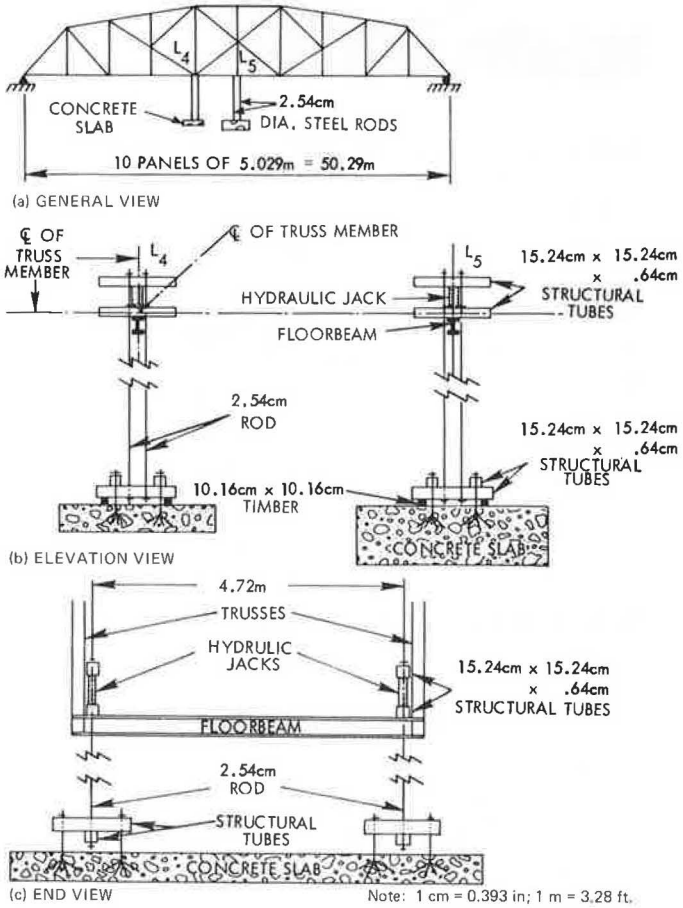

Note: 1 cm = 0.393 in; 1 m = 3.28 ft.

Figure 5. Strain gauge locations.

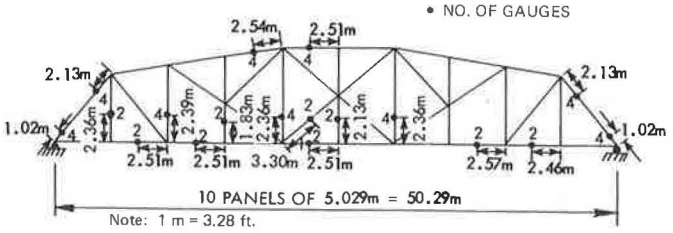

Note: 1 m = 3.28 ft.

Figure 6. Distortion of lower chord at L_5.

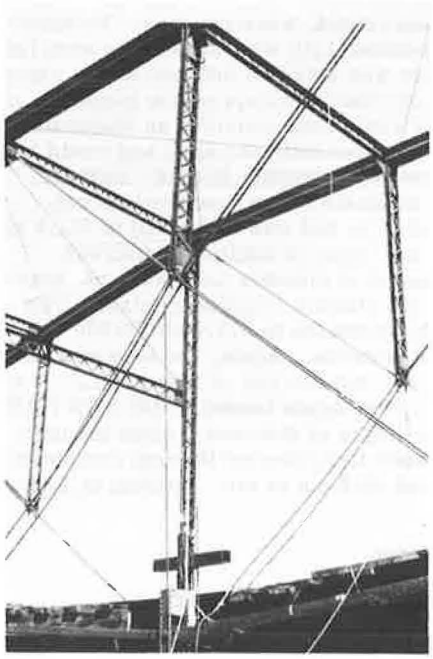

Figure 7. Damaged member after collapse.

Figure 8. Total load-vertical deflection at L_5 for truss test.

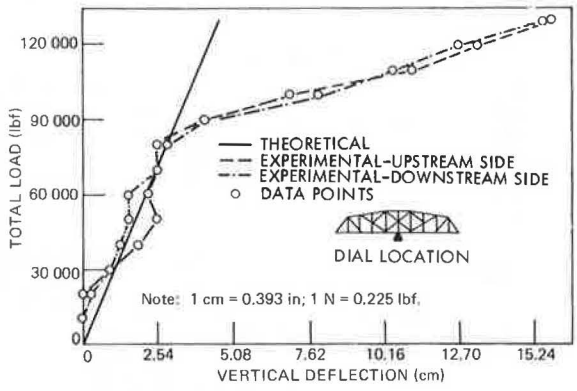

Figure 9. Total load-vertical deflection at L_3 and L_7 for truss test.

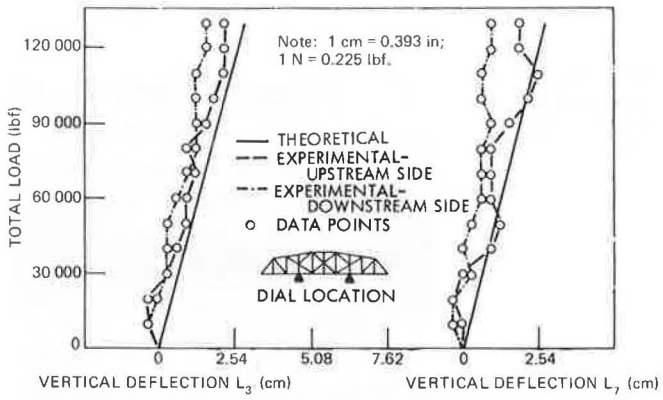

Figure 10. Total load-force in member L_5M_5.

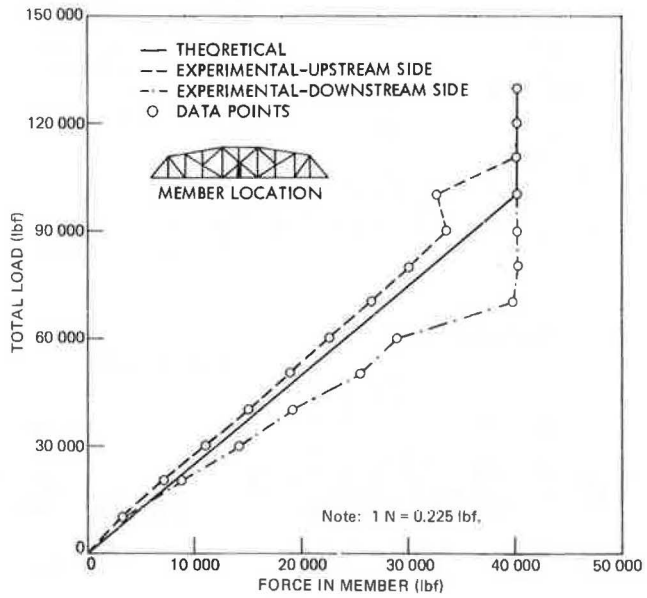

Figure 11. Total load-force in member L_0U_1.

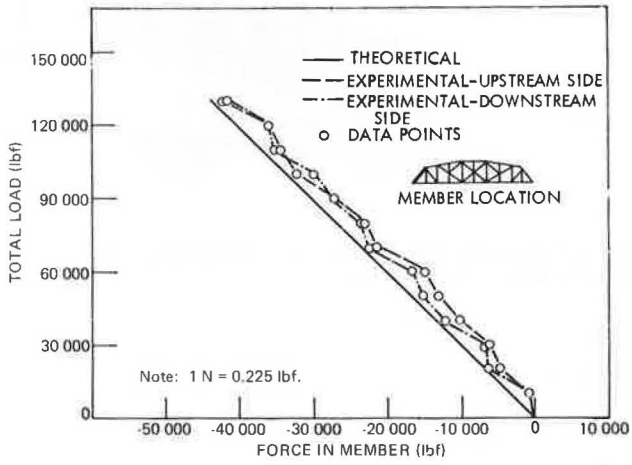

again applied and reached 173.5 kN (39 000 lbf) before the member collapsed upon itself, forming a complete but shorter member at the cut location (Figure 7). The load was then increased to 320.3 kN (72 000 lbf) with no further distress of the truss. The load was removed and all testing terminated. It was postulated that, if a greater gap had been provided in L_2U_2 so that the two sections had not met when initial collapse occurred, the truss might well have collapsed completely.

Results and Analysis

The behavioral indicators for the truss test were the deflection readings taken at midspan and at the 0.3 points and the forces in the truss members that were computed from the strain guage readings taken during the test. Figure 8 shows the theoretical and experimental load-deflection curves for the vertical deflection at midspan, and indicates that yielding began to occur in member L_5M_5 at a total load of approximately 355.8 kN (80 000 lbf). The curve is relatively linear at loads less than 355.8 kN (80 000 lbf), whereas above 355.8 kN (80 000 lbf) the slope of the curve decreases indicating yielding of member L_5M_5. The small nonlinearities at loads below 355.8 (80 000 lbf) indicate the effect that rusting of the members and pins and the distorted shape of some members had on the behavior of the truss. Figure 9 shows the theoretical and experimental load-deflection curves for the vertical deflection at L_3 and L_7 and indicates no yielding or nonlinearity up to the maximum load at which readings were taken. Figure 9 shows that both of the deflection readings taken at the 0.3 points exhibit fairly linear behavior. Although there is some agreement between the two sides of the truss, the small magnitude of the deflections and the apparent effect of the rusted condition of the truss made it difficult to determine whether this agreement was valid. The horizontal deflections of the truss were negligible.

Figure 10 shows the total load-force in truss member L_5M_5, and indicates that this truss member exhibited approximately the same behavior shown in the total load-vertical deflection curve in Figure 8. Representative samples of the curves for other total load-force in truss members are shown in Figures 11, 12, and 13. These curves indicate linear behavior up to the maximum load at which readings were taken.

The theoretical forces shown in Figures 10, 11, 12, and 13 were obtained by analyzing the structure of the truss and by assuming that all of the members were held together by pins at the joints. Most of the experimental forces determined from strain gauge readings agreed quite closely with the theoretical forces determined by analysis. However, in a few cases the experimental data differed in magnitude from the theoretical curves. In these cases, the experimental results were less than the theoretical results. This behavior was due, in part, to the "frozen" condition of the joints that resulted from the rusted members and pins.

Thus, although the actual conditions in the joints were unknown, to consider that the truss was pin-connected provides a realistic method for truss analysis of these old bridges. The tremendous flexibility of the members that allows accommodation of any joint restraint also contributes to this conclusion.

The capacity of the hangers at L_5, calculated by using data from coupon tests, was 489.3 kN (110 000 lbf) [337.2 MPa (48 900 lbf/in^2)]. This was larger than the load that actually caused the fracture of one of these hangers. The actual stress at fracture was 326.8 MPa (47 400 lbf/in^2) thereby indicating that the "lap" near fracture was about 97 percent effective. The current practice in Iowa is to assume that the lap is only 40 percent effective, which is much lower than the actual capacity of the member.

One of the significant portions of this study was the rating of the test span and the comparison of that rating with the actual capacity. Field inspection was used as the basis for the rating calculations and was made by the Maintenance Department of the Iowa State Highway Commission. This information was forwarded to the agencies cooperating in this phase of the study: U.S. Army Corps of Engineers, Iowa State Highway Commission, and Iowa State University. Using these base data, each agency computed bridge rating in accordance with the 1970 AASHO maintenance manual (4).

The operating-level truss ratings (H11.4, H12.7, and H11.9) determined by the three different agencies were quite consistent and were about 18 percent of the test capacity (H66.5). Even though the ratings considered dynamic effects, they still appeared conservative.

Figure 12. Total load-force in member L_2L_3.

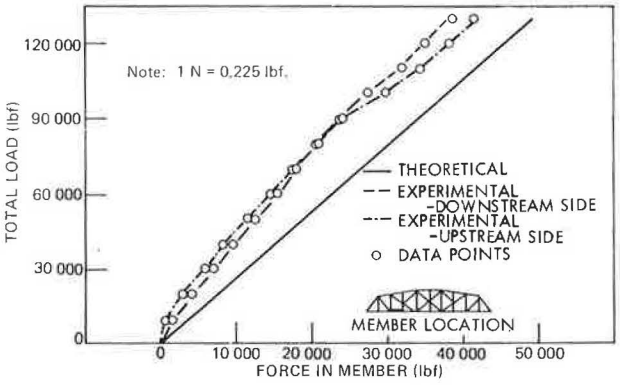

Figure 13. Total load-force in member U_3U_4.

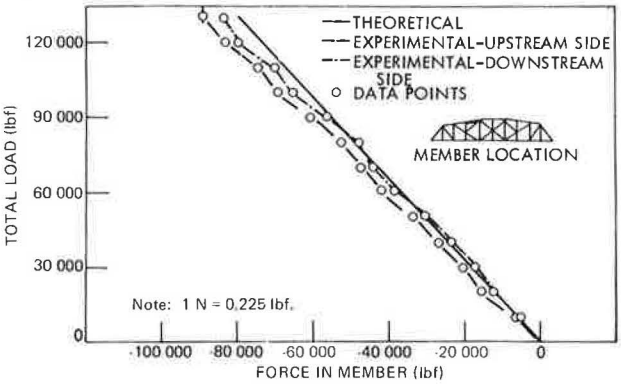

SUMMARY AND CONCLUSIONS

The purpose of the ultimate load tests was to relate currently used bridge design and rating procedures to field behavior of this type of truss bridge. The general objective of the test program was to provide data regarding the behavior of this bridge type in the overload range up to collapse. As a result of the ultimate load test performed on this truss bridge, the following conclusions were reached:

1. The experimental forces determined for the truss members agreed closely with those forces determined by analysis for the same members. This indicates that to assume the members were pin-ended was valid for this particular truss.
2. The theoretical capacity of the hangers at L_5

agreed closely with the load capacity that actually caused the fracture of one of these hangers.

3. The current practice of assuming that the lap of an eye-bar must be only 40 percent effective is quite conservative. However, additional tests are required before any recommendation to change this assumption is warranted.

4. The truss ratings averaged about 18 percent of capacity.

At the conclusion of this project, a final summary report will be prepared that will include recommendations for implementation of the findings.

ACKNOWLEDGMENTS

The program was conducted by the Engineering Research Institute of the Iowa State University and funded by the Iowa Department of Transportation and the Federal Highway Administration; supplemental funding was provided by the Engineering Research Institute. In addition to these direct sponsors, services were provided for the research by the Boone County Engineer's Office and the U.S. Army Corps of Engineers. The Hubby Bridge was provided through the cooperation of these latter two agencies.

The opinions, findings, and conclusions expressed are those of the authors and not necessarily those of the Federal Highway Administration, the U.S. Department of Transportation, or the Iowa Department of Transportation.

REFERENCES

1. C. P. Heins, Jr. and C. F. Galambos. Highway Bridge Field Tests in the United States, 1948-70. Public Roads, Vol. 36, No. 12, Feb. 1972, pp. 271-291.
2. Standard Specifications for Highway Bridges, Eleventh Ed. AASHO, 1973.
3. G. S. Vincent. Tentative Criteria for Load Factor Design of Steel Highway Bridges. American Iron and Steel Institute, Bulletin 15, March 1969.
4. Manual for Maintenance Inspection of Bridges. AASHO, 1970.
5. Dynamic Studies of Bridges on the AASHO Road Tests. HRB, Special Rept. 71, June 1972.
6. The AASHO Road Test: Report 4—Bridge Research. HRB, Special Rept. 61D, 1962.
7. A. Rosli and H. Hofacker. Test on the Glatt Bridge at Opfikon. Cement and Concrete Association, London, Translation 106, Aug. 1973.
8. E. G. Burdette and D. W. Goodpasture. Final Report on Full-Scale Bridge Testing: An Evaluation of Bridge Design Criteria. Department of Civil Engineering, Univ. of Tennessee, Dec. 31, 1971.
9. S. K. Doyle and E. G. Burdette. A Comparison of Measured and Computed Load-Deflection Relationships for Four Highway Bridges. Department of Civil Engineering, Univ. of Tennessee, Research Series 13, March 1973.
10. E. G. Burdette and D. W. Goodpasture. A Comparison of Measured and Computed Ultimate Strengths of Four Highway Bridges. HRB, Highway Research Record 382, 1972, pp. 38-49.
11. R. F. Varney. Preliminary Research Reports of a Highway Bridge Loading Study With the HET-70 Main Battle Tank Transporter. U.S. Bureau of Public Roads, 1970.
12. E. G. Burdette and D. W. Goodpasture. Tests of Four Highway Bridges to Failure. Journal of the Structural Division, Proc., ASCE, Vol. 99, No. ST3, March 1973, pp. 335-348.
13. H. Salane, R. Duffield, R. McBean, and J. Baldwin. An Investigation of the Behavior of a Three-Span Composite Highway Bridge. Missouri Cooperative Highway Research Program, Univ. of Missouri, Columbia, Rept. 71-5, 1972.
14. W. W. Sanders, Jr. and H. A. Elleby. Feasibility Study of Dynamic Overload and Ultimate Load Tests of Full-Scale Highway Bridges. Engineering Research Institute, Iowa State Univ., Ames, Final Rept., Jan. 1973.
15. W. W. Sanders, Jr., H. A. Elleby, and F. W. Klaiber. Field Test Details for Research Study HR-169 on Ultimate Load Behavior of Full-Scale Highway Truss Bridges. Engineering Research Institute, Iowa State Univ., Ames, interim rept., May 1974.
16. W. W. Sanders, Jr., F. W. Klaiber, H. A. Elleby, and L. W. Timm. Ultimate Load Behavior of Full-Scale Highway Truss Bridges: Phase 1—Ultimate Load Tests of the Hubby Bridge—Boone County. Engineering Research Institute, Iowa State Univ., Ames, interim rept., April 1975.

Abridgment

Lateral Load Distribution for Two Continuous Steel Girder Highway Bridges

Edwin A. McDougle, Ross H. Bryan, Inc., Nashville
Edwin G. Burdette and David W. Goodpasture, University of Tennessee

Three Tennessee state highway bridges and one Franklin County highway bridge were located in an area that has been inundated as a part of the Tennessee Valley Authority (TVA) Tims Ford Reservoir. These bridges were made available by the TVA, the Tennessee Department of Highways, and the Franklin County Highway Department for testing purposes. Descriptions of this testing program have been published by Burdette and Goodpasture (1, 2, 3, 4).

This paper presents the results obtained as a part of the full-scale bridge testing program (FSBT) of the University of Tennessee and tank transporter tests by the Bureau of Public Roads to determine the lateral distribution of load on two multispan continuous steel beam and slab bridges.

The results of an ICES STRUDL II finite element analysis relating to lateral load distribution for each bridge (6, 7) are compared with the experimental results from FSBT. Both the analytical and experimental results are then compared to the empirical design equation in the 1973 AASHO specifications (8) and the proposed revisions to the AASHTO specifications made by Sanders and Elleby (9).

Further background information and derivation of all formulas may be found in the author's original thesis (10).

DESCRIPTION OF BRIDGES

Each of the four bridges tested in the full-scale bridge testing program was a two-lane deck girder bridge with four longitudinal girders. The Bureau of Public Roads (BPR) tests were performed on three of these four bridges (5). The findings reported herein are limited to two of the FSBT bridges, one of which was the BPR bridge. These bridges are numbered 1 and 4 in the FSBT final report (1) and will be so referenced here. A description of the bridges is given in Table 1. Both of the bridges appeared to be structurally sound before testing. Approximate average daily traffic volumes in 1968 for bridges 1 and 4 were 600 and 200 respectively.

ROLLING LOAD TESTS

To determine the lateral distribution of applied loads, four different vehicles were driven across the bridges in each of the traffic lanes at speeds ranging from a crawl to 56 km/h (35 mph).

The vehicles used to load the bridges were as follows:

Vehicle	Load (Mg)
Federal Highway Administration	32.7
University of Tennessee	59.9
M-60 track-laying combat tank	47.6
Army HET-70 tank transporter	88.4

When the FHWA test vehicle is loaded, it closely simulates HS-20 design vehicle loading and is referred to as HS-20 here. When the University of Tennessee test vehicle is loaded with solid concrete blocks, its axle loads are almost double those of the HS-20 design vehicle load and it is therefore referred to as HS-40. The Army HET-70 tank transporter has eight pneumatic-tired axles.

STATIC LOAD TESTS TO FAILURE

To determine the lateral distribution of loads at high load levels and how the distribution changes with increasing load, static tests to failure were performed on each bridge. Application of the loads simulated an HS truck in each lane, and they were located in the approximate position to cause maximum positive moment near the center of the span. The points on the span at which load was applied were at the positions of the eight rear wheels of the two simulated trucks. A complete description of the tests and test results is given in the literature (1, 2, 3, 10).

EXPERIMENTAL DATA AND RESULTS

The lateral distribution of loads as determined by the bending moment supported by each girder is computed by using the measured strain in the top and bottom fibers

Publication of this paper sponsored by Committee on Dynamics and Field Testing of Bridges.

Table 1. Description of bridges.

Bridge Number	General Description	Span (m)	Girder Spacing (m)	Skew (deg)	Location	Date	Loading
1	Four-span continuous, 91-cm steel rolled beams, composite in positive moment regions	21, 27, 27, 21	2.54	90	Tenn-130 over Elk River	1963	HS-20
4	Three-span continuous, 68.6-cm steel rolled beams, noncomposite	14, 18, 14	2.24	90	Mansford Road over Elk River	1956	HS-15

Note: 1 cm = 0.39 in; 1 m = 3.28 ft.

Figure 1. Comparison of actual and theoretical distribution factors for bridge 1.

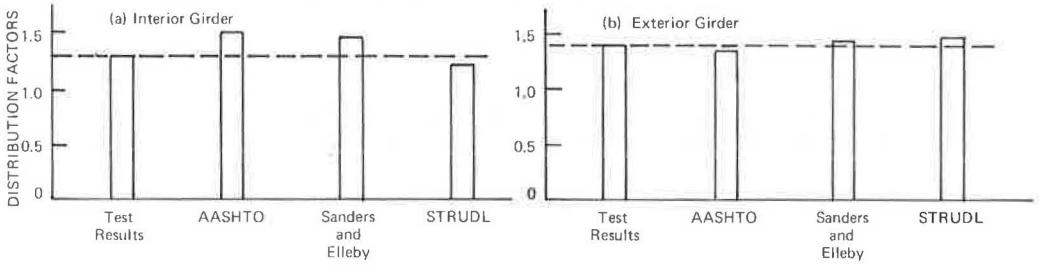

Figure 2. Comparison of actual and theoretical distribution factors for bridge 4.

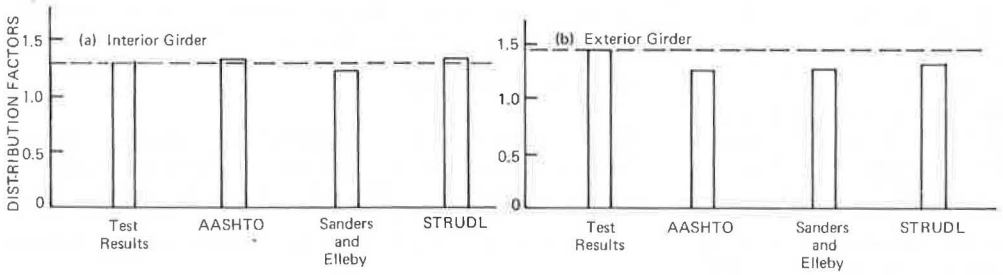

in combination with the properties of the girder cross section.

Instrumentation

Lateral distribution of loads was determined by mounting a foil gauge on the underside of the top and bottom flanges of each of the four girders at the point of maximum moment. These gauges were monitored with a minicomputer connected with a digital-to-analog converter interface.

Data Interpretation

From the measured strains in the top and bottom flanges, the moment in each individual girder was computed. The exact method used is discussed elsewhere (10).

Results

The term load distribution coefficient is used to denote the percentage of total live load bending moment supported by a particular longitudinal girder. McDougle (10) lists these coefficients for rolling load tests and static load tests for both subject bridges.

PREDICTION OF LATERAL DISTRIBUTION

The theoretical analysis of bridges to determine the lateral distribution of load is a difficult, time-consuming, and expensive process. For more than 30 years, AASHTO has published and authorized the use of an empirical method of distribution to simplify the problem. Since that time, numerous researchers have advanced their own theories and proposed revisions to the AASHTO load distribution equation. A comparison of the results of the proposed revisions by Sanders and Elleby, the current AASHTO specifications, and a STRUDL analysis of each bridge is given below.

AASHTO Specifications

The current AASHTO specifications (8) state that, for a two-lane bridge with a concrete deck over I-beam stringers spaced not more than 4.3 m (14 ft) apart, the live load bending moment for each interior stringer shall be determined by applying the fraction S/5.5 (S = stringer spacing) of a wheel load to the stringer. For a similar bridge, the live load bending moment for an exterior stringer is determined by applying the fraction S/(4.0 + 0.25S) of a wheel load.

Sanders and Elleby Proposal

In their final report, Sanders and Elleby (9) recommend significant changes to the AASHTO specifications for determining lateral distribution of load. Specifically, they recommend for beam and slab bridges that the live load bending moment for each beam (both interior and exterior) be determined by applying the fraction of a wheel load determined by their formula, which is based on bridge geometry and material properties.

STRUDL II Analyses

Both bridges were modeled by using the STRUDL II subset of the ICES computer program. The models included a combination of plate bending elements to simulate the concrete deck and grid members to simulate the longitudinal beams. Distribution coefficients were computed by loading these models of the bridges. Distribution factors for interior and exterior girders were then determined by superimposing distribution coefficients for two trucks in the desired position.

Rolling Load Tests

Rolling load tests were performed in each lane on each bridge. Distribution factors are computed by superimposing the distribution coefficients of a given girder for two tests to obtain the maximum value for comparison with AASHTO values.

Comparisons of distribution factors for bridges 1 and 4 are shown in Figures 1 and 2.

CONCLUSIONS

From the data and comparisons made here, the following conclusions relating to the lateral distribution of load are offered.

1. The rolling load data suggest that, for a particular bridge, the lateral distribution of load depends almost entirely on the lateral position of the vehicle on the bridge. Although axle spacing, magnitude of vehicle load, and vehicle speed have a measurable effect on the total moment at a bridge cross section, these parameters appear to have only a minor effect on the lateral distribution of load to supporting girders.
2. The static load test data indicate that, as the load on a bridge is increased up to the order of magnitude that produces first yield of the steel, the load distribution coefficients are not significantly affected.
3. The AASHTO specifications require distribution factors that are slightly conservative for interior girders and slightly unconservative for exterior girders, indicating that they do not fully account for the additional stiffness contributed to the exterior girder by curbs and rails.
4. The Sanders and Elleby equation yields distribution factors that are conservative for the composite bridge and somewhat unconservative for the noncomposite bridge. If the noncomposite equation proposed in their report is adjusted to include partial slab participation, the factors are in closer agreement. Their exclusion of the effects of curbs and handrails is shown to be invalid.
5. The distribution factors predicted by the STRUDL II models were not entirely consistent with the experimental values. The relative stiffness of the interior girder-slab section and the exterior girder-slab-curb section appears to have a great deal of effect on the distribution of load. These parameters must be carefully evaluated and adjusted to ensure that the model acts like the real structure.
6. Although the AASHTO requirements did not predict the actual maximum distribution factors precisely as determined by test results, they were just as accurate, on the average, as any of the other methods reported here.
7. The M-60 and HET-70 loads were more evenly distributed to the longitudinal girders because of the vehicles' track and wheel spacings.

REFERENCES

1. E. G. Burdette and D. W. Goodpasture. Final Report on Full Scale Bridge Testing—An Evaluation of Bridge Design Criteria. Department of Civil Engineering, Univ. of Tennessee, Dec. 31, 1971.
2. E. G. Burdette and D. W. Goodpasture. Comparison of Measured and Computed Strengths of Four Highway Bridges. HRB, Highway Research Record 382, 1972, pp. 38-50.
3. E. G. Burdette and D. W. Goodpasture. Tests of Four Highway Bridges to Failure. Journal of Structural Division, Proc., ASCE, March 1973.
4. E. G. Burdette, D. W. Goodpasture, and S. K. Doyle. Comparison of Measured and Computed Load-Deflection Behavior of Two Highway Bridges. TRB, Transportation Research Record 507, 1974, pp. 17-25.
5. R. F. Varney. Preliminary Research Report of a Highway Bridge Loading Study With the HET-70 Main Battle Tank Transporter. Bureau of Public Roads, 1969.
6. A. C. Bogaty, Jr. A Study Concerning Data Input Into a Finite Element Analysis of a Highway Bridge. Univ. of Tennessee, Knoxville, MS project paper, 1973.
7. A. W. Rush, Jr. A Study of Wheel Load Distribution in a Highway Bridge. Univ. of Tennessee, Knoxville, MS project paper, 1973.
8. Specifications for Highway Bridges. AASHO, Washington, D.C., 1973.
9. W. W. Sanders, Jr., and H. A. Elleby. Distribution of Wheel Load on Highway Bridges. Engineering Research Institute, Iowa State Univ., Ames, 1968.
10. E. A. McDougle. Comparison of Measured and Computed Lateral Load Distribution for Two Continuous Steel Girder Highway Bridges. Univ. of Tennessee, Knoxville, MS thesis, 1975.